MASS ANGULAR SCATTERING POWER METHOD APPLIED TO THE THERAPEUTICAL ELECTRON BEAMS

By

FATİH İŞBAKAN

B.S. in Physics , Boğaziçi University, 1993

Submitted to Biomedical Engineering Institute
in partial fulfillment of the requirements of
Master of Science
in
Biomedical Engineering

Boğaziçi University

1997

MASS ANGULAR SCATTERING POWER METHOD APPLIED TO THE THERAPEUTICAL ELECTRON BEAMS

By

FATİH İŞBAKAN

APPROVED BY:

Prof. Dr. Yekta ÜLGEN .....
(Thesis Supervisor)

Yr.Doç.Dr.Albert Güveniş .....

Prof.Dr.Vural Altın .....

DATE OF APPROVAL : 17.6.1997

ACKNOWLEDGMENTS

I would like to thank Prof.Dr.Yekta ÜLGEN for his supervision and help during the course of study. I also thank to General Electric Medical Systems Turkey and Kartal Devlet Hospital for their support in my experiments. In addition, I would like to express my gratitude to Zeynep Özen İşbakan, Nural Öztürk and Berrin Yılmaz for their constant support and assistance in the preparation of the experimental setting.

ABSTRACT

A method for determining the kinetic energies of therapeutical electron beams is described. The theoretical basis of the mass angular scattering power method is analysed. The kinetic energy of therapeutical electron beams is determined from the Gaussian spread of a pencil beam. The pencil beam is obtained from a broad electron beam by using a simple technique. The data taken with a "closed collimator" are subtracted from those measured with the "open collimator" in order to isolate the pencil beam dose distribution. The spatial spread of a pencil electron beam in air is, as predicted by the Fermi-Eyges Theory,is Gaussian whose variance is a function of the mass angular scattering power, which in turn is related to the kinetic energy. The dose distribution is measured by an ion chamber which is moved by an "empty" water phantom system. The energies obtained by the mass scattering power method in air are significantly close to measured values obtained with the range method in water. The mass angular scattering power method is driven from the inelastic collisions in air and uses a probabilistic approach while the range method uses emprical formulas.

RADYOTERAPİDE KULLANILAN ELEKTRON IŞINLARININ ARDARADA SAÇINIM TEORİSİNE DAYANAN ENERJİ ÖLÇÜM METODU

ÖZET

Radyoterapide kullanılan elektron ışınlarının kinetik enerjilerinin ölçümleri için halen kullanımda olmayan bir metod açıklanmaktadır. Kütle açısal saçınım gücü adı verilen bu metodun teorik temelleri incelenmektedir. Elektronların kinetik enerjileri, geniş alanlı bir elektron ışınının, merkezinde dar bir delik bulunan bir kurşun plaka şeklindeki açık kolimatör ve aynı kalınlıkta herhangi bir deliği olmayan kapalı kolimatörün ışınlanmasıyla elde edilen doz profillerinin birebir farkından elde edilen doz dağılım profillerinden yararlanılarak bulunmaktadır. Kullanılan metodda, kapalı kolimatörden geçen radyasyon bize arka plandaki dozu vermektedir. Fermi-Eyges teorisinin öngördüğü üzere, dar bir elektron ışınının havadaki uzaysal saçınmı bir Gauss dağılım eğrisidir. Bu Gauss eğrisinin varyansı bulunarak kullanılan elektronun kütlesel saçınım gücü hesaplanmakta buradan da elektronun kinetik enerjisi belirlenmektedir. Havada saçınıma uğrayan elektronların uzaysal dağılımı bir iyon odası ve boş bir su fantomu ile ölçülmektedir. Elektronların enerji tayini için kullanılan sudaki erişim metodu amprik formüllere dayandığı halde kütle açısal saçınım metodu yüksek enerjili elektronların havadaki atomlarla elastik çarpışmalarının sonuçlarını kullanmakta ve atomik düzeydeki etkileşimlerden çıkan direkt formüllere dayanmaktadır.

TABLE OF CONTENTS

LIST OF FIGURES

LIST OF SYMBOLS

a	Atomic radius
A	Atomic mass
b	Impact parameter
c	Speed of light in vacuum
d	Thickness of the material
D_{eff}	Effective distance between electron-nucleus and electron-orbital electron
e	Electron charge
E_0	Energy at the absorber surface
Ez	Energy at depth z in a medium
$\hbar$	Planck constant divided by 2π
l	Length ,distance
m	Mass
m_0	Rest mass
m_e	Relativistic mass
M	Mass of nucleus
N_A	Avagadro's number
M_A	Molar mass of subtance A
P	Momentum
r	Radius of nucleus

R_p	Therapeutic range
R_{50}	Half-value depth
t	Thickness
T/ρ	Mass angular scattering power
χ	Distance
χ_0	Relative length
$Z(\vartheta)$	Collisional probability
z	Depth in a medium
β	Velocity of the electron with respect to the velocity of light in vacuum
ε_0	Permittivity of space
$\lambda\!\!\!^{-}$	Wavelength divided by 2π
ϑ	Angle of scattering of an electron
$\langle\vartheta^2\rangle$	Mean square angle of scattering
ϑ^2_a	The charge in mean square angle of scattering per unit length
ρ	Density
σ	Cross section

I. INTRODUCTION

1.1. Objective of The Study

Kinetic energy is one of the parameters affecting the clinical and dosimetric properties of electron beams and therefore should be known for clinically used electron beams .
Due to the high flux rates of pulsed linear accelerators, typically of the order of 10^{11} electrons / cm^2.s at the isocenter at 1 Gy/min particle-by-particle measurement in the beam is usually impossible [1] .
A few techniques, most of them very complex, are currently known for the determination of the kinetic energy of clinical electron beams. The most obvious technique is based on magnetic spectrometers which, unfortunately, are not yet available in radiotherapy departments and would also be difficult to use on the relatively large sized clinical electron beams. The International Commision on Radiation Units and Measurements (ICRU) suggests three different measurement techniques from which kinetic energies of clinical electron beams may be determined (ICRU 1984) :
a) Range of electrons in medium ,
b) Cerenkov radiation threshold angle ,
c) Nuclear radiation threshold [2].
The main objective of this research is to show that, from the in air measurement of the mass angular scattering power of a pencil electron beam, one can obtain energies that are comparable to the energies obtained with the range method. The mass angular scattering power method for determining the kinetic energy of clinical electron beams is described. The method is based on the measurement in air of the spatial spread of a pencil electron beam which is produced from the broad clinical electron beam. As predicated by the Fermi-Eyges theory, the dose distribution measured in air on a plane, perpendicular to the incident direction of the initial pencil electron beam, is Gaussian. The square of its spatial spread is related to the mass angular scattering power which in

turn is related to the kinetic energy of the electron beam, from the known relationship between mass angular scattering power and kinetic energy. The mass angular scattering power is relatively cumbersome, however, allows us to determine the kinetic energies of electron beams from the first principles, in contrast to the empirical methods based on range measurement in water.

II. ELECTRON BEAM IN RADIOTHERAPY

2.1. The Radiation Therapy

Therapeutical electron beams that are in use today are in the range of 4.5 and 25 MeV [3]. Radiotherapy is a branch of medicine dealing with the treatment of cancer using radiation [4]. The term radiation applies to the emission and propagation of energy through space or a material medium. There are mainly two kinds of radiation:

a) Particle radiation

b) Electromagnetic radiation

By particle radiation we mean energy propagated by traveling corpuscles that have a definite rest mass and within limits have a definite momentum and defined position at any instant. However, the distinction between particle radiation and electromagnetic waves, both of which represent modes of energy travel, became less sharp when in 1925, De Broglie introduced a hypothesis concerning the dual nature of matter. He theorized that not only do photons (electromagnetic waves) sometimes appear to behave like particles (exhibit momentum) but material waves such as electrons, protons and atoms have some type of wave motion associated with them (show refraction and other wave-like properties).

Protons, neutrons and electrons, many other atomic and subatomic particles have been discovered. These particles can travel with high speeds, depending on their kinetic energies, but never attain the speed of light in a vacuum. Also they interact with matter and produce varying degrees of energy transfer to the medium. The elemantary particles encountered in Radiotherapy are basically electrons, positrons, protons, neutrons, neutrinos and mesons.

Besides electromagnetic radiation constitues the mode of energy propagation for such phenomena as light waves, heat waves, radio waves, microwaves, ultraviolet rays,

X-rays and γ rays. These radiations are called "electromagnetic" because they were first described, by Maxwell, in terms of oscillating electric and magnetic fields. The wave nature of electromagnetic radiation can be demonstrated by experiments involving phenomena such as interference and diffraction of light. Similar effects have been observed with X-rays using crystals which possess interatomic spacing comparable to the X-ray wavelengths. However, as the wavelength becomes very small or the frequency becomes very large, the dominant behaviour of electromagnetic radiation can be explained by their particle or quantum nature [3], [4].

2.2. The Purpose of Radiation Therapy

The objectives of any form of cancer treatment is the destruction of the tumour and its extensions into the neighbouring lymph system. Three methods of treatment are currently in use: surgery, radiation therapy and chemotherapy. None of these alternatives are exclusive and treatments may in general be a combination of two or more of these techniques. Of the these techniques, surgery would be ideal, were it not for the tendency of tumours to extend rapidly into the adjoining healthy tissue. Radiation therapy is thus often used to reduce the tumour volume before surgery and to sterilize those lymph nodes not erradicated by the operation.

Chemotherapy drugs are highly toxic and often cannot be adminestered in sufficient quantities to reduce cell proliferation. Combinations of chemotherapy and radiotherapy are thus designed to accomplish this with minimum side effects.

It should be emphasized here that there are few hard and fast rules which apply to radiotherapy. Certain cancers (i.e. skin cancers) respond well to the teletherapy and experience has dictated presciptions which are successful in many cases. However, radiotherapy is an art with the success of treatment depending on many diverse factors [5].

2.3. Methods of Radiation Treatments

Presently two differents methods are used in radiotherapy, dependent upon the source. External source irradiation from an orthovoltage X-ray machine, Cobalt-60 teletherapy unit, or linear accelerator is the most important technique, while complementary to this is the internal irradiation from active needles and tubes. If there is easy access to the tumour and target volume is small and well defined, then the internal irradiation technique (brachytherapy) may be used alone.

The objectives of radiotherapy are to deliver a known dose to a known tumour volume. Ideally, the dose would be delivered only in the tumour volume with no irradiation of healthy tissue. The problem of radiotherapy is to approach this ideal. The tumour volume must be precisely defined. This can be done using a variety of techniques, among which radiography, tomography, contour planning, magnetic resonance and simulation are popular.

The choice of radiation source is also important, and is governed by the position and volume of the tumour to be treated, the dose required and the equipment available at the cancer center [5], [6].

2.4. Clinical Applications of Electron Beams

The features of the electron beam that make it a unique therapeutic tool are related to physical characteristics rather than to any special biological effectiveness of electrons. The most attractive characteristic in radiotherapy application is the depth dose curves (see Figure 2.1.) [7].

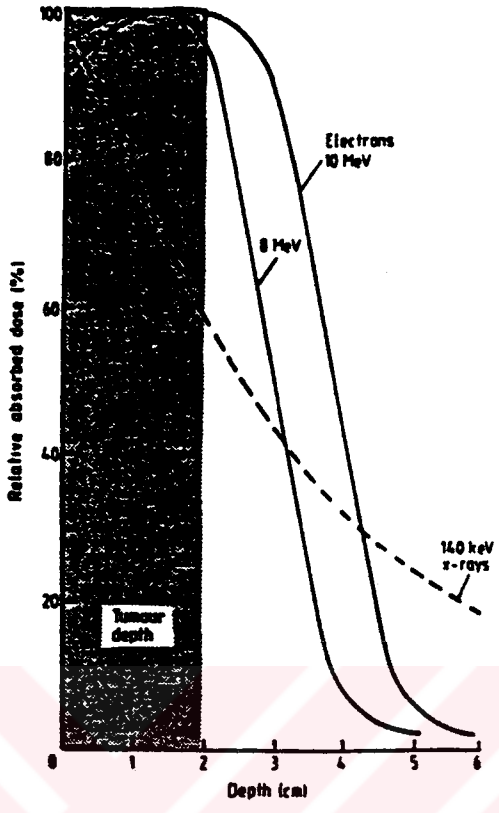

Figure 2.1. Comparison of the central axis distributions obtained with low-energy x-ray and electron beams [7].

The curve displays a moderately flat plateau in the first few centimeters of tissue, followed by a rapid fall in the absorbed dose to a small "tail" produced by X-rays generated in the scattering foil, the collimating system and the irradiated medium. The advantages to be drawn from the depth dose pattern area, therefore, suggesting the use of electrons for irradiation of sub-dermal tumours with the benefit of sparing the underlying tissues. The characteristic which are of particular significance in clinical applications are:

(a)The dose distribution from a single beam is such as to allow the treatment of a surface slab of tissue to relatively uniform doses whilst sparing underlying, deeper regions of healty tissues. The sharp cut off beyond the 80% depth dose is present for all

energies up to about 20 MeV, by 30 to 35 MeV the depth dose curves have a long tail resembling depth doses for low energy X-rays.

(b) The depth dose pattern with electrons of lower energy offers rapid and simple treatment set-ups, with the use of one field in many cases.

(c) There is an absence of increased absorption of energy in bone. The absorption of electrons is primarily determined by the electron density in the absorbing material. Since the number of electron per gram is almost the same in most biological materials, the absorbed dose is essentially the same in bone as in soft tissue.

(d) There is no difference in the biological effectiveness of electrons compared with megavoltage photon radiation.

(e) The build-up of absorbed dose below the skin is rapid; thus the skin sparing effect is smaller than with high energy photons.

(f) The dose distribution in tissue suffers perturbation if tissue inhomogeneities are present within the beam.

The dependance of depth dose distribution on energy has influenced the clinical application of electrons. The most useful in radiotherapy are electrons of 4-20 MeV, although higher energies are sometimes used as an alternative to photons for treatment of deep sited tumours [7], [8].

2.4.1. Electrons of Energy Below 20 MeV

The sharp fall-off of dose with depth makes electrons of energies up to 20MeV eminently suitable for treatment of tumours from surface up to depths of about 6cm. In this application, simple single direct fields are employed although multiple adjacent fields, seperated by 0.5 or 1.0 cm are also used if the area to be treated is large.

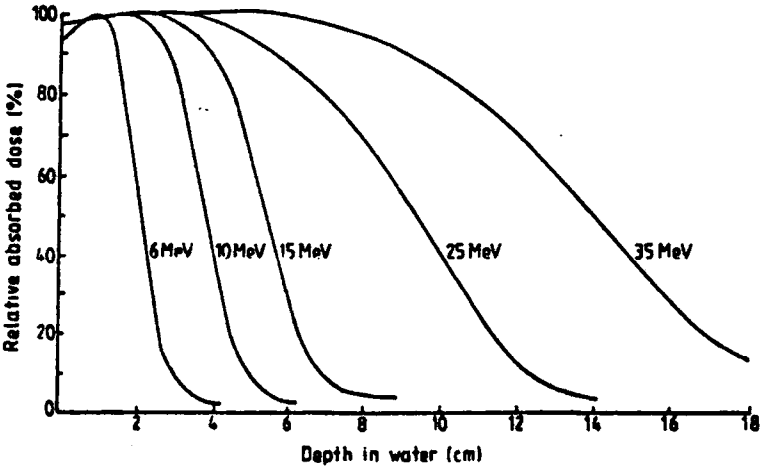

Figure 2.2. Central axis depth absorbed dose curves obtained at various electron beam energies [7] .

The electron beam distribution is more uniform over the target volume in comparison with a superficial X-ray treatment technique. This is evident in Figure 2.1., which shows that, up to the depth of 2.0 cm, the dose delivered by electrons varies by no more than 10% whilst the dose produced by 140 keV X-rays is seen to fall continously from the skin surface, giving a dose difference in a comparable depth range up to 40%. At a depth of 4cm, the 8 MeV electron beam has a depth dose of only 5% compared with 30% produced by the photons, and thus the sparing of tissues beyond the desired treatment depth is more pronounced with electrons.

Electrons of lower energy are therefore ideal for the irradiation of all skin and lip cancers, as well as operation scars and residual tumours. They are particullarly useful in the treatment of the nose and ear. Further applications extend to lymphomas located on or near the surface and sarcomas on the dorsum of the hand or foot. Electrons can also be used for large lesions in the area of the face and for lesions that have received treatment by cautery or surgical excision. Lesions of the floor of the mouth and the under-surface of the tongue can be treated adequately using an intraroral cone. Also,

small and superficial lesions of the gingiva and the soft palate can be treated by 8-10 MeV electrons.Electron beam therapy offers an excellent technique for providing additional dosage (top-up) to a limited area; for example, boost irridation to nodes. This technique can be applied to more extensive lesions of the floor of the mouth. The intraoral "boost" should be given prior to the external beam therapy in order to visualise the lesion and to be able to deal with the discomfort associated with the mucosal reaction. Electrons of 8-10 MeV can be used in combination with interstitial γ-ray therapy in the treatment of buccal mucosa lesions, but if the lesion is thick, 15-18 MeV electrons are required. There are clinical cases which can be satisfactorily treated with photon beams, but where an electron beam may also offer a simple technique. For instance, an 8 MeV straight-on electron beam is an elegant method of treatment of the chest wall which avoids the high doses to the lung evident when using glancing Cobalt-60 fields. For the same reason, electrons are preferred for the irradiation of the peripheral lymphatic areas and the chest wall after radical mastectomy. The supraclavicular field can be treated with 10 MeV electrons which provide the required tumour dose at 3cm. depth. However, for the internal mammary node chain an energy of 15 MeV is needed to reach the depth of 4cm. Other clinical situations which require electrons of 15-20 MeV are upper respiratory digestive track lesions and lymphatic of the neck.

The fixed beam technique is difficult to use in cases like long scars or tumours extending across the midline or on the inferier or posterior thorax. These are best treated with a rotating arc beam.

Sometimes, in cases of deeper lesions, because of the intensity of the skin reaction and the degree of subcutaneous fibrosis, electrons are combined with photons in the course of the treatment [7].

III. DETERMINING THE KINETIC ENERGY

3.1. Introduction

The term "beam quality" is often used as a general and reasonable attempt to describe the radiation beam ability to penetrate through matter. With electrons, this concept is related to the specification of energy and the energy spectrum of the beam [3].

Knowledge of the radiation quality of a high energy beam is necessary for several reasons. In clinical circumstances, treatment parameters can only correctly be selected if the beam energy is known. This applies to the determination of depth doses, radiobiological effectiveness etc. Knowledge of the beam is necessary for a meaningful comparison of characteristics of beams from various machines or data from various centres. It also plays an important role in the comparison of clinical results. In dosimetry, knowledge of the beam quality is essential for the choice of energy dependent factors used in dosimetry, such as chamber calibration factors, the ionisation to absorbed dose conversion factor C1, stopping power ratios, the perturbation and other correction factors [7].

3.2. Methods for Energy Determination

A few methods have been developed for the kinetic energy determination of the clinical electron beams. The methods described in ICRU Report No 35 are :

1) Magnetic Spectroscopy:

The most unambigous and accurate method of characterizing the primary electron beam in the patient plane is magnetic spectroscopy, which has long been known to be capable of very high resolution in spectral determination. Unfortunately, magnetic spectrometers are not yet readily available in radiotherapy depatments [1].

2) Method based on the thresholds of Nuclear Reactions [(Pohlit 1969), Lazl (1969), St. George and Anderson (1982) Ross and Shortt (1985)] :

An interaction of an electron or a photon with an atomic nucleus can lead to a nuclear reaction and to the emission of nucleons. The energy threshold for this type of reaction is determined by the difference between the rest energy of the target material and that of the residual nucleus plus the emitted nucleons.

The experimental method makes use of the fact that the activated nucleus will undergo a radioactive transformation whose emission can be measured by a radiation detector [1].

3) The Cerenkov Method [de Almeida (1974)] :

When a charged particle passes through a dielectric medium at a velocity of light in that medium, electromagnetic radiation, called Cerenkov radiation is emitted.

The maximum energy of the electron beam can be determined by measuring the Cerenkov emission threshold and employing the following relation [1] :

$$E = m \cdot c^2 \left[\left(1 - \beta^2\right)^{-1/2} - 1 \right] \qquad (3,1)$$

where $m.c^2$ is the rest energy of the electron and β is the ratio between the velocities of the electron and light in vacuum [9].

The Cerenkov method provides a method for determining the entire spectral range. However, the experimental requirements for good energy resolution are severe, since the derived energy spectrum is proportional to the numerical second derivative of the pressure versus the light intensity curve [1].

4) Practical Range Method :

This is the method that is routinely used in clinics today. In order to obtain the range for the broad and parallel electron beams, a semi-infinite water phantom ,on which

electrons are incident perpendicularly ,is used. It is difficult to set a limit beyond which a clinical beam can be considered as a broad beam, i.e. when the central axis depth dose distributions become independent of the field size, as it will depend on the energy and angular spread of the beam. Mostly, the manufacturers specifications will be taken as reference for the field size in the range method. An ionization chamber is traveled in depth till the dose absorbed is nearly zero, where only the bremsstrahlung tail is observed. Absorbed dose versus depth gives a curve similar to that of Figure 3.1 [10]. The practical range R_p and the half value depth R_{50} are of special importance for range-energy measurements. R_p is defined as the depth where the tangent to the descendent part of the curve intersects the prolongation of the bremsstrahlung tail. R_{50} is defined as the depth where the absorbed dose is 50 % of the maximum [10], [8].

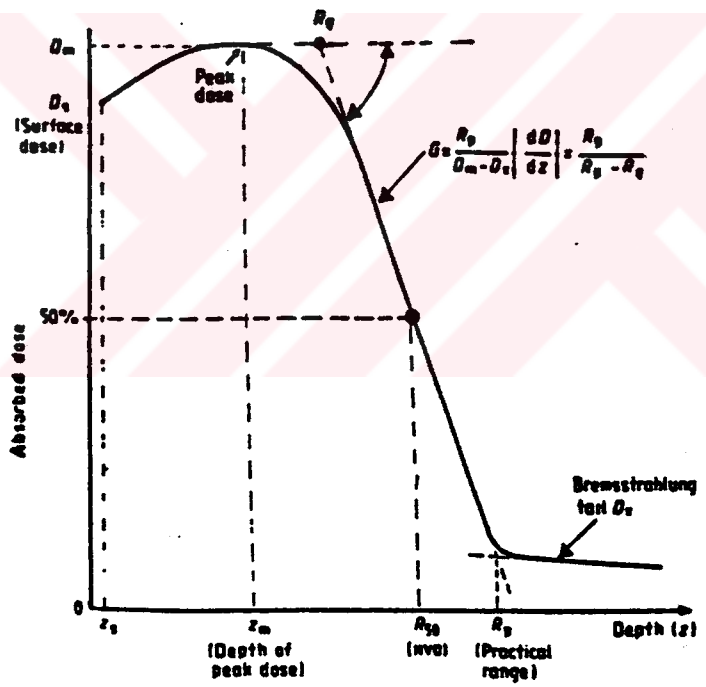

Figure 3.1. Characteristic parameters of the central axis depth dose curve [7].

The most probable energy at the surface ,is related to the practical range by the following empirical relation:

$$E_{p,o} = C_1 + C_2 R_p + C_3 R_p^2 \qquad (3,2)$$

with $C_1 = 0.22$ MeV, $C_2 = 1.98$ MeV.cm^{-1}, $C_3 = 0.0025$ MeV.cm^{-2}.

This equation is valid for broad beams and for most of the existing accelerators.

The mean energy at the phantom surface, is related to the half-value depth R_{50} by means of the expression:

$$\overline{E}_o = C_4 R_{50} \qquad (3,3)$$

where $C_4 = 2.33$ MeV.cm^{-1}

The mean energy as a function of depth is normally determined by means of approximate relations. For monoenergetic electron beams with the electron energy E_o at the phantom surface, Harder suggested that the depth dependence of the mean energy could be approximated by the simple relation :

$$\overline{Ez} \approx Eo \left[1 - \frac{Z}{R_P}\right] \qquad (3,4)$$

where Z is the depth and Rp is the practical range in a water phantom for an initial energy Eo [10].

3.3. An Alternative Method For Measuring The Kinetic Energy

The Mass Angular Scattering Power Method

The primary theme of this research is that, from the in air measurement of the mass angular scattering power of a pencil electron beam, we can obtain energies that are comparable to the energies obtained with the range method.

As an electron penetrates a medium, such as tissue or air, the Coulomb interactions of the electron with nuclei and orbital electrons of the medium result in multiple electron

scattering and in degradation of the kinetic energy of the electron. With the small angle scattering approximation and the central limit theorem (Reichl 1984) it can be shown that the mean square angle $< \theta^2 >$ for multiple electron scattering is linearly proportional to the mass thickness, ρt of the absorber, and the proportionality constant is equal to the mass scattering power, T/ρ. The mass angular scattering power is expressed analytically by the following equation [2], [11], [12].

$$\frac{T}{\rho} = \frac{\langle \theta 2 \rangle}{\rho t} = \frac{N_A \pi D_{eff}^2}{A} \left[\ln\left(1 + \frac{\vartheta_{min}^2}{\vartheta_{max}^2}\right) - 1 + \left(1 + \frac{\vartheta_{max}^2}{\vartheta_{min}^2}\right)^{-1} \right] \qquad (3,5)$$

This equation implicitly contains the kinetic energy of the electron in the expressions for θ_{min}, θ_{max} and D_{eff}. N_A in equation (3,5) is Avagadro's number, while A and ρ are the atomic mass and density of the absorber, respectively. D_{eff} is a characteristic distance counting for the electron-nucleus and electron-orbital electron interactions and is given by [9], [12]:

$$D_{eff} = \frac{\sqrt{Z(Z+1)}\ e^2}{4\pi\varepsilon_o (m_e \beta^2 c^2/2)} \qquad (3,6)$$

Where Z is the atomic number of the absorber nucleus, e the charge of the electron, ε_o is the permittivity of free space, m_e is the relativistic mass of the electron and βc the velocity of the electron.

In equation (3,5), θ_{max} is defined as the maximum scattering angle for which the nuclear point source approximation is still valid. It is given by [9], [12] :

$$\theta_{max} = 280\, A^{-1/3} \left(mc/p \right) \qquad (3,7)$$

where A and p are the atomic mass of the atom and the momentum of the electron respectively.

In clinical electron energy range and for low atomic number materials, equation (3,7) results in θ_{max} being larger than π, and therefore we can set $\theta_{max}=\pi$ under these conditions. The cut-off angle, θ_{min}, in equation (3,5) is given by [9], [12]:

$$\theta_{min} = \frac{Z^{1/3}}{137} \left({}^{mc}/_{p} \right) \qquad (3,8)$$

which for example, for a 10 MeV kinetic energy electron incident on hydrogen or aliminium atoms, corresponds to angles of 0.02° and 0.05° respectively. Since θ_{max} is assumed constant, it follows that T/ρ is dependent on kinetic energy only through the cut-off angle, θ_{min}, and the characteristic distance, D_{eff}.

In Figure 3.1. the plot of equation (3,5), i.e. τ/ρ in air, as a function of E_k, in the energy range from 1 to 100 MeV. The relationship on a log-log scale shows a steady and almost linear drop of T/ρ with an increase in E_k, suggesting a relatively simple means for kinetic energy determination from a measurement of the mass angular scatting power T/ρ [12].

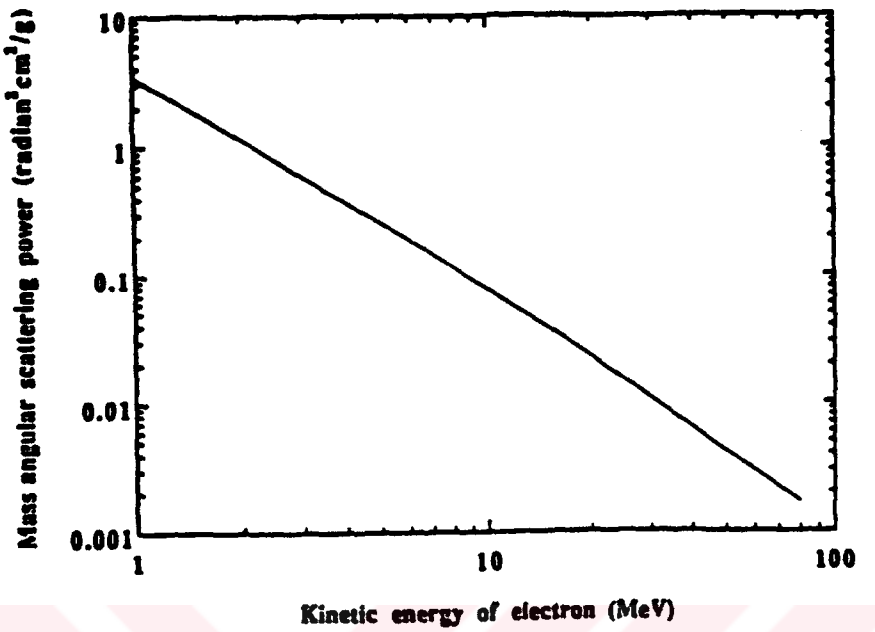

Figure 3.2. Mass Angular Scattering Power in air as a function of the kinetic energy of electron in the energy range from 1 to 100 MeV [12].

The propagation of a pencil beam in a medium is described by a distribution function, which is given by the Fermi-Eyges solution to the Fermi differential equation (Eyges 1948, Rossi and Greisen 1941). The Fermi-Eyges theory predicts that, the dose distribution in a medium on a plane perpendicular to the incident direction of the initial pencil electron beam is given by a Gaussian distribution with a spatial spread proportional to its variance. In air, the square of the spatial spread of the pencil electron beam σ^2, is related to the mass angular scattering power and the thickness of air layer, X, from a pencil beam origin through the expression:

$$\sigma^2(X) = \left(T/\rho\right)\frac{\rho X^3}{6} \qquad (3,9)$$

In deriving the above equation, the following assumptions are made:

a) Only small angle scattering events, are considered.

b) The air layer X is much smaller than the electron range in air, i.e. the energy loss of electrons in air is neglected.

c) The secondary electrons, set in motion by the incident electron beam are ignored.

d) The brehmsstrahlung contamination of the electron beam is ignored.

The function σ^2, as given by equation (3,9), is a linear function of X^3 with the slope proportional to T/ρ, which in turn is a function of the electron beam kinetic energy Ek, as given in equations (3,5), (3,6), (3,7), and (3,8) above. From a measurement of $\sigma^2(X)$, the spatial spread of a pencil beam in air, in different distances from the pencil beam origin; T/ρ, the mass angular scattering powers are determined [12].

IV. THEORETICAL BASIS OF THE MASS ANGULAR SCATTERING POWER METHOD

4.1. Introduction

The transport and penetration of electrons in matter in the energy range of interest in radiation therapy involves interactions which result either in direct energy losses or scattering, or a combination of both. The most important interactions include elastic nuclear scattering involving a nucleus (Coulomb Scattering), inelastic interactions with orbital electrons and radiative collisions with both nuclei and orbital electrons. The mode of interaction is largely determined by the energy of the passing electron and the distance of electron approach to the atom or nucleus with which it interacts [13].

4.2. Energy Losses of Electrons

Collisions which lead to direct energy loss by the passing electron are of primary interest, since such events give rise to a direct deposition of energy and hence absorbed dose, in the irradiated medium. The energy losses usually take place in small increments and an electron must therefore suffer many collisions before it losses all its energy. A 10 MeV electron will go some 100 000 interactions before coming to rest. Two principally different energy loss processes may occur: collisional losses and radiative losses. The fundamental difference between them is that the collisional loss involves the outer atomic electrons while the radiative losses involve the atomic nucleus [14].

4.3. Scattering Processes

An important aspect of electron interaction with atoms, apart from the energy losses, is the change in direction of the electron motion leading to scattering. Most of the collision type interactions are also accompanied by electron scattering [7].

It is possible to treat the energy loss and scattering separately, although they are inseparable.

As a general rule, the elastic scattering can be divided into 3 classes:

a) Single scattering ,

b) Plural scattering ,

c) Multiple scattering .

Single scattering results in a large angular deflection of the electron whereas small-angle deflections are associated with multiple scattering. The intermediate case is known as the plural scattering.

Two interaction processes are particularly important in scattering: interactions of the passing electron with the Coulomb field of the nucleus and electron-orbital electron collisions.

If the thickness x of the layer transversed is small, $x << 1 / \sigma N$, where σ is the cross section and N is the number of scattering atoms per cm^3, there will be practically one single scattering; i.e. most of the electrons are scattered by only one nucleus. For larger values of thickness, $d \sim 1 / \sigma N$, we get plural scattering, there is more probability that the scattering angle is due to a number of successive single scattering processes. When the thickness becomes so large that the mean number of processes is larger than 20 - 30, the term multiple scattering is used [11].

4.4. Deflection and Energy Transfer In a Coulomb Collision

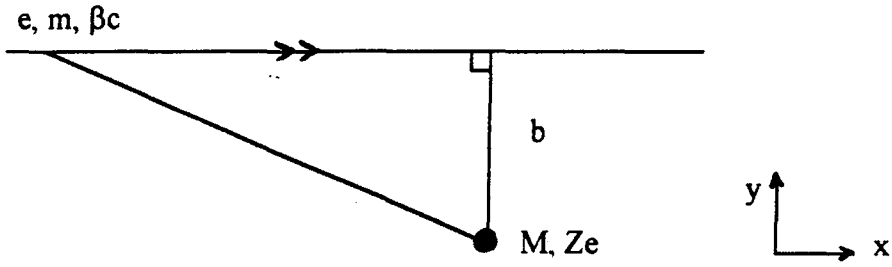

Figure 4.1. Collision of an electron with a nucleus.

Consider an electron of mass m and charge e collides with a heavy nucleus of mass M and charge Ze in an atom, with an impact parameter b and velocity βc. Here the electron and the nucleus can be treated as free particles.

The mass of the nucleus is much larger than the mass of the nucleus (M >> m). As the electron passes through, in the position of the nucleus, only the transverse electric field has a nonvanishing time integral; the longitidunal forces vanish each other during the collision time. Consequently, the momentum impulse Δp is in the transverse direction (y direction) and has a magnitude of:

$$\Delta p = \int_{-\infty}^{\infty} Ze\, E_2(t)\, dt = \frac{2Ze^2}{b\beta c} \qquad (4,1)$$

It should be noted that Δp is independent of γ and the energy transfer to the nucleus is:

$$\Delta E(b) = \frac{(\Delta p)^2}{2m} = \frac{2Z^2e^4}{M\beta^2c^2}\left(\frac{1}{b^2}\right) \qquad (4,2)$$

Because the mass of the target nucleus is much larger than that of the electron, the energy transfer is negligible.

From Newton's third law, it follows that the incident particle (electron) acquires a transverse momentum of the same magnitude in the opposite direction. The angular deflection of the incident particle is given by $\theta \approx \Delta p / p$, provided that $\Delta p << p$, thus for small deflections [14]:

$$\theta \cong \frac{2Ze^2}{b\beta cp} \qquad (4,3)$$

4.5. Differential Cross Section and Differential Scattering Probability of Electron with Atoms of Matter

Collision of electrons with the atoms of the material occur at random, and their observable effects are therefore described in terms of probability distributions and averages. We need to specify not only the probability of a collision but also the probability that, after the collision, the energy (or momentum) of this particle be within a given differential interval and its direction of motion lie within a given element solid angle. The quantities used for these purposes are the differential cross sections.

The "size" of the atomic and subatomic particles are not easily defined. For example, an electron which passes at a distance b of a nucleus is scattered by the Coulomb field of the nucleus, which extends its effective size for scattering far beyond the "boundary" of the nucleus.

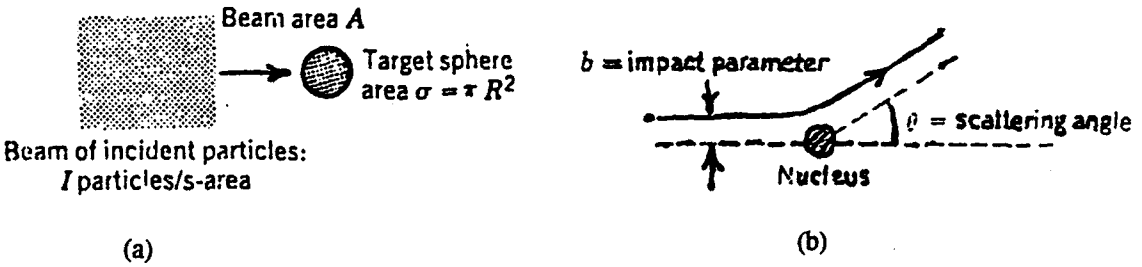

Figure 4.2. (a) A beam of particles incident on a target sphere. (b) Positively charged particle scattered from a stationary positive nucleus [11] .

As indicated in Figure 4.3.a, particles incident with impact parameters between b and b+db will have deflection angles between θ and θ+dθ. The cross sectional target area enclosed by the annulus of radius b and of width db is just $d\sigma = 2\pi b db$. It is often customary to express dσ in terms of the differential solid angle dΩ instead of the polar angle dθ.

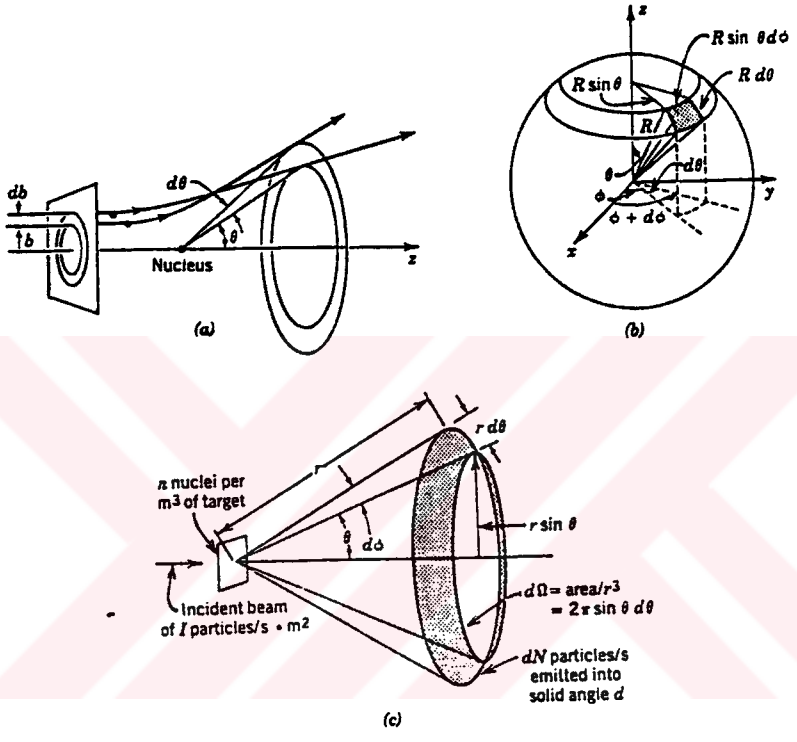

Figure 4.3. (a) Correspondence between the impact parameter b and the scattering angle θ. (b) Area on a sphere subtended by dθ and dφ (c) Azimuthally symmetric solid angle corresponding to dθ [11].

The solid angle, expressed in units of steradians (sr), corresponding to a polar angular interval dθ and a azimuthal angular interval dφ, is just the corresponding area on a unit sphere centered at the origin, that is the scattering center. We can write the area on the sphere of radius R subtended by dθ and dφ at the origin as :

$$dA = (Rd\theta)(R \sin\theta \, d\phi) = R^2 \sin\theta \, d\theta \, d\phi \qquad (4,4)$$

setting R=1 for the unit sphere then yields,

$$d\Omega = \sin\theta \, d\theta \, d\phi \ (sr) \qquad (4,5)$$

as a general expression for $d\Omega$. The solid angle that corresponds to $d\theta$ is found by integrating $d\Omega$ in equation (4,5) over ϕ to obtain :

$$d\Omega = 2\pi \sin\theta \, d\theta \ \ (sr) \qquad (4,6)$$

When the electron passes in the neighborhood of a nucleus, one can neglect the radiation emitted during the process. Since the nucleus is very heavy with respect to the incident electron, the energy of the latter does not change appreciably and the collision is an elastic one [1].

In the case of elastic collisions (and if the target particle is at rest), the energy and the momentum of the incident particle after the interaction are entirely determined by its angle of scattering, i.e. by the angle between the directions of motion of the particle before and after the interaction. In our case, we shall assume that there is no preferential orientation of either the incident particles or target particles. Then all information about the collision in question is confined in a function of the incident energy E_k and the angle of scattering θ, to be denoted by $d\sigma/d\Omega$ and defined by the following condition: If K particles of energy E_k are incident perpendicularly upon a layer of very small thickness dx, then $K(d\sigma/d\Omega) d\Omega dx$ represents the number of particles scattered into the element of solid angle $d\Omega$ at the angle θ to the incident beam. In the same manner, one can define a differential scattering probability $Z(\theta)$. Let $Z(\theta)d\Omega \, dx$ represent the probability that a particle of momentum p and velocity βc, transversing a thickness of dx gcm^{-2},

undergoes a collision which deflects the trajectory of the particle into the solid angle $d\Omega$ at an angle θ to its original motion. Then one can conclude that :

$$Z(\theta)\, d\Omega\, dx = \frac{d\sigma}{d\Omega}\, N\, dx\, d\Omega \qquad (4,7)$$

which yields,

$$Z(\theta)\, d\Omega = N \left(\frac{d\sigma}{d\Omega}\right) d\Omega \qquad (4,8)$$

If N is the number of atoms per cm^3, A is the atomic number then the probability of a collision with impact parameter in db at b on traversal of 1 gcm^{-2} is:

$$\frac{N}{A} 2\pi b db = \pi \left(\frac{N}{A}\right) d\left(b^2\right) \qquad (4,9)$$

Equation (4,3) gives, in absolute value:

$$d\,(b^2) = \left(\frac{2Ze^2}{\beta cp}\right)^2 2\frac{d\vartheta}{\vartheta^2} \qquad (4,10)$$

since $d\Omega = 2\,\pi\,\theta\,d\theta$, we obtain:

$$Z(\theta)\, d\Omega = \frac{N}{A}\left(\frac{2Ze^2}{\beta cp}\right)^2 \frac{d\Omega}{\theta^4} \qquad (4,11)$$

If we substitute $r_e = e^2/mc^2$, the classical radius of the electron we have [11], [15]:

$$Z(\theta)\, d\Omega = 4\, N \frac{Z2}{A} r_e^2 \left(\frac{mc}{\beta p}\right)^2 \frac{d\Omega}{\theta^4} \qquad (4,12)$$

4.6. The Limits of the Rutherford Scattering Formula

The expression for the scattering probability were derived under the assumption that the electric field of a nucleus is that of a point charge Ze. Departures come from the point Coulomb-field approximation at large and small angles, corresponding to small and large impact parameters. At large b, the screening effects of the atomic electrons cause the potential to fall off more rapidly than (1/r). In the Fermi -Thomas model the potential can be approximated roughly by the form:

$$V(r) \cong \frac{kZe^2}{r}\exp\left(-\frac{r}{a}\right) \qquad (4,13)$$

where $a \cong 1.4a_o z^{-1/3}$.

The length $a_o = \hbar^2 / m_e c^2$ is the hydrogenic Bohr radius. For impact parameters of the order of or greater than a, the rapid increase of the potential (4,13) will cause the scattering angle to vanish much more rapidly with increasing b than is given by (4,3). This implies that the scattering cross section will flatten off at small angles to a finite value at $\theta = 0$, rather than increasing as θ^{-4}. Goudsmit and Saunderson obtained the following expression (valid for small values of θ):

$$Z(\theta)\, d\Omega = 4\,N\,\frac{Z2}{A} r_e^2 \left(\frac{mc}{\beta p}\right)^2 \frac{d\Omega}{\left(\theta^2 + \theta_{mn}^2\right)^2} \qquad (4,14)$$

where θ_{min} is the cut-off angle. The minimum angle θ_{min} below which the differential scattering probability (or the cross section) departs appreciably from the simple result (4,12) can be determined either classically or quantum mechanically. Classically θ_{min} can be estimated by putting b = a in (4,3). This gives:

$$\theta_{min} \cong \frac{2Ze^2}{p\beta ca} \qquad (4,15)$$

Quantum mechanically, the finite size of the scatterer implies that, the approximately classical trajectory must be localized to within $\Delta x<a$; the incident particle must have a minimum uncertainity in transverse momentum $\Delta p \geq \hbar / a$. For collisions in which the momentum transfer (4,1) is large compared to $\hbar/a$,the classical Rutherford formula will apply. But for smaller momentum transfers, we expect the quantum-mechanical smearing cut to flatten off the cross section. This leads to a quantum mechanical θ_{min}:

$$\theta_{min} = \frac{\hbar}{pa} \tag{4,16}$$

For the screening radius a, (4,16) becomes:

$$\theta_{min} = \frac{Z^{1/3}}{137}.\frac{mc}{p} \tag{4,17}$$

where p is the incident momentum ($p = \gamma M\beta c$) and m is the electronic mass.At comparatively large angles, the Rutherford Scattering formula (4, 12)fails because of the finite size of the nucleus. The charge distribution of the atomic nucleus can be crudely approximated by a uniform volume distribution inside a sphere of radius R, falling rapidly to zero outside R. This means that the electrostatic potential inside the nucleus is not 1/r, but rather parabolic in shape, with a finite value at r = 0:

$$V(r) = \begin{cases} \frac{3}{2}\frac{Ze^2}{R}\left(1 - \frac{r^2}{3R^2}\right) & \text{for } r < R \\ \frac{Ze^2}{r} & \text{for } r > R \end{cases} \tag{4,18}$$

It is a peculiarity of a point charge Coulomb field that the quantum-mechanical cross section is the classical Rutherford formula. For a nucleus of finite size, the De Broglie

wavelength of the incident particle is taken into account. When we consider wave packets incident on the relatively constant (inside r = R) potential, there will be departures from the simple formula (4,12) Since the particle wavelength is $\lambda\!\!\!^{-} = \hbar/p$, the maximum scattering angle, beyond which the scattering probability falls significantly below θ^{-4} law, is:

$$\theta_{max} \cong \frac{\hbar}{pa} \tag{4,19}$$

Using the simple estimate $R \cong (1/2)(e^2/mc^2) = 1.4\ A^{-1/3}\ 10^{-13}$

$$\theta_{max} = 280\ A\text{-}1/3\left(\frac{mc}{p}\right) \tag{4,20}$$

In the clinical electron energy range for low atomic number materials, equation (4,20) results in θ_{max} being larger than π, and therefore we can set $\theta_{max}=\pi$, as the maximum scattering angle for which the nuclear point source approximation is valid.

The general behaviour of the cross section is shown in Fig 4.4. The dotted curve is the small-angle Rutherford approximation, while the solid curve shows the qualitative behaviour of the cross section; including the screening and finite nuclear size [9], [11], [12].

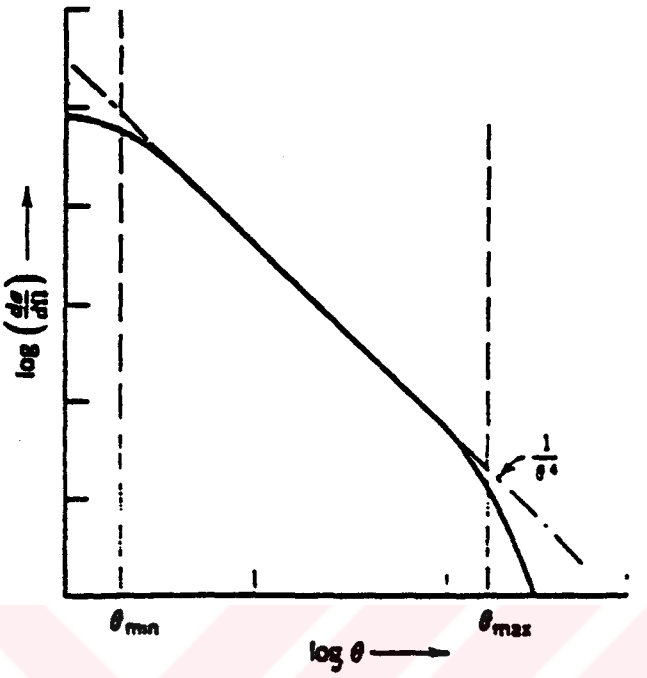

Figure 4.4. Atomic scattering, including effects of electronic screening at small angles and finite nuclear size at large angles [9]

4.7. The Mean Square Angle of Scattering

When a charged particle traverses a plate of finite thickness, it undergoes a large number of collisions, most of which produce very small angular deflections. One may want to compute the probability that, as a result of these successive collisions, the particle emerges from the plate with a given lateral displacement and with an angular deflection.

As a first step, we shall compute the mean square angle of deflection, $\langle\theta^2\rangle$, as a function of the thickness x, of matter traversed. According to a general rule on the superposition of small and independent variations, the value $\langle\theta^2\rangle$ at x+dx equals the value of $\langle\theta^2\rangle$ at x plus the mean square angle of scattering in dx:

$$\langle\theta^2\rangle\,(x+dx) = \langle\theta^2\rangle\,(x) + \int \theta^2\, Z(\theta)\, d\Omega \qquad (4,21)$$

which yields,

$$d\langle\theta^2\rangle = dx \int \theta^2 Z(\theta) d\Omega$$

This equation can be written as follows:

$$\frac{d\langle\theta^2\rangle}{dx} = \theta^2_a \qquad (4,22)$$

where $$\theta^2_a = \int \theta^2 Z(\theta) d\Omega = \int \theta^2 Z(\theta)\, 2\pi\, \theta\, d\theta \qquad (4,23)$$

If one assumes that $Z(\theta) = 4N \frac{Z^2}{A} r_0^2 \left(\frac{mc}{\beta p}\right)^2 \frac{d\Omega}{\theta^4}$ for $\theta_{min} < \theta < \theta_{max}$ and is zero

for $\theta < \theta_{min}$ or $\theta > \theta_{max}$, equation (4,23) yields :

$$\theta^2_a = 8\pi\, N \frac{Z^2}{A} r_0^2 \left(\frac{mc}{\beta p}\right)^2 \ln\left(\frac{\theta_{max}}{\theta_{mn}}\right) \qquad (4,24)$$

or with the derived values for θ_{min} and θ_{max}:

$$\theta^2_a = 16\pi\, N \frac{Z^2}{A} r_0^2 \left(\frac{mc}{\beta p}\right)^2 \ln\left[196 Z^{-1/6} \left(\frac{Z}{A}\right)^{1/2}\right] \qquad (4,25)$$

The coefficient that multiplies $Z^{-1/3}$ in the logarithm varies from a value of 175 in the light elements (where A = 2 Z) to a value of 163 in the heavy elements (where A = 2.5 Z). The difference between these coefficients is not theoretically significant and has a negligible effect on the result. If we introduce E_s with the dimensions of energy

$$E_s = \left(\frac{4\pi}{\alpha}\right)^{1/2} m_e c^2 = 21 \times 10^6 \text{ eV} \qquad (4,26)$$

where $\alpha = 1/137$, we may write:

$$\theta^2_a = \left(\frac{E_s}{\beta cp}\right)^2 \frac{1}{X_0} \qquad (4,27)$$

where X_o (radiation length) is given for different materials given in ICRU 35.
Instead of considering the total deflection θ, it is convenient to consider the projection, θ_x, of the polar angle θ in the x-z plane and θ_x the projection in the y-z plane. For small angles, we have $\theta^2 = \theta^2_x + \theta^2_y$ (4,28) and as the distributions are symmetric:

$$\overline{\theta^2} = 2\overline{\theta^2_x} = 2\overline{\theta^2_y} \qquad (4,29)$$

Thus, we can write:

$$\langle\theta^2\rangle = \frac{1}{2}\,\theta^2_a\, x \qquad (4,30)$$

We have so far neglected scattering in the field of atomic electrons. Presumably one can take this effect into consideration by replacing Z^2 with $Z(Z+1)$ in the expressions for the scattering probability and for the root mean square angle of scattering [16], [17].

4.8. The Distribution Function

Let us consider a parallel and infinitely narrow beam of particles incident on a plate of some scattering substance. The particles are all supposed to have the same energy and their energy loss in scattering substance is neglected. We wish to compute the spatial and angular distributions of the beam after traversal of a thickness x of the scattering substance.

Let us take a system of Cartesian coordinates with the origin at the point of incidence and one of the axes in the direction of the motion of the incident particles. This axis will be denoted as the x axis, while the other two will be the y and z axes, respectively. Let us consider the projection of the motion of the particles on the (x, y) plane and let F(x, y, θ) dy dθ be the number of particles at the thickness x having a lateral displacement (y, dy) and traveling at an angle (θ, dθ) with the x axis. For the reasons of symmetry, the same function F describes also the space and angular distributions in the (x, z) plane. Since deflections in the two orthogonal directions y and z are independent of eachother, the number of particles having a lateral displacement with components (y, dy) and (z, dz) and an angular deflection with components (θ_y,$d\theta_y$) and (θz,$d\theta z$) at the thickness x is given by F(x, y, θ_y) F(x, z, θ_z) dy dz $d\theta_y$ $d\theta_z$. We want to calculate the distribution function F under the usual assumption that the angle θ is small. Let $\rho\Delta x(\theta)d\theta$ be the probability that a particle traversing the thickness Δx will be deflected through an angle (θ, dθ). The deflection θ is not necessarily caused by a single collision. Hence, the function ρ(θ) is not immediately related to the function Z(θ) defined previously. By its definition, ρ(θ) satisfies the following equations:

$$\rho\Delta x(\theta) = \rho\Delta x(-\theta) \tag{4,31}$$

$$\int_{-\infty}^{\infty} \rho\Delta x(\theta)d\theta = 1 \tag{4,32}$$

$$\int_{-\infty}^{\infty} \theta\rho\Delta x(\theta)d\theta = 0 \tag{4,33}$$

$$\int_{-\infty}^{\infty} \theta^2 \rho\Delta x(\theta)d\theta = \langle\theta^2\rangle A_v = \frac{1}{2}.\frac{Ea^2}{\rho^2\beta^2c^2}.dx \tag{4,34}$$

Since ρ has a very sharp maximum at θ = 0 and goes rapidly to zero on both sides of the maximum, the integrals can be extended from -∞ to +∞. We ask now for the

change that the function F undergoes in the layer from x to x+Δx. The function F changes because both the space distribution and the angular distribution of particles are modified by the transversal of the layer Δx. The scattering in this layer represents only a second order effect and can be disregarded as far as the change in the space distribution is concerned. It follows that the particles having a lateral displacement y at the thickness x+Δx are those which had a lateral displacement y-θΔx at the thickness x. Hence, neglecting the change in the angular distribution,

$$F(x+\Delta x, y, \theta) = F(x, y-\theta\Delta x, \theta) = F(x, y, \theta) - \theta\Delta x\left(\frac{\partial F}{\partial y}\right) \qquad (4,35)$$

In order to calculate the effect of the change in the angular distribution, let us consider two angular intervals (θ, dθ) and (θ′, dθ′). There are F(x, y, θ′)dy dθ′ particles in (θ′, dθ′) at the thickness x with a lateral displacement (y, dy) and a fraction ρΔx(θ-θ′)dθ of these particles is scattered into the angular interval (θ, dθ) while traversing the layer Δx. Hence, if we neglect the change in the space distribution,

$$F(x+\Delta x, y, \theta) = \int_{-\infty}^{\infty} F(x, y, \theta') \rho\Delta x(\theta - \theta')d\theta' \qquad (4,36)$$

Since ρΔx(θ - θ′) is different from zero only for very small values of the argument, F can be developed in Taylor series (θ - θ′). Dropping the terms beyond the second order and taking into account equation (4,36), we obtain:

$$F(x+\Delta x, y, \theta) = F(x, y, \theta) + \frac{1}{4}\frac{Ea^2}{\rho^2\beta^2c^2}\left(\frac{\partial^2 F}{\partial\theta^2}\right)\Delta x \qquad (4,37)$$

Hence the total change of the distribution function F in the layer Δx is :

$$-\theta\left(\frac{\partial F}{\partial y}\right)\Delta x+\frac{1}{4}\frac{Ea^2}{\rho^2\beta^2c^2}\left(\frac{\partial^2 F}{\partial\theta^2}\right)\Delta x \qquad (4,38)$$

If we set :

$$\omega = 2p\beta / E\alpha$$

we obtain for F the differential equation :

$$\frac{\partial F}{\partial x}=-\theta\frac{\partial F}{\partial y}+\frac{\theta^2}{4}\frac{\partial^2 F}{\partial\theta^2} \qquad (4,39)$$

We look for a solution of (4,39) which corresponds to a single incident particle. The function F will then represent the probability for a certain lateral displacement and a certain angular deflection at the thickness x. It can easily be proved that such a solution (given by Fermi):

$$F(x, y, \theta)=\frac{2\sqrt{3}}{\pi}\frac{1}{\theta a^2x^2}\exp\left[-\frac{4}{\theta a^2}\left(\frac{\theta^2}{x}-\frac{3y\theta}{x^2}+\frac{3y^2}{x^3}\right)\right] \qquad (4,40)$$

Indeed, it is seen upon substitution that (4,39) satisfies (4,40). That the boundary conditions are also fulfilled will be made apparent by what follows.

By integrating the distribution function F over y, one obtains a function G(x, θ) which represents the angular distribution irrespective of lateral displacement:

$$G(x,\theta)=\int_{-\infty}^{\infty}F(x,y,\theta)dy=\frac{1}{\sqrt{\pi}}\frac{1}{\theta_a x^{1/2}}\exp\left(-\frac{\theta 2}{\theta_a^2 x}\right) \qquad (4,41)$$

Similarly, by integrating the function F over θ one obtains a function H(x, y) which represents the distribution in space, irrespective of angle.

$$H(x, y) = \int_{-\infty}^{\infty} F(x,y,\theta)d\theta = \sqrt{\frac{3}{\pi}}\frac{1}{\theta_a x^{3/2}}\exp\left(-\frac{3y^2}{\theta_a x^3}\right) \qquad (4,42)$$

It follows from H and G functions that, for all values of x:

$$\int_{-\infty}^{\infty} G(x,\theta)d\theta = \int_{-\infty}^{\infty} H(x,y)dy = 1 \qquad (4,43)$$

Moreover, at the limit for x=0, G is zero for all values of θ except θ=0, and H is zero for all values of y except y=0; i.e.:

$$G(0, \theta) = \delta(\theta)$$
$$H(0, y) = \delta(y)$$

where δ is Dirac's improper function.

This proves that the solution (4,40) actually corresponds to a single particle incident at x=0, y=0 in the direction of the x axis.

Equation (4,41) shows that, at every thickness, the angular distribution irrespective of position is Gaussian. The mean square angle of scattering is given by:

$$\langle\theta^2\rangle(x) = \frac{1}{2}\theta_a^2 X \qquad (4,44)$$

in agreement with our previous discussion.

Similarly, Eq (4,42) shows that at every thickness the distribution in space, irrespective of angle, is Gaussian.

The mean square displacement is:

$$\sigma_y^2 = \langle y^2\rangle(x) = \frac{\theta_a^2 x^3}{6} = \frac{1}{6}\left(\frac{T}{\rho}\right)\rho x^3 \qquad (4,45)$$

since $\theta_a^2 = \frac{d\theta^2}{dl} = \frac{T}{\rho}$ as seen in equation 4,46 and equation 4,22 [11], [17].

4.9. Mass Angular Scattering Power

The multiple scattering of electrons traveling a path length l, is usually described by the mean square scattering angle, $\langle\theta^2\rangle$. By analogy with the mass stopping power, the quotient $\langle\theta^2\rangle/\rho l$ may be called "mass angular scattering power" of the material. The mass angular scattering power, which is defined as the increase in the mean square angle of scattering $d\theta^2$ per unit mass thickness traversed $\rho.dl$ [2] :

$$\frac{T}{\rho} = \frac{d\theta^2}{\rho.dl} \quad [rad^2cm^2g^{-1}] \qquad (4,46)$$

Using the derivation for $\langle\theta^2\rangle$ in equation (4,25), we can express T/ρ as :

$$\frac{T}{\rho} = \frac{\langle\theta^2\rangle}{\rho l} = 16\pi N_A \frac{Z^2}{M_A} r_e^2 \left(\frac{mec^2}{\beta pc}\right) \log\left[196 Z^{-1/6}\left(\frac{Z}{A}\right)^{1/2}\right] \qquad (4,47)$$

where r_e electron radius = e^2/mec^2 (= 2.818x10-5m),

M_A = molar mass of the substance A.

T/ρ for different materials is calculated in ICRU 21 using the above formula [18].

Another formula, which has been driven by Rossi, was used in ICRU 35 report. In this approach, Rossi used a screened Rutherford cross section which is finite at zero degrees and explicitly includes the same screening angle θmin . This leads to Equation (3.5).The formula 3.25 is used in ICRU Report No 35 to calculate T/ρ for different materials [12].

4.10. T/ρ Versus Kinetic Energy

If we plot T/ρ given in ICRU 35 report and kinetic energy on a log-log scale, it gives a steady and almost linear drop of T/ρ with an increase in electron energy, suggesting a relatively simple relation, $T/\rho \alpha E^{-n}$, where n is in the range of 1.5-2.0 depending on E. Werner has found n to be equal to 1.78 for materials from water to aliminium in an energy range of 5-20 MeV and calculated the T/ρ values for different materials for ICRU Report No 21 [13].

An approximate estimation of the mass scattering power for electrons of kinetic energy Ek can be made by using the formula [11] :

$$\frac{T}{\rho} = \frac{\left(\frac{E_s}{E}\right)^2}{\beta X_0} \qquad (4,48)$$

where Es has a constant value of 21.2 MeV and X_o, the radiation length, has been calculated in ICRU 35.

This suggests us that the determination of T/ρ of an electron beam in a given medium (air in our case) will give us the kinetic energy of this electron beam, since we can find T/ρ versus kinetic energy tables in ICRU Reports No 21 and ICRU Reports No 35.

V. MATERIALS AND METHODS

A linear accelerator,General Electric model Saturne 41F, producing electrons in the nominal energy range from 4.5 to 16 MeV, was used in my experiments. The electron beams were studied at the radiotherapy port (Kartal Devlet Hastanesi - Radiation Oncology Center) and their kinetic energies were determined using both the "range method" and the "mass angular scattering method".

In the range method, broad electron beams, a water phantom and an ionization chamber were used. The gantry was in zero degrees of the rotation angle, water phantom was filled with water, and the water surface was brought to 100 cm from the target bar of the linac. The simulation light, simulating the irradiation field, was opened 10 cm x10 cm at this particular position. The ionization chamber IC 10 was placed into the holding mechanism and brought to the centre of the crosshairs shadow on the water surface. The center of the crosshair should be the radiation and mechanical axis of the collimator. Choosing the depth dose measurement option in the Dosimeter System - Wellhaufer 600-,the ionisation chamber is traveled in depth on the central axis of the beam and the ion pairs caused by the irradiation are calculated and the electrometer gives us the relative dose at each point in depth. The dosimeter system gives us a depth dose curve which enables us to calculate R_p, R_{50}, E_o, E_p. Wellhaufer 600 automatically calculates R_p, E_o of the beam. The kinetic energies of electron beams with nominal energies 12, 13.5 and 16 MeV were measured by the range method in the water phantom.

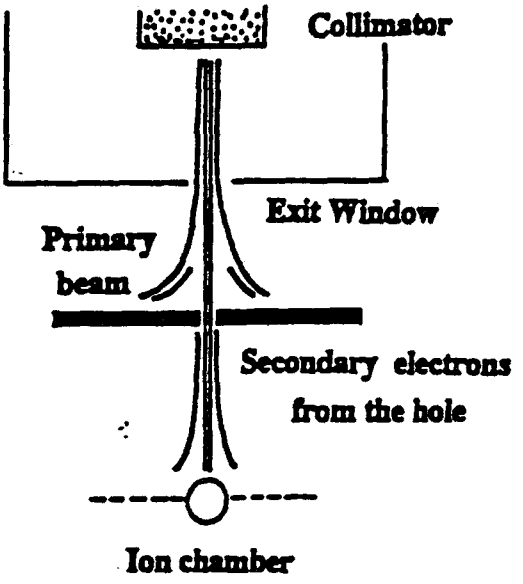

Figure 5.1. Experimental set-up for the measurement of the mass angular scattering power for the pencil electron beams obtained from a broad clinical electron beam [12] .

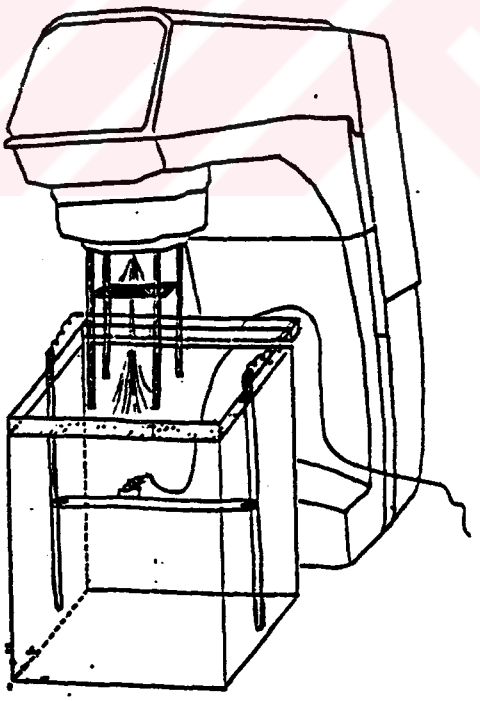

Figure 5.2. Illustration of the experiment for the mass angular scattering power method.

A pencil beam of a much smaller diameter than the broad electron beam, is produced by a square (20 cm x 20 cm) lead sheet with an aperture, in the intersection point of the diagonals of 2mm. diameter. In the output (exit window) of the linear accelerator, the electron beam, is a pencil beam of usually 2-3 mm diameter, however is broadened by two scattering foils therefore we use a lead sheet with a small aperture of 2mm. in order to get a pencil beam of electrons.

The X-ray collimator is opened to a field of 4 cm x 4 cm at the isocenter (the intersection of the axis of the gantry rotation and the axis of the collimator rotation) and a lead sheet with an aperture is placed to an SSD (distance from the target bar) of 65 cm. After the lead sheet, the electrons passing through the aperture produce a pencil beam which is scattered in the air. The ion chamber (IC 10 - 0.14 cc), the empty water phantom mechanism and the Wellhaufer dosimeter system is used to measure the amount of electrons scattered in the crossplane (which is the axis of the water tank perpendicular to the gun-target direction of the accelerator). The lead sheet is supported by a four leg apparatus installed in the accessory holder tray and between the legs were the foam blocks holding the square lead sheet without perturbating the pencil beam distribution.

The ion chamber is placed first to the central axis, which is also the center of the aperture light when the gantry is at zero degrees, at a distance of 100cm. SSD. Next, the ion chamber is placed to the build up point of the particular electron beam in water but again the measurement is in air. For both points, the ionization in the crossplane is measured by traveling the ion chamber in the given axis. The dosimeter system gives us a relative dose distribution curve. However, when we examine the relative dose distribution profiles, we see that the distribution is not Gaussian.

To understand this dose profile shape, four features of the production of the pencil beam should be noted:

a) Some electrons may be transmitted through the lead sheet,

b) Some electrons may be scattered in the pencil beam aperture,

A pencil beam of a much smaller diameter than the broad electron beam, is produced by a square (20 cm x 20 cm) lead sheet with an aperture, in the intersection point of the diagonals of 2mm. diameter. In the output (exit window) of the linear accelerator, the electron beam, is a pencil beam of usually 2-3 mm diameter, however is broadened by two scattering foils therefore we use a lead sheet with a small aperture of 2mm. in order to get a pencil beam of electrons.

The X-ray collimator is opened to a field of 4 cm x 4 cm at the isocenter (the intersection of the axis of the gantry rotation and the axis of the collimator rotation) and a lead sheet with an aperture is placed to an SSD (distance from the target bar) of 65 cm. After the lead sheet, the electrons passing through the aperture produce a pencil beam which is scattered in the air. The ion chamber (IC 10 - 0.14 cc), the empty water phantom mechanism and the Wellhaufer dosimeter system is used to measure the amount of electrons scattered in the crossplane (which is the axis of the water tank perpendicular to the gun-target direction of the accelerator). The lead sheet is supported by a four leg apparatus installed in the accessory holder tray and between the legs were the foam blocks holding the square lead sheet without perturbating the pencil beam distribution.

The ion chamber is placed first to the central axis, which is also the center of the aperture light when the gantry is at zero degrees, at a distance of 100cm. SSD. Next, the ion chamber is placed to the build up point of the particular electron beam in water but again the measurement is in air. For both points, the ionization in the crossplane is measured by traveling the ion chamber in the given axis. The dosimeter system gives us a relative dose distribution curve. However, when we examine the relative dose distribution profiles, we see that the distribution is not Gaussian.

To understand this dose profile shape, four features of the production of the pencil beam should be noted:

a) Some electrons may be transmitted through the lead sheet,

b) Some electrons may be scattered in the pencil beam aperture,

4) The Bremsstrahlung radiation produced in the lead sheet,

5) The inherent photon contamination of the broad electron beam [20].

Placing an identical lead plate without any hole on it may provide us the background radiation data. Subtracting the relative doses at each particular point, we can get a well Gaussian distribution of electrons generated from the pencil beam.

When the lead sheet with the pinhole is irradiated by a broad electron beam, primary electrons from the beam will be able to go through and form a narrow beam. For a depth X, less than the practical range of electron in the air $R_{p,a}$ and a distance r from the central axis; the absorbed dose can be divided into three components:

a) The dose coming from the pencil electron beam.

b) The primary electrons transmitted through the lead plate plus the secondary electrons produced within the lead plate.

c) The photons due to the Bremsstrahluhg radiation produced in the lead sheet plus the inherent photon contamination of the broad beam. With the pinhole, the dose at a point (X, r) is given by:

$$D_{ph}(X, r) = D_{apb}(X, r) + (1- R)\, D_{plate}(X, r) + D_{cont}(X, r) \qquad (5,1)$$

where D_{ph} is the absorbed dose in case of the pinhole, D_{apb} is the dose distribution of the approximate pencil beam formed, R is the ratio of the pinhole area to that of the irradiation field on the plate; (1-R) Dplate (X,r) thus represents the dose contribution Due to the amount of lead plate irradiated. D_{cont} (X,r) is the dose due to the beam contaminants made up of electrons scattered by the pinhole edges and Bremsstrahlung photons. If the lead sheet with no hole on it is replaced then the dose distribution at a point (X,r) is composed of both an electron component due to Bremsstrahlung generated within the plate and air. Hence, the dose at (X,r) with a plane lead plate is:

$$D_{nph}(X,r) = D_{plate}(X,r) + D_{cont}(X,r) \qquad (5,2)$$

If the two dose distributions, one with and one without the pinhole present are subtracted, then the resulting dose distribution is given by:

$$\begin{aligned}\Delta D(X,r) &= D_{ph}(X,r) - D_{nph}(X,r) \\ &= D_{apb}(X,r) - R\, D_{plate}(X,r) \\ &= D_{apb}(X,r) + \varepsilon(X,r) \qquad (5,3)\end{aligned}$$

where $\varepsilon(X,r)$ is an "error" term to be minimized in order to improve the measure of the approximate pencil beam dose distribution [21], [22].

The effects of the electron contaminants remaining may be reduced using a sufficiently thick plate, a small enough pinhole and by tapering the pinhole edge. There are other methods to form a narrow pinhole such as either collimating or magnetically focusing the incident broad beam. As it is generally impractical to magnetically focus the electron beam from a therapy accelerator to very small widths, the only alternative is to use a collimator. However, such a technique introduces scattered electrons and Bremsstrahlung photons into the beam and, hence, complicates the measurements. By replacing the lead sheet with aperture of the same thickness but without the aperture, the components of dose due to the transmitted electrons and Bremssstrahlung photons are obtained. Subtracting the relative doses at points of the same distances from the central axis of the beam, we can suppress the dose contributions from the electrons transmitted though the lead sheet, the Bremsstrahlung produced in the lead sheet and inherent photon contamination of the broad electron beam and isolate the pencil beam contribution as seen in Figure 5.3. The subtraction of two dose profiles gives us a well Gaussian distribution curve.

The variance of the Gaussian curve may be determined easily from the $1/\sqrt{e}$ times the peak amplitude of the curve. The distance of the point corresponding to the $1/\sqrt{e}$ of the

peak amplitude, gives us the variance σ of the Gaussian distribution. σ^2, the square of the spatial spread of the pencil electron beam, can be used to calculate T/ρ values and, hence, the kinetic energy of the electron beam.

The thickness of the lead sheet was increased to see how the dose distribution curves would be effected. 2mm, 4mm. and 6mm. thick lead plates were utilized for the measurements. The results for the kinetic energies were compared for different thickness of the lead plates.

In order to compare the obtained results for the kinetic energies of the electron beams, range method was also used to obtain energies. The mean energy and the most probable energy of the broad electron beam ,has been calculated in order to compare with the results obtained with the mass angular scattering power method.

The range measurements are based on the collisional and radiative energy loss of electrons and a well defined range of these electrons in the medium. While mass angular scattering power method measurements are based on the inelastic collisions and spatial spread in air.

In both the mass scattering power method in air and the range method in water, since we have to correct the ion chamber measurements and the density of the air, we have to know the pressure and the temperature of the air in the treatment room.

5.2. The Linear Accelerator : A General Overview

5.2.1. Introduction:

The use of natural radioactive sources in teletherapy is limited in that energies available for therapy are fixed by the characteristic decay scheme of the source. However, artificial sources of radiation provide variable energies allowing the therapist a choice of energy to suit the treatment. The linear accelerator, is the most widely used machine for radiotherapy.

Essentially, there are two functions of a teletherapy unit.

i) The beam generating device must produce a beam with well-defined dosimetric and geometric properties.

ii) The beam adjusting devices and patient's couch must ensure that the beam intersects the target volume.

Constraints to these two functions are patient safety and the reliability of the equipment. The choice of an accelerator over other instrumentation is governed by two basic consideration.

a) For therapy, aside from skin cancers, only radiations of a quality with sufficient penetration to reach deep seated tumours are viable. For most tumours, a 50% dose at 10cm is a minimum requirement.

b) It is essential that clinical equipment be flexible and reliable in operation.

These two criteria are somewhat contradictory. The first consideration leads to sophisticated accelerators with high power, high energy outputs which are complex to build and operate. The second condition, explains why there is such a long time lap between the initial design of the machine and its utilization in clinical work.

The high energy electron (4.5 to 25 MeV) are produced in betatrons or the linear accelerators. Usually, the linear accelerators is more universal and convinient for clinical use. The electron linear accelerator is a machine in which a high-frequency, high-power microwave is employed to accelerate electrons traveling in a straight line to high energies. These electrons can either be used directly for electron irradiation or stopped in a target where, when slowed down, they produce a strong-energy X-ray, which is used for photon irradiation [5], [23].

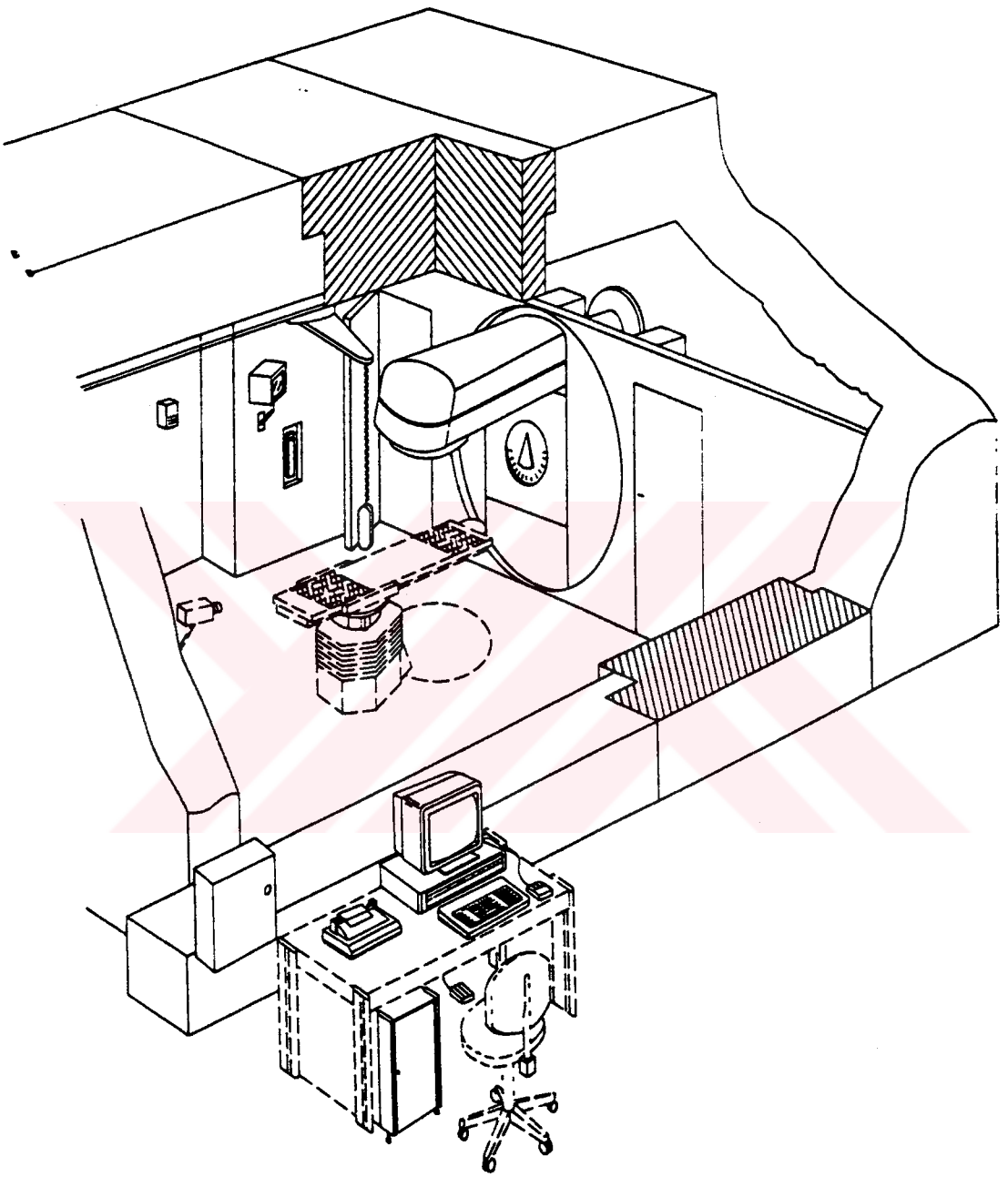

Figure 5.4. A typical linear accelerator room [23].

5.2.2. Principle of the Accelerator Electron Beam Production

An accelerator is made up of a gun, which produces electrons, followed by an accelerating waveguide means to accelerate the electrons emitted by the gun.

The heart of the accelerator is the wave guide, which acts as a conductor of microwaves and is where the actual acceleration takes place. The energy required by a microwave (RF) power source. This power is delivered to the waveguide in the form of short duration pulses of microwaves which travel close to the speed of light along the accelerating structure. Attached to the front end of the waveguide is an electron gun which provides electrons and injects then simultaneously with the pulses of radio frequency wave and are accelerated by it, achieving a velocity almost equal to the velocity of light. Having passed through the waveguide the electrons enter a bending chamber surrounded by a strong magnet where the electron beam is bent towards the isocenter of the machine to make patient irradiation conditions easier.

The process of the acceleration of electrons to high energy takes place in three stages. The first stage of acceleration occurs when the gun injects electrons with a certain initial velocity into the waveguide. The gun is made up of a cathode which is heated, and brought to a negative potential in regard to an anode which is set to ground potential. The cathode emits electrons through a thermoionic effect; the potential difference extracts these electrons and supplies them with an energy of approximately 50keV. An electron at a modest energy of 50keV when injected into the waveguide has a velocity of 0.41 of the velocity of light c. The next stage takes place in the bunching section of the waveguide and is characterized by a steady increase of electron velocity, accompanied by a continous energy gain. The electrons quickly reach a velocity which is very close to the velocity of light c and this marks the start of the last stage, during which the electrons gain energy relativistically. The buncher is the part of the section, which is about 20cm. long and is made up of cavities of increasing thickness. Cavities of equal thickness make up the rest of the accelerating waveguide.

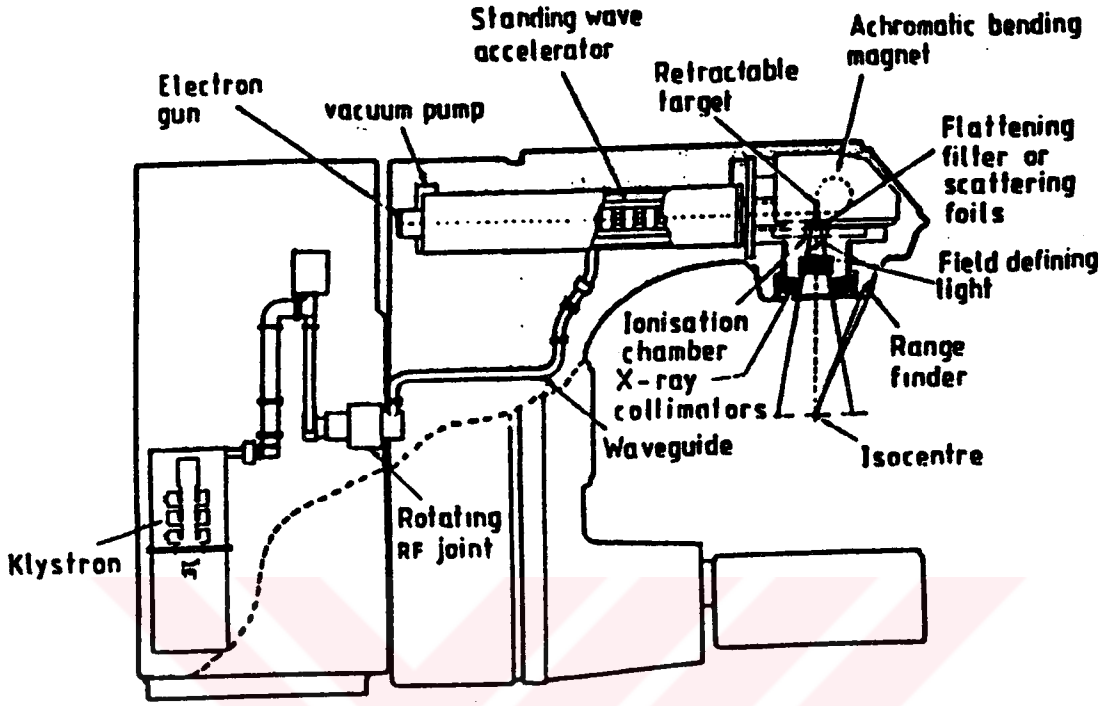

Figure 5.5. Major accelerator subsystems [7].

1 MeV and 5 MeV electrons have velocities of 0.94 c and 0.996 c respectively. Note that the relative velocity changed only about 6% in this example, while the kinetic energy has changed by a factor of 5. It is seen that, when the second stage of acceleration is reached, the electron velocity remains almost constant. The progressive energy gain must therefore be thought of as an increase of electron mass.

The relativistic mass gain is given by:

$$\frac{m}{m_0} = \left(1-\beta^2\right)^{-1/2} \tag{5,4}$$

where β is the ratio of the velocity of the electron the velocity of light c, m_o is the rest mass of the electron and m is the mass of the particle at velocity βc.

The result of the gain in the electron mass ,is a gain in the electron kinetic energy, since mass and energy are interchangeable in a relativistic sense. The kinetic energy E_k which the electron gains is proportional to the difference between the relativistic and rest masses (m-mo) as is incident from the equation:

$$E_k = eV = (m-mo)c^2 \qquad (5,5)$$

The total energy being equal to $E=E_k+moc^2$. The energy of a particle is defined by the product of the electronic charge e and the accelerating potential V and expressed in MeV.

The energy acquired by the electrons at the end of the accelerating waveguide depends on a number of parameters such as the electric field value, the phase and frequency [3], [4], [7], [23].

5.2.3. Pulse Characterizing Emitted Radiation

There are several types of linear accelerator designs, but the ones used in radiotherapy accelerate electrons either by traveling or stationary electromagnetic waves of frequency in the microwave region (~ 3000 megacycles / sec)

The difference between traveling wave and stationary wave accelerators is the design of the accelerator structure. Functionally, the traveling structure requires a terminating load in order to absorb the residual power at the end of the structure, thus preventing a backward reflected wave. On the other hand, the standing wave structures provide maximum reflection of the waves at both ends of the structure so that the combination of forward and reverse traveling waves will give rise to stationary waves. The average electric field needed for the acceleration ranges from 10 to 20 megavolts per meter in order for a 20 MeV energy to be communicated in less than 2 meters. An RF wave power of several megawatts is needed to generate such a field; therefore, it can be a

continous wave. The electromagnetic wave is then pulsed in 5μs pulses, with a repetition frequency of 50, 100, 150, 200 and 300 Hz according to the flow rate and the energy of the wanted beam. Consequently, the emitted radiation is pulsed. Moreover, the electrical field inside the cavities oscillates with the 3 Ghz wave frequency. Only one polarity allows the acceleration to take place; the emitted radiation is therefore pulsed twice as much; inside each pulse electrons are gathered in bunches following eachother at intervals of 0.33 nanosecond.

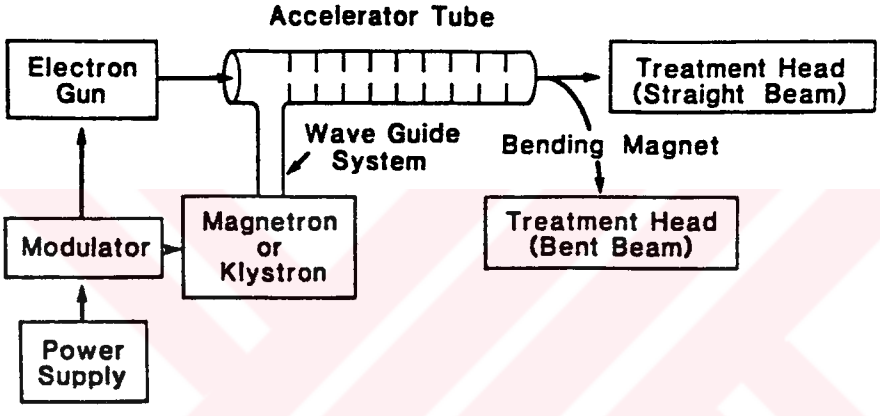

Figure 5.6. A block diagram of typical medical linear accelerator [3] .

Figure 5.2. is a block diagram of a medical linear accelerator showing major components and auxiliary systems. A power supply provides DC power to the modulator, which includes the pulse - forming network and a switch tube known as hydrogen thayratron. High voltage pulses from the modulator section are flat-topped DC pulses of a few microseconds in duration. These pulses are delivered to the magnetron or klystron and simultaneously to the electron gun. Pulsed microwaves produced in the magnetron or klystron are injected into the accelerator tube or structure via a waveguide system. At the proper instant electrons, produced by the electron gun are injected into the accelerator structure [3], [7], [24].

5.2.4. Method Used To Obtain The Various Energies

An accelerator supplied by an RF power Po, can be considered as a generator with an internal impedance R. For an accelerated current I, the acquired energy U is given by the relation (called load line):

$$U = Uo - RI \tag{5,6}$$

in which Uo ; no load condition energy is linked to

$$Uo = k\sqrt{Po} \tag{5,7}$$

As Po varies, the load line can be modified as in Figure 5.3. The maximum current which can be accelerated corresponds to a certain P power consumption rate.

Because a range between 4.5 to 16 MeV is to be covered, the RF power must vary within a ratio equal to

$$\frac{P_0}{P_1} = \left(\frac{16}{4.5}\right)^2 = 12.6 \tag{5,8}$$

This value is much too high, since the buncher does not tolerate such a variation. In practice, a very quick decrease of the accelerated maximum current with the power is noticed. In response to this problem, the energy is obtained by varying the RF frequency:

- If this frequency corresponds to the resonance frequency of the waveguide then, the intensity of the electrical field generated in the cavities is high and the energy transmitted to the electron bunches is maximal,
- If this frequency is shifted in relation to the resonance frequency of the waveguide, the intensity of the electrical field in the cavities is lower and the electron bunches are

slowed. To obtain the required value, the beam energy should be adjusted by slowly modifying the RF power [24].

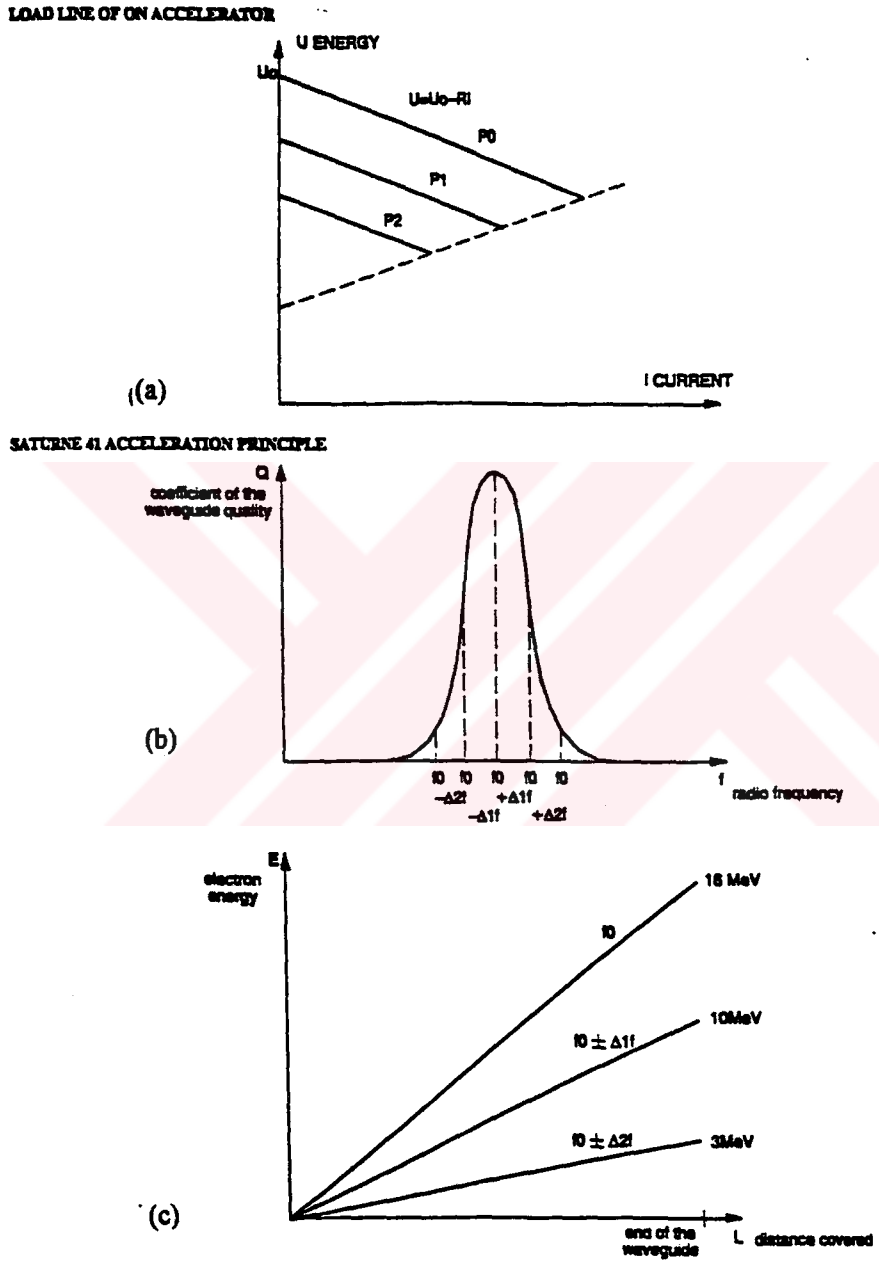

Figure 5.7. (a)Load line of an accelerator. (b), (c)Saturne 41 Acceleration principle [23].

5.2.5. The Output Components of a Linac

As the high-energy electrons emerge from the exit window of the accelerator structure, they are in the form of a pencil beam of about 3mm. in diameter. In most linacs, the accelerator structure is too long and therefore is placed horizontally or at an angle to the horizontal. The electrons are then bent through a suitable angle (usually 90° or 270°) between the accelerator structure and the target. The precision bending of the electron beam is accomplished by the beam transport system consisting of bending magnets, focussing coils and other components. The beam path, from the gun to the exit window from the bending assembly, is performed in a vacuum to avoid unwanted interaction between the electrons and the material, and maintain the electrical field. Vacuum is maintained by an ion pump. In the electron mode of operation, the electron beam, instead of striking a target, is made to strike an electron scattering foil in order to spread the beam as well as get a uniform electron fluence across the treatment field. The scattering foil consists of a thin metallic foil, usually of lead. The thickness of the foil is such that most of the electrons are scattered instead of suffering Bremsstrahlung. However, a small fraction of the total energy is still converted into Bremsstrahlung and appears as X-ray contamination of the electron beam [3], [7].

The treatment head consists of a thick shell of high density shielding material such as lead, tungsten or lead-tungsten alloy. It contains an X-ray target, scattering foil, flattering filter, ion chamber, fixed and movable collimator, and light localizer system. The head provides sufficient shielding against leakage radiation in accordance with radiation protection guidelines [25].

The treatment beam is first collimated by a fixed primary collimator located immediately beyond the X-ray target. In the case of X-ray beam or the electron beam is incident on the dose monitoring chambers. The monitoring system consists of several ion chambers or a single chamber with multiple plates.

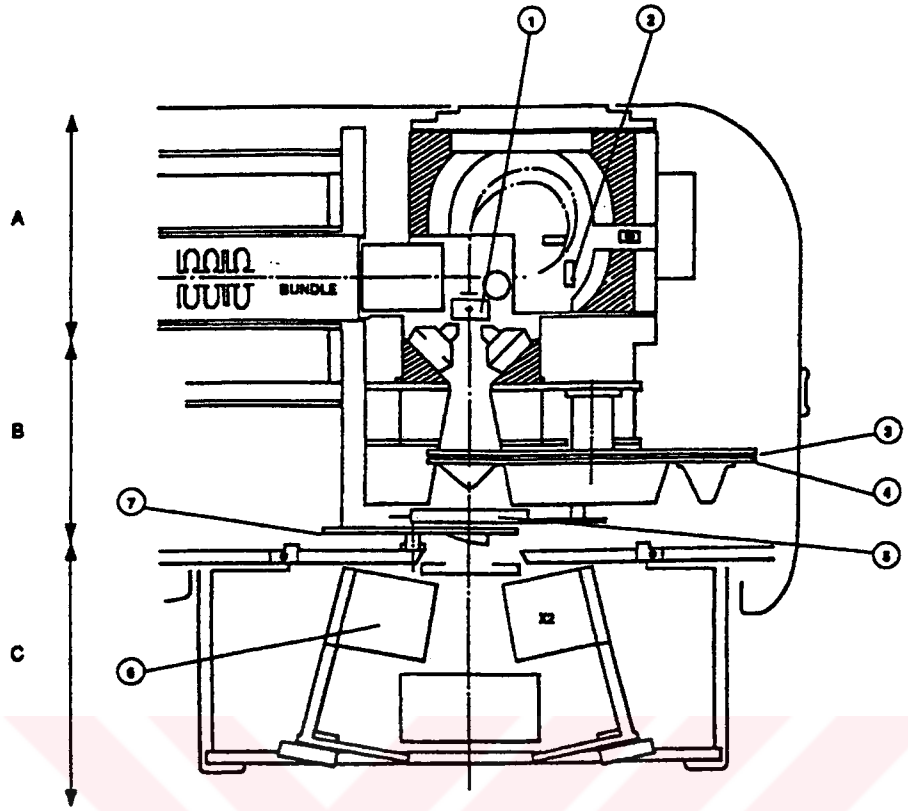

Figure 5.8. The treatment head of an accelerator [25].

The function of the ion chamber in a linac, is to monitor dose rate, integrated dose, and field symmetry. After passing through the ion chambers, the beam is further collimated by a continously movable X-ray collimator. This collimator consists of two pairs of lead and tungsten blocks (jaws) which provide a rectangular opening from 0x0 to maximum field size (40cm x 40cm or a little less/projected at a standart distance such as 100cm from X-ray source.

Whereas the X-ray collimation systems of most medical linacs are similar, the electron collimation systems vary widely. Since electrons scatter readily in air, the beam collimation must be achieved close to the skin surface of the patient. There is a considerable scattering of electrons from the collimator surfaces including the moveable

jaws. Dose rate can change by a factor of two or three as the collimator jaws are opened to maximum field size limits. If the electrons are collimated by the same jaws, as for X-rays, there will be an extremely stringent requirement on the accuracy of the jaw opening, since output so critically depends on the surface area of the collimator. This problem has been solved by keeping the X-ray collimator wide open and attaching an auxiliary collimator for electrons in the form of trimmers extended down to the skin surface. It should be noted that due to the electron scattering, the dose distribution the collimation system provided by the machine. Most of the linear accelerators currently produced are constructed so that the source of radiation can rotate about a horizontal axis. As the gantry rotates, the collimator axis (supposedly coincident with the central axis of the beam) moves in a vertical plane. The point of the intersection of the collimator axis and the axis of rotation of the gantry is known as the isocenter [3], [4].

5.2.6. The Energy Characteristic of Saturne 41 Linear Acceleration

The experiments and measurements in this study was done with a Saturne 41-linear accelerator, based in Kartal Devlet Hastanesi, Radiation Oncology Center. Saturne 41 is produced by General Electric Medical Systems Company. The RF wave is generated by a magnetron. The machine uses standing wave .

The high voltage needed for the magnetron to operate is generated by the modulator assembly (HV cabinet and magnetron panel) The high voltage generated by the modulator assembly is also used at the electron gun level as a cathode-anode extraction voltage. Further information is given in the data sheets in APPENDIX A[23].

5.2.7. Measurement method of Electron Intensity in The Mass Angular Scattering Method:

In order to measure the relative amount of scattered electrons in air in the crossplane of each distance from the central axis, an ion chamber IC 10 is used. The same ion chamber was used in measuring the depth doses of the electron beams in water.

IC 10 is a gas filled thimble chamber with a chamber volume of 0.14 cc. When the electrons enter the chamber volume, positive and negative ions are produced as ion pairs. The chamber has two electrodes: The central electrode with a positive voltage and the negative electrode as the inner surface of the thimble wall coated by a special material to make it electrically conducting. A DC voltage is applied between the two electrodes which can vary according to the type of radiation measured. In all the measurements in this work, a polarisation voltage of 400 V is used. When the polarisation voltage is applied, the negative ions produced during the irradiation, travel to the positive electrode and the positive electrons travel to the negative electrode. The higher the polarisation voltage is, the faster the ions move to the electrodes. The current of moving ions, the ionization current, indicates the ionization rate in the ionization chamber[26].

In order for the thimble chamber to be air equivalent, the effective atomic number of the wall material and the central electrode must be such that the system as a whole behaves like a free air chamber, the chamber wall of IC-10 is made up of graphite.

IC-10 is waterproof and is suitable for using in water and solid phantoms. It is also ventilated therefore one has to correct the measurements according to the air pressure and temperature of air in the treatment room.

The ionization chamber, among the other radiation measuring systems, is specially suited for accurate measurements of high radiation fields such as clinical therapy electrons and photon beams. The amount of current produced in an ion chamber is directly related to the energy deposited in the chamber and is reasonably independent of the HVL of the beam. Ionization chambers are also used as calibration instruments in

order to accurately measure the ionization due to the high energy electron and photon beams. In the experiments of this thesis, the measurements were relative hence we did not need to use the calibration values.

The electrometer to which the ion chamber was connected was WP 5007. The electrometer supplies the high voltage for the ion chamber and processes the signals coming from the ion chamber. The system has the options of measuring the integrated dose and the ionization current. The ion chamber and the electrometer is calibrated together so that the reading is converted into exposure [26].

The water phantom is a container for water and the driving mechanism of the radiation detector. The holding box for the ion chamber is driven by small DC motors and plastic belts controlled by the computer.

For the "in water" measurements, the tank is filled tap city water. The table which is holding the tank, is raised to a height where the isocenter is high enough to get the depth that one wants to measure. In order for the beam to come diagonally to the water surface, the tank is levelled by a three point levelling system. The tank has a cross target at the bottom and two strings at the top passing from the mid-points of the sides of the tank. For a diagonally incoming beam, the crosshair of the linac, the strings at the top of the tank and the target at the bottom of the tank should line up [26].

By the manual control, we take the ion chamber to the water surface while the chamber is half in the water. We define this level as the water surface level. Next, we place the ion chamber to the central axis on the surface of the water so that the active point of the ion chamber is where the crosshairs intersect. We define this point as the central axis. After that we do not touch the water phantom and the make the measurements.

For the in air measurements, we use the same phantom without water. We use the defined central axis. We get measurements at two depths, one with air thickness of 35 cm and another distance varying with energy where we can receive dose data for dose profiles.

VI. RESULTS

The kinetic energies of the nominal energies 12, 13.5 and 16 MeV electrons were measured using both the mass angular scattering method and the range method. In the range method, the most probable energy E_p was calculated using equation 3.2 with the measured R_p and the mean energy E_0 was calculated using equation 3.3 with the measured R_{50}.

In the scattering method, the variances of the Gaussian curves give us T/ρ values by the equation 3.9. The relative dose profiles of the pencil electron beams, from the theory of multiple scattering, have the shape of Gaussian curves.

The experimental setting was changed with the parameters such as the thickness of the lead sheet and the distance between the lead sheet and the measurement axis X. Although we used a very small ion chamber, we observed that the sensitivity of the ion chamber-electrometer system was not enough to measure the dose distribution after some distance from the lead sheet. However, it is not also very convinient to measure the dose distribution at very near distances from the lead sheet, since the spatial spread due to the multiple scattering is more pronounced at larger distances and the low energy scattering of electrons at the edge of the aperture is effective at near distances. Therefore, we chose a distance X of 35 cm.and one bigger distance varying for each energy.

The dose profiles obtained with the lead sheet with aperture and those obtained with the lead sheet without an aperture and the subtraction results of these two are given in the following pages from Figure 6.2 to Figure 6.19. In these figures, the profile with the biggest peak is the one obtained with a lead sheet with an aperture, the middle one is the profile obtained with a lead sheet without an aperture and the lowest one is the difference of these two curves. We find the mass angular scattering power and hence the energy by calculating the variance of the difference curve.

We measured the energy of each beam in two different distances and with three different lead sheet thicknesses. The Wellhaufer 600 dosimeter system gives the dose

distributions in an analog curve.We measured the dose corresponding to each one millimeter of distance from +4.5 to -4.5 cm. therefore we digitize the curve into 90 channels. By subtracting the dose amount at each one millimeter of the dose profile with the open collimator from that with the closed collimator, we get a well Gaussian distribution .

Since the experimentally measured dose data contain experimental noise and errors, the following approach is used in estimating σ.The general expression for a Gaussian function has the form,

$$d(y) = d(0).\exp\left(-\frac{y^2}{2\sigma^2}\right) \tag{5,8}$$

symmetrical with respect to y=0,

This can also be expressed as:

$$\ln\frac{d(0)}{d(y)} = \frac{y^2}{2\sigma^2} \tag{5,9}$$

If we call d(y) as the amount of measured dose at a particular distance y from the central axis , by plotting $\ln\frac{d(0)}{d(y)}$ against $y^2/2\sigma^2$ and linearly fitting the measured dose data; the slope of the fitted line namely $1/2\sigma^2$ can be used to estimate the value of σ, as seen in Figure 6.1.

The discrepancy from the linearity at large distances from the central axis of the beam is attributed to the large angle single scattering which is omitted in the Fermi-Eyges theory but plays an increasing role with increasing distances from the central beam

axis.Therefore, the linear portion of the graph $y^2/2\sigma^2$ versus $y^2/2\sigma^2$ is used to calculate the value of σ.

Next, we calculate the T/ρ values from the variances of the Gaussian curves by means of Equation 3.9. Each of these values correspond to one particular electron energy in air which is determined from the log-log graph of T/ρ versus kinetic energy values.

It is seen that T/ρ values obtained with different thicknesses of the lead sheets are close to each other for each energy. However, the dose signal is weaker and with more peaks as the thickness is increased for the plane lead sheet. This is because the radiation is significantly absorbed with increasing thickness. With a 6 mm thick lead plate, the primary electrons are nearly stopped for 12, 13.5 and 16 Mev electron energies however the background dose is mainly due to the photon contamination and the secondary electrons. With a 2mm thick lead plate, the primary electrons passing through the lead sheet are added to the dose distribution more effectively .

A comparison of measurement results obtained from the mass scattering power method and the conventional R_p and R_{50} methods is shown in Table 1.This comparison clearly demonstrates that results in all three methods are in good agreement.

NOMINAL ENERGY		SCATTERING METHOD							R-50 METHOD			RP METHOD	
		2 mm Pb		4 mm Pb		6 mm Pb		AVERAGE	R50	EK		RP	EK
		x=35 cm	x=35+dma	x=35 cm	35+dmax	x=35	x=35+dmax						
12 MeV		11.5	11.7	12	11.9	10.5	11.5	11.52	4.52	10.53		5.59	11.99
13.5 MeV		13	13	12.5	12.5	12.5	12.7	12.7	5.2	12.12		6.32	13.05
16 MeV		14.25	15.25	13.5	15	13	14.8	14.3	6.02	14.79		7.29	14.45

TABLE 1: COMPARISON OF THE RESULTS FROM THREE KINETIC ENERGY METHODS.

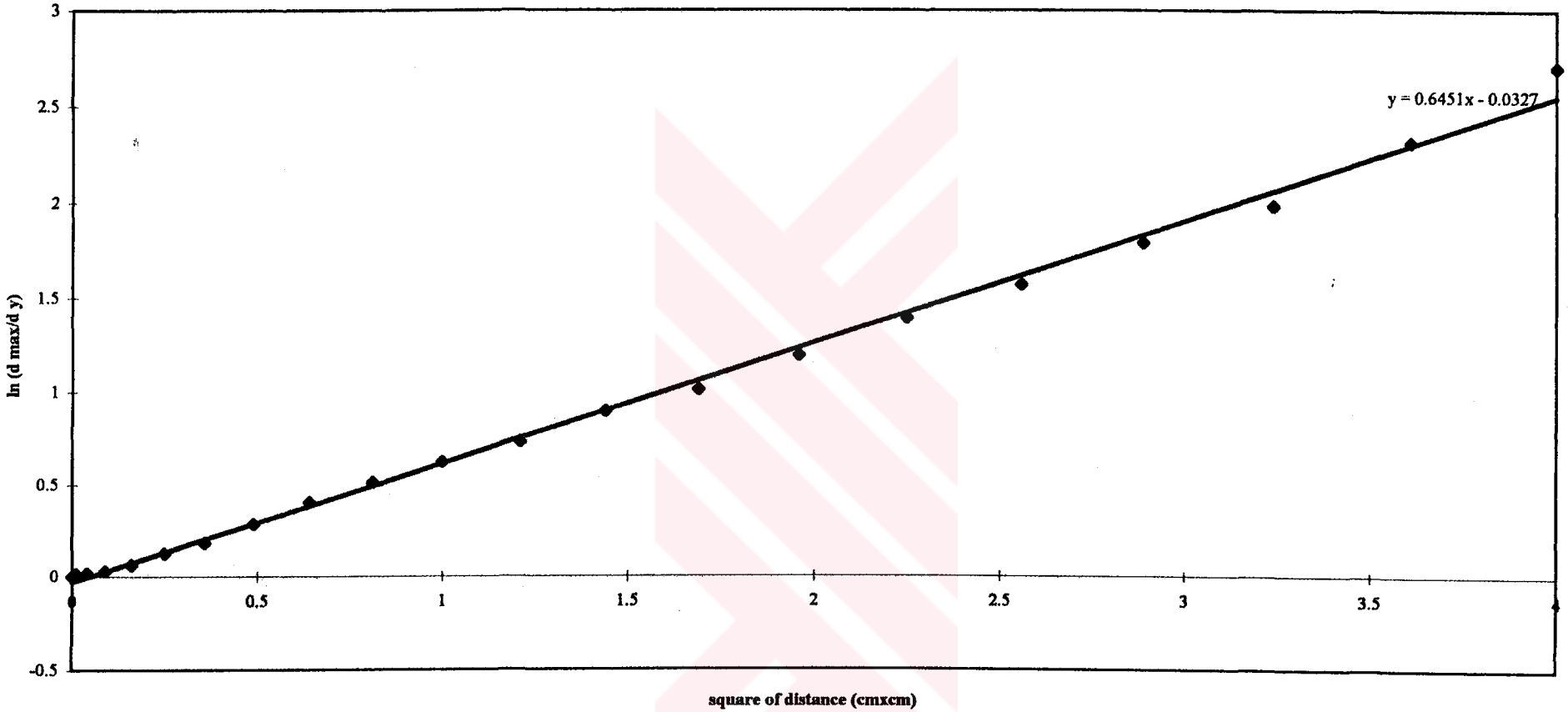

Figure 6.1. The dose profile data of the pencil beam for 13.5 MeV electrons measured at a distance of x= 35 cm. by using a 6 mm. lead sheet is observed as ln (d max / d y) versus square of the distance from the central beam axis.Note that the dose values at large distances are not used for finding the variance since Fermi-Eyges theory fails in large distances because of the not accounted single scattering events.

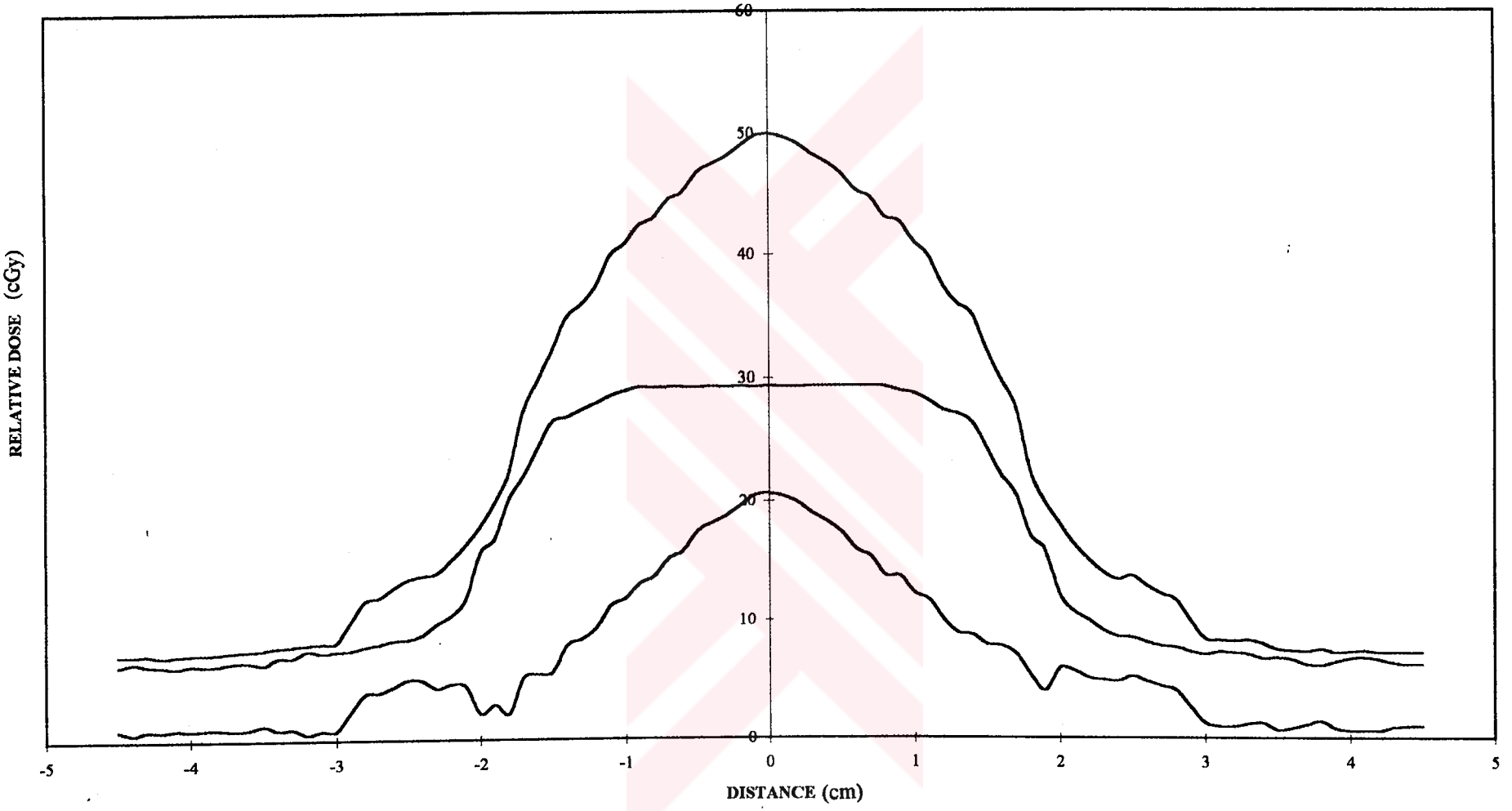

Figure 6.2 Electron Dose Profile for E=12 MeV, x=35+0 cm and lead sheet thickness=2 mm.

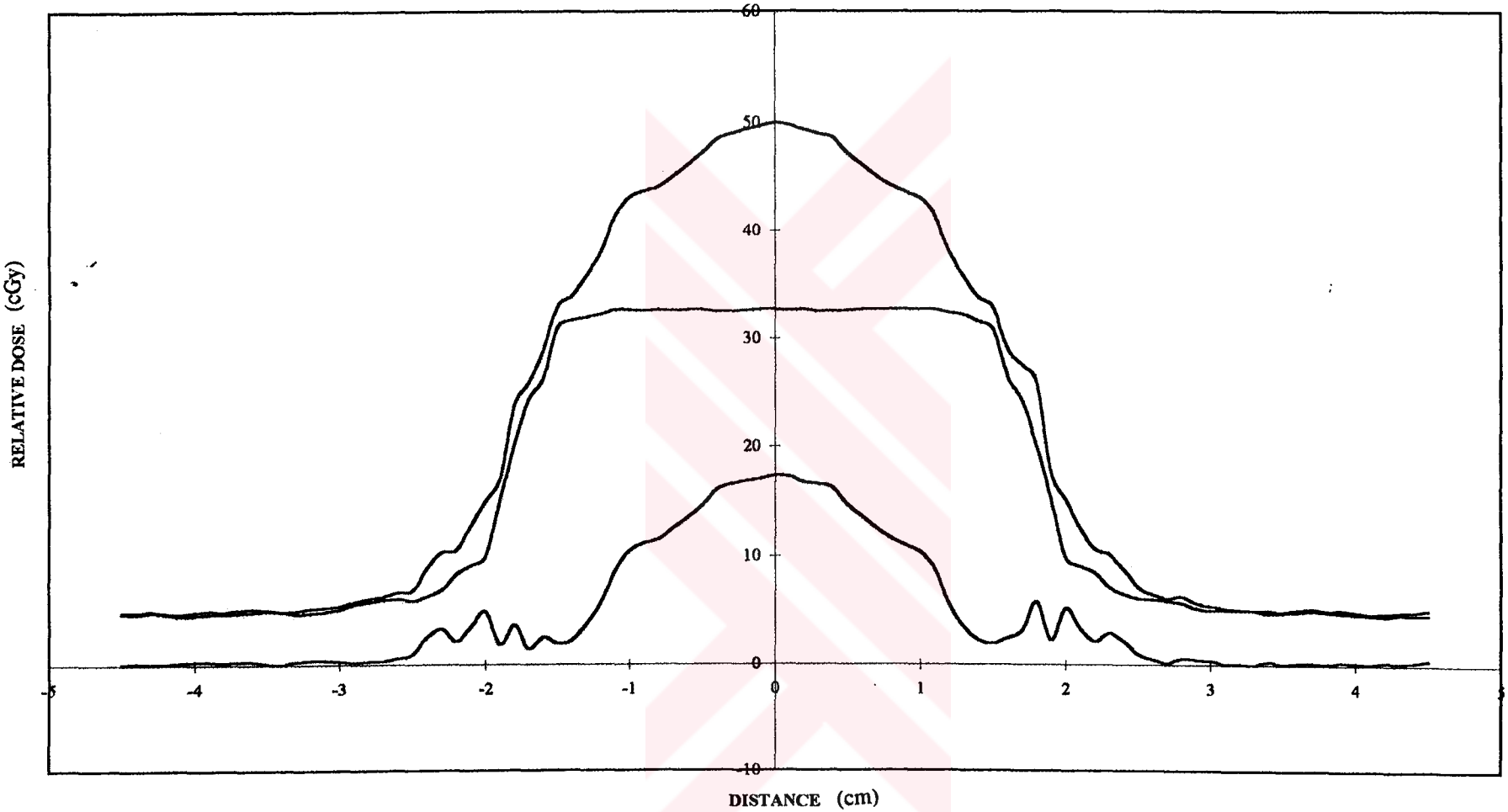

Figure 6.3. Electron Dose Profile for E=12 MeV, x=35+2.32 cm and lead sheet thickness=2 mm.

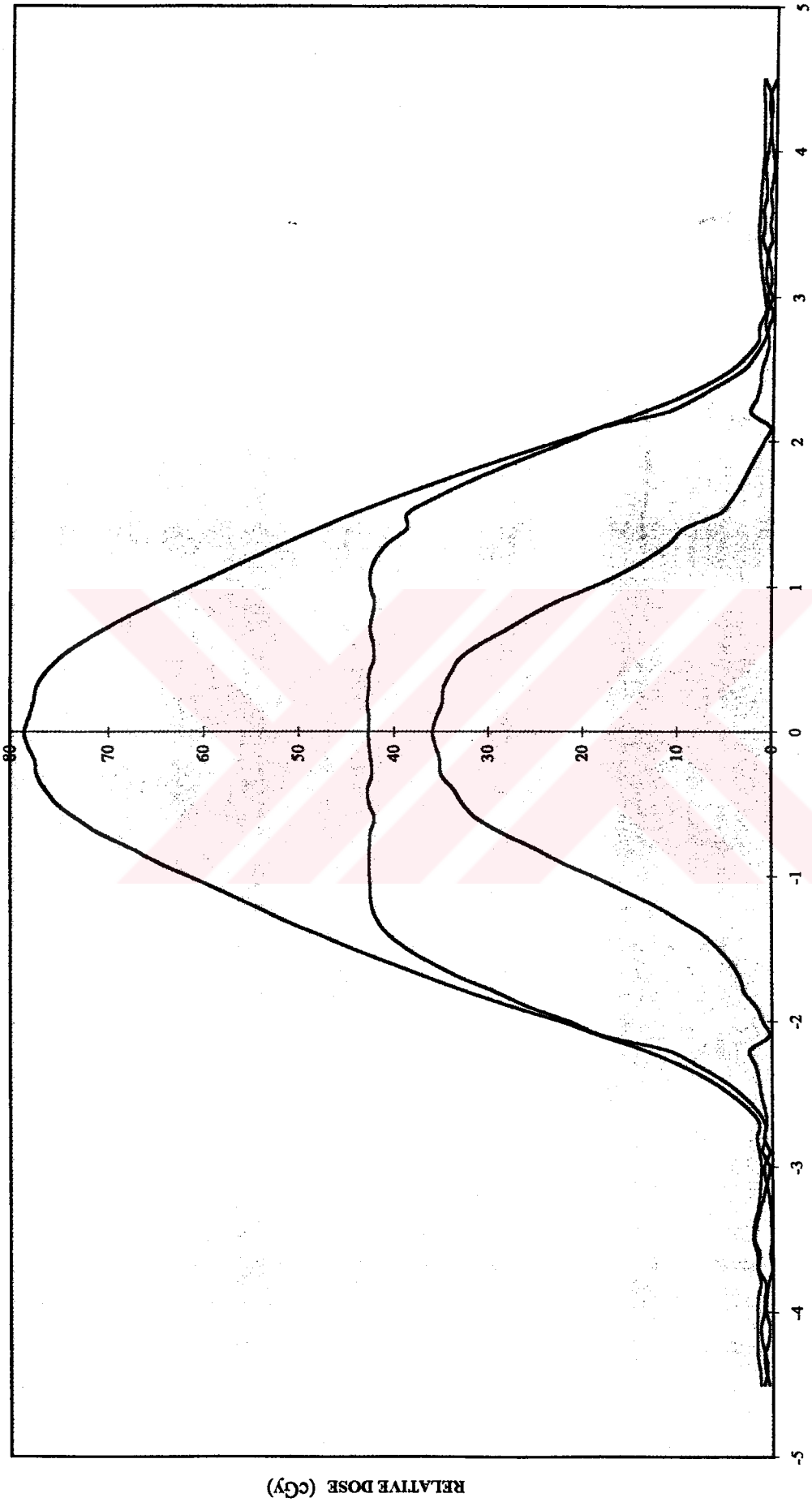

Figure 6.4. Electron Dose Profile for E=12 MeV, x=35+0 cm and lead sheet thickness=4 mm.

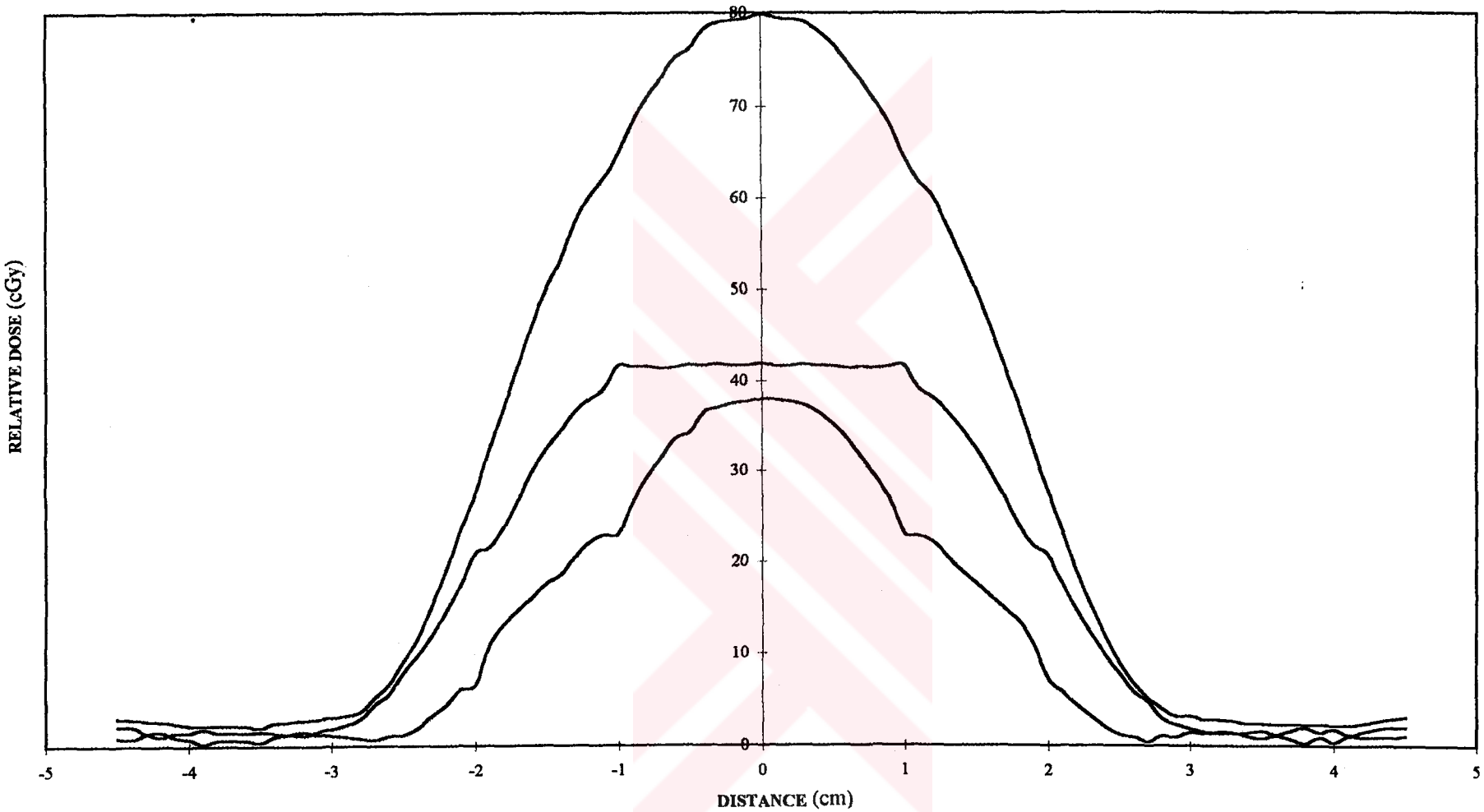

Figure 6.5. Electron Dose Profile for E=12 MeV, x=35+2.36 cm and lead sheet thickness=4 mm.

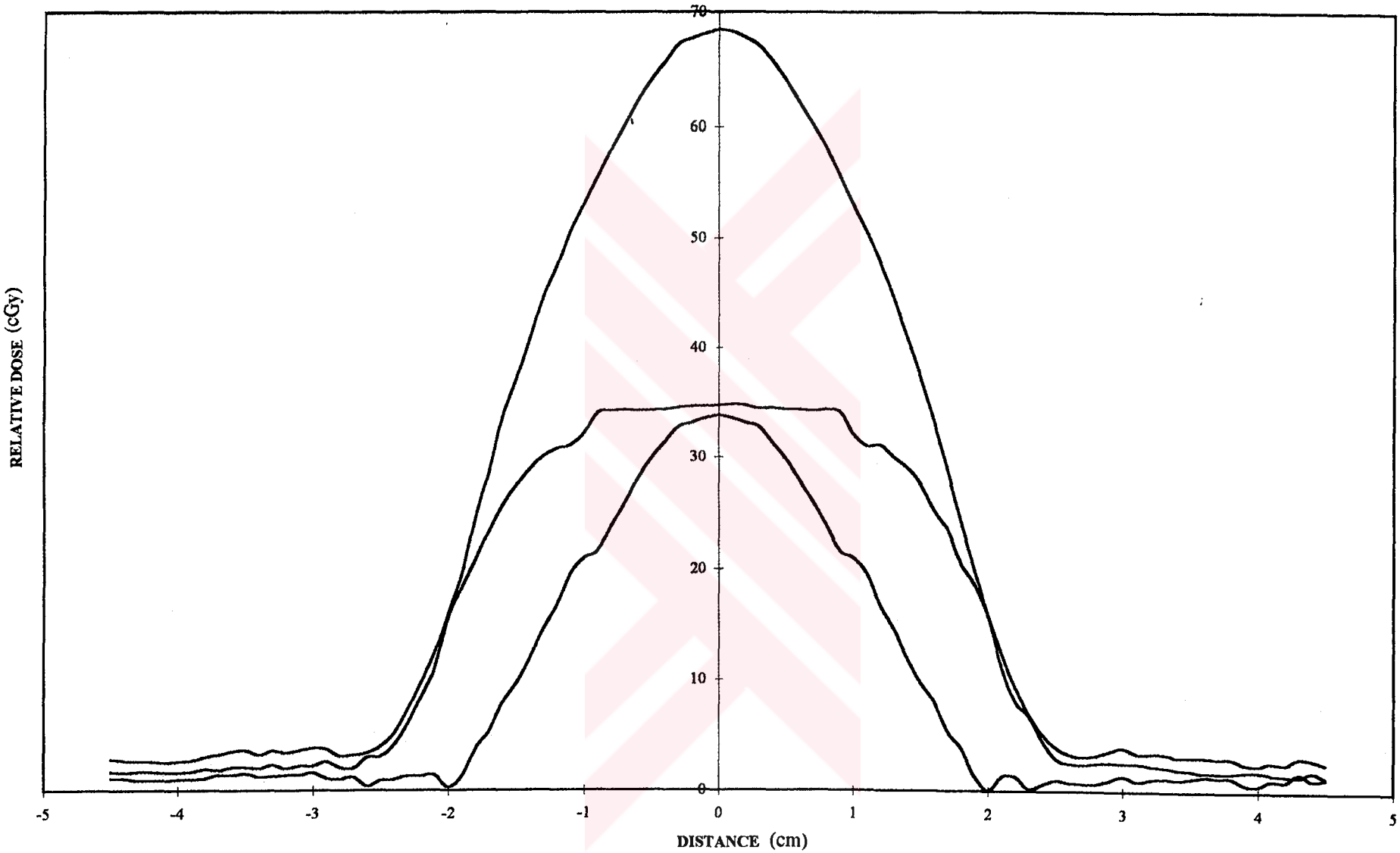

Figure 6.6 Electron Dose Profile for E=12 MeV, x=35+0 cm and lead sheet thickness=6 mm.

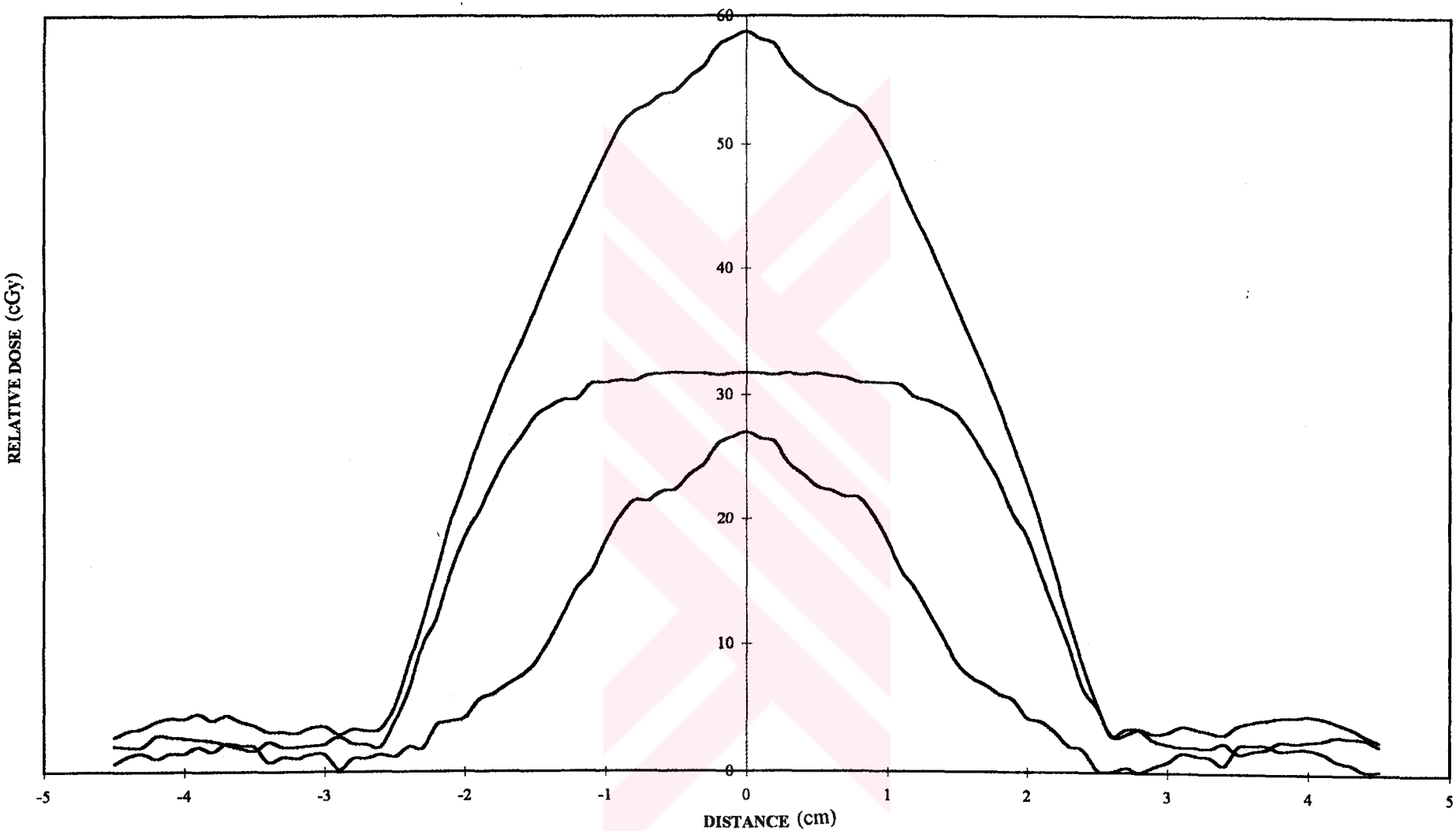

Figure 6.7. Electron Dose Profile for E=12 MeV, x=35+2.39 cm and lead sheet thickness=6 mm.

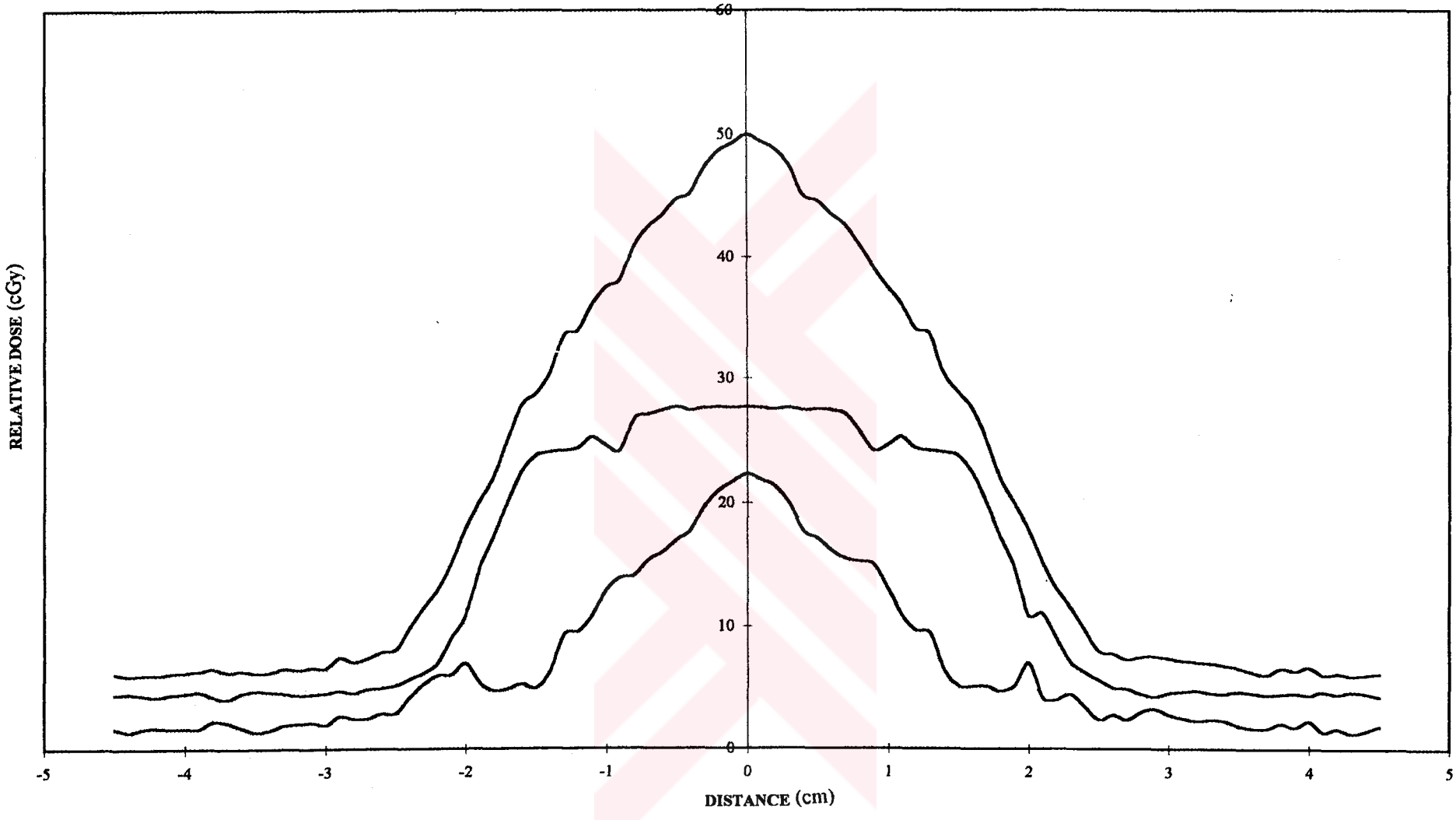

Figure 6.8. Electron Dose Profile for E=13.5 MeV, x=35+0 cm and lead sheet thickness=2 mm.

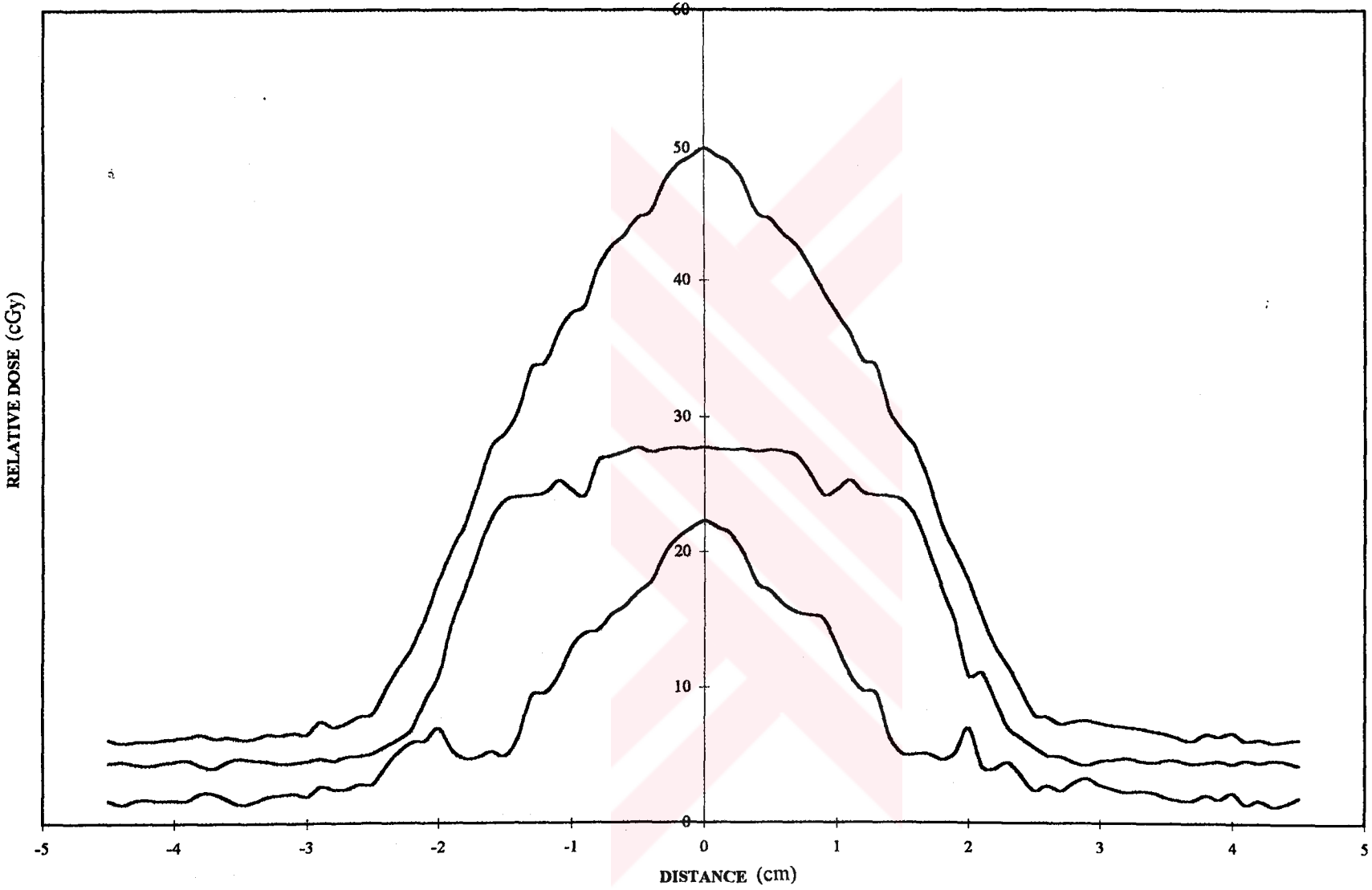

Figure 6.9. Electron Dose Profile for E=13.5 MeV, x=35+2.65 cm and lead sheet thickness=2 mm.

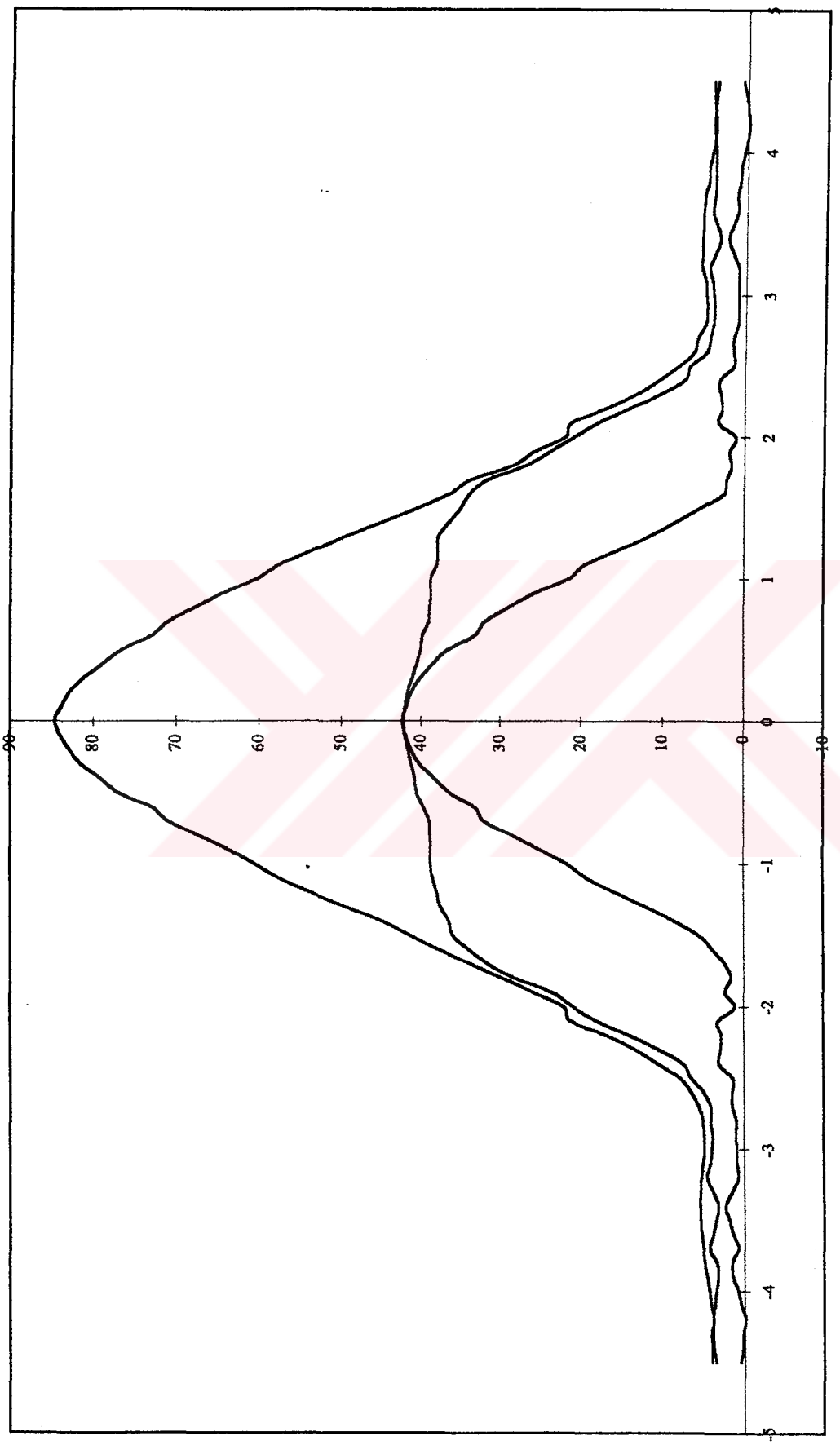

Figure 6.10. Electron Dose Profile for E=13.5 MeV, x=35+0 cm and lead sheet thickness=4 mm.

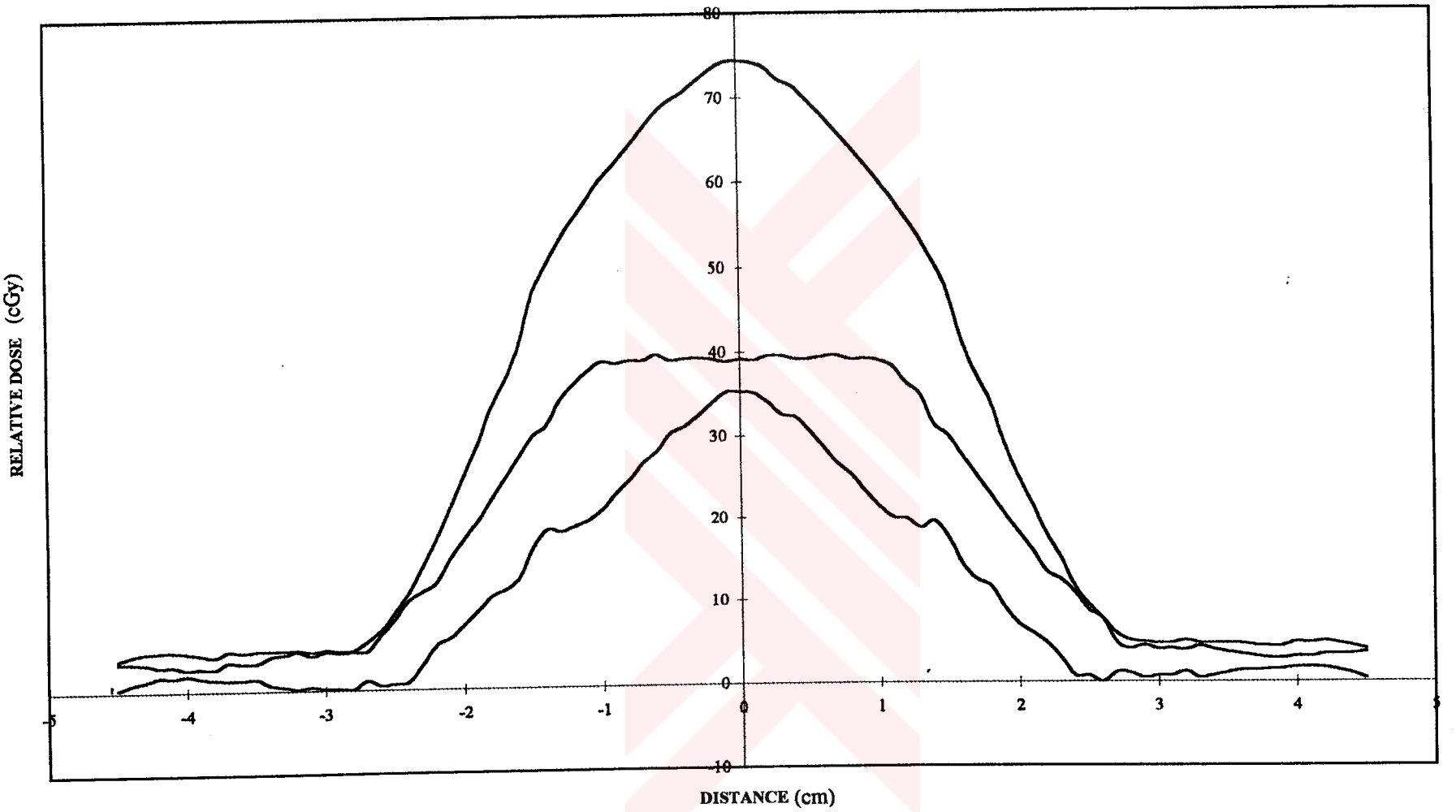

Figure 6.11. Electron Dose Profile for E=13.5 MeV, x=35+2.65 cm and lead sheet thickness=4 mm.

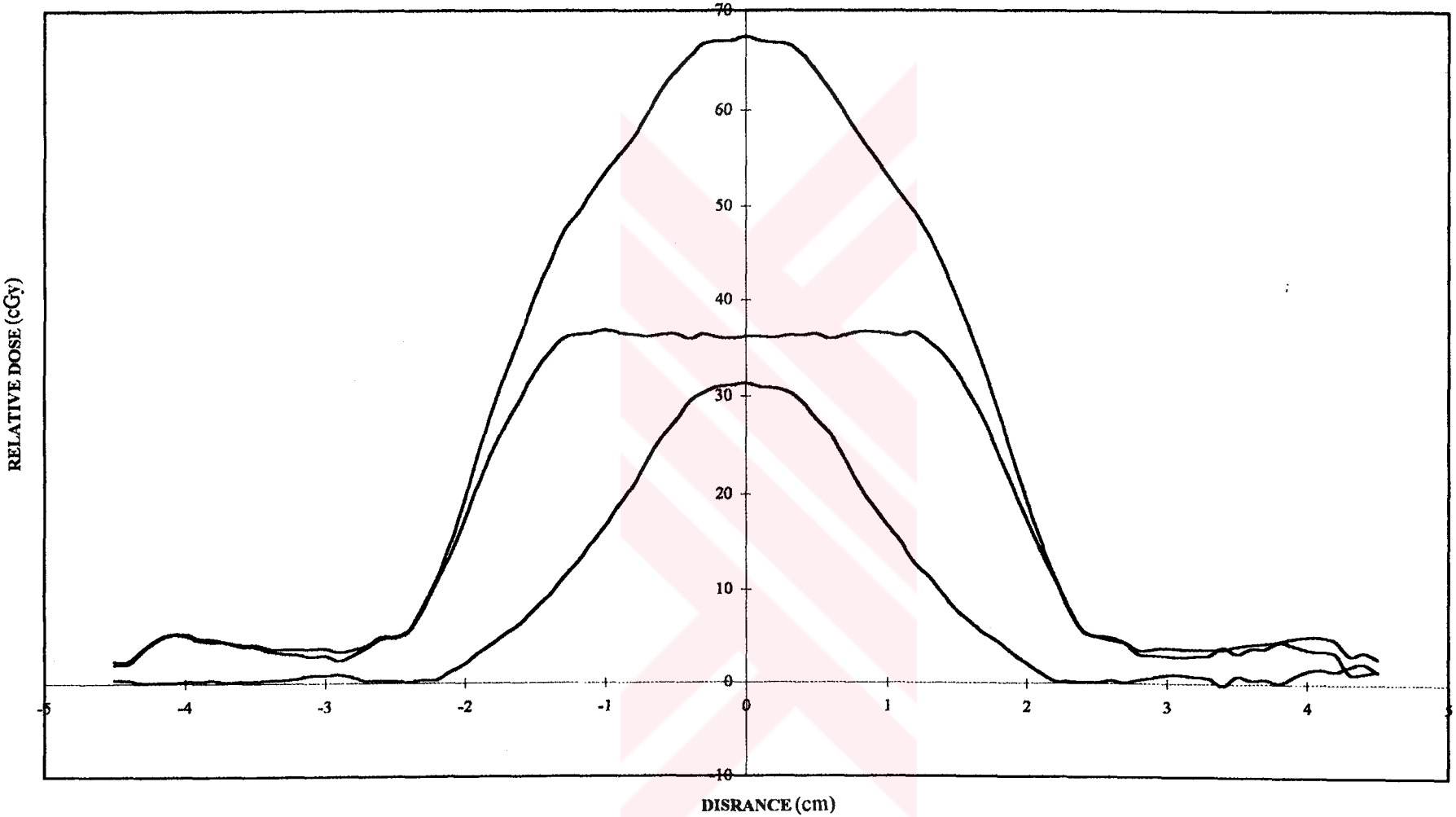

Figure 6.12. Electron Dose Profile for E=13.5 MeV, x=35+0 cm and lead sheet thickness=6 mm.

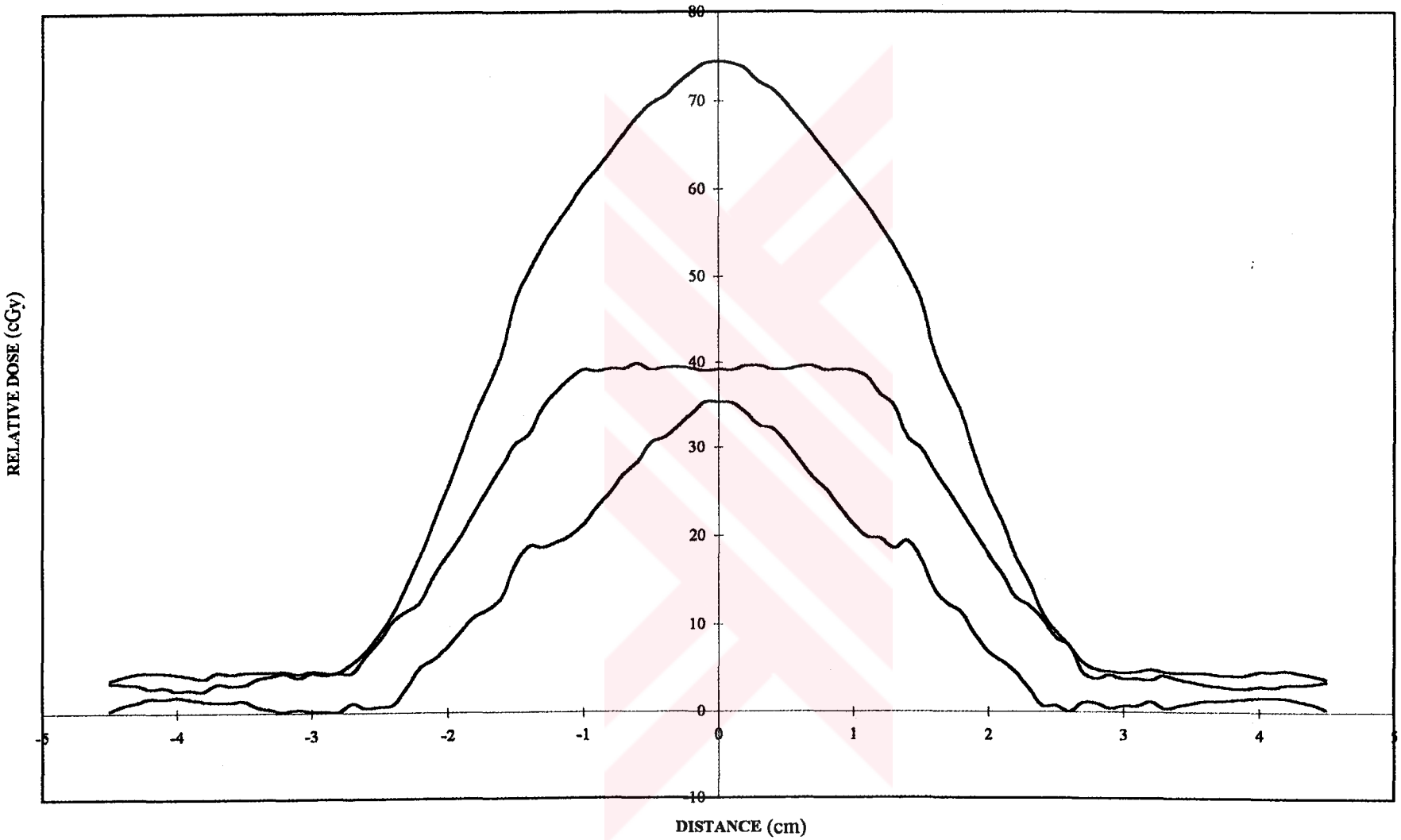

Figure 6.13 Electron Dose Profile for E=13.5 MeV, x=35+2.65 cm and lead sheet thickness=6 mm.

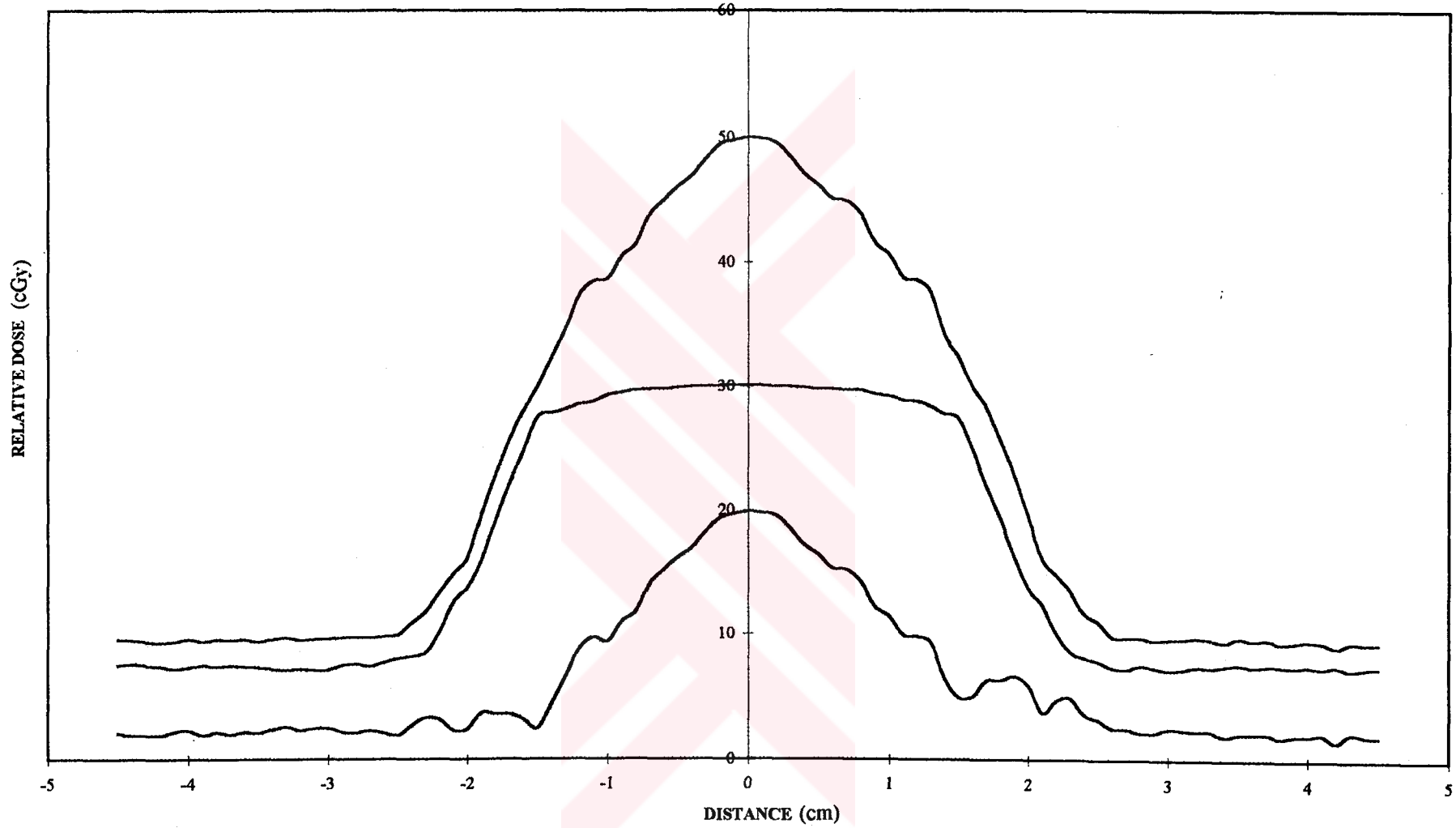

Figure 6.14. Electron Dose Profile for E=16 MeV, x=35+0 cm and lead sheet thickness=2 mm.

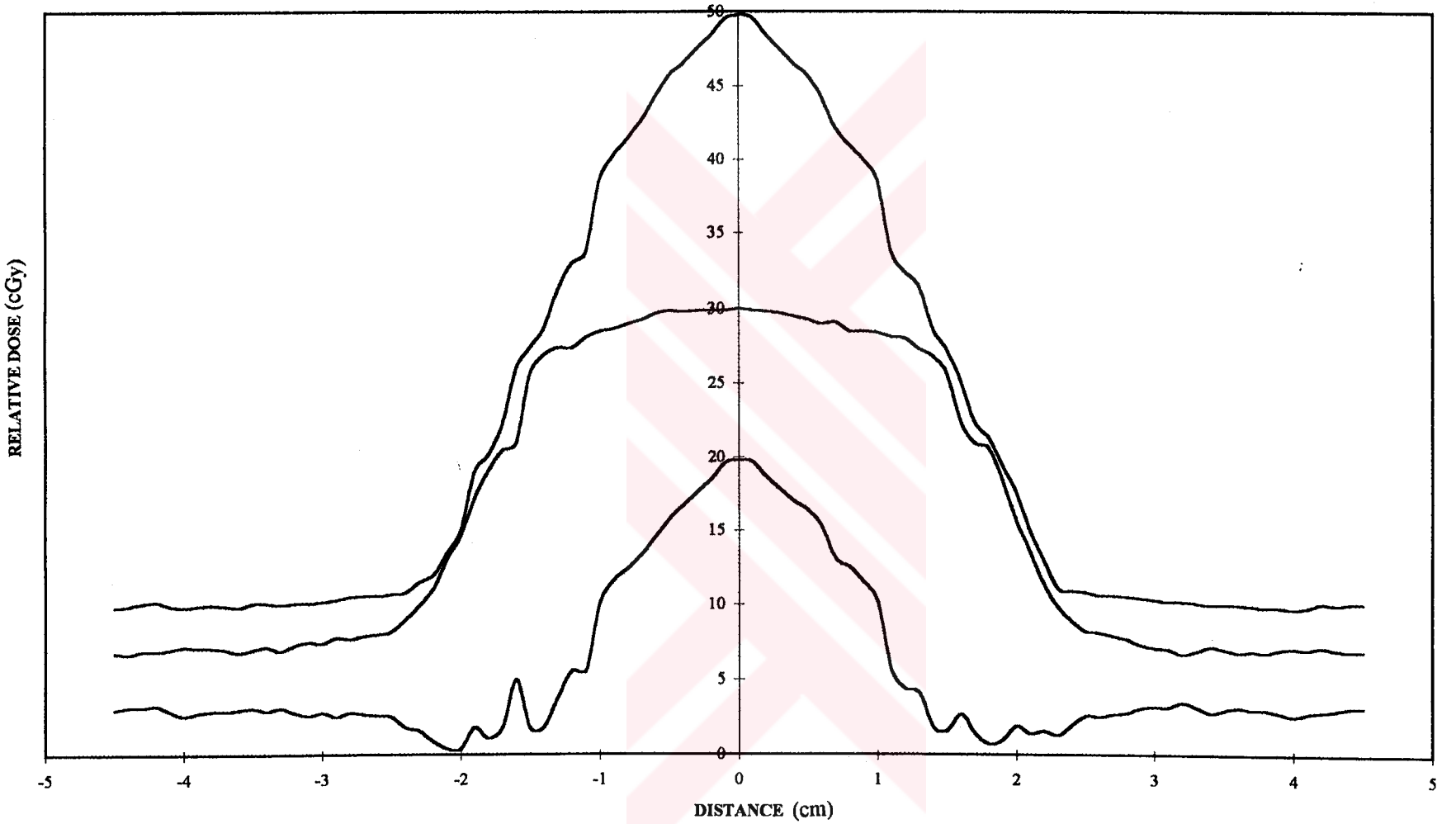

Figure 6.15. Electron Dose Profile for E=16 MeV, x=35+3.2 cm and lead sheet thickness=2 mm.

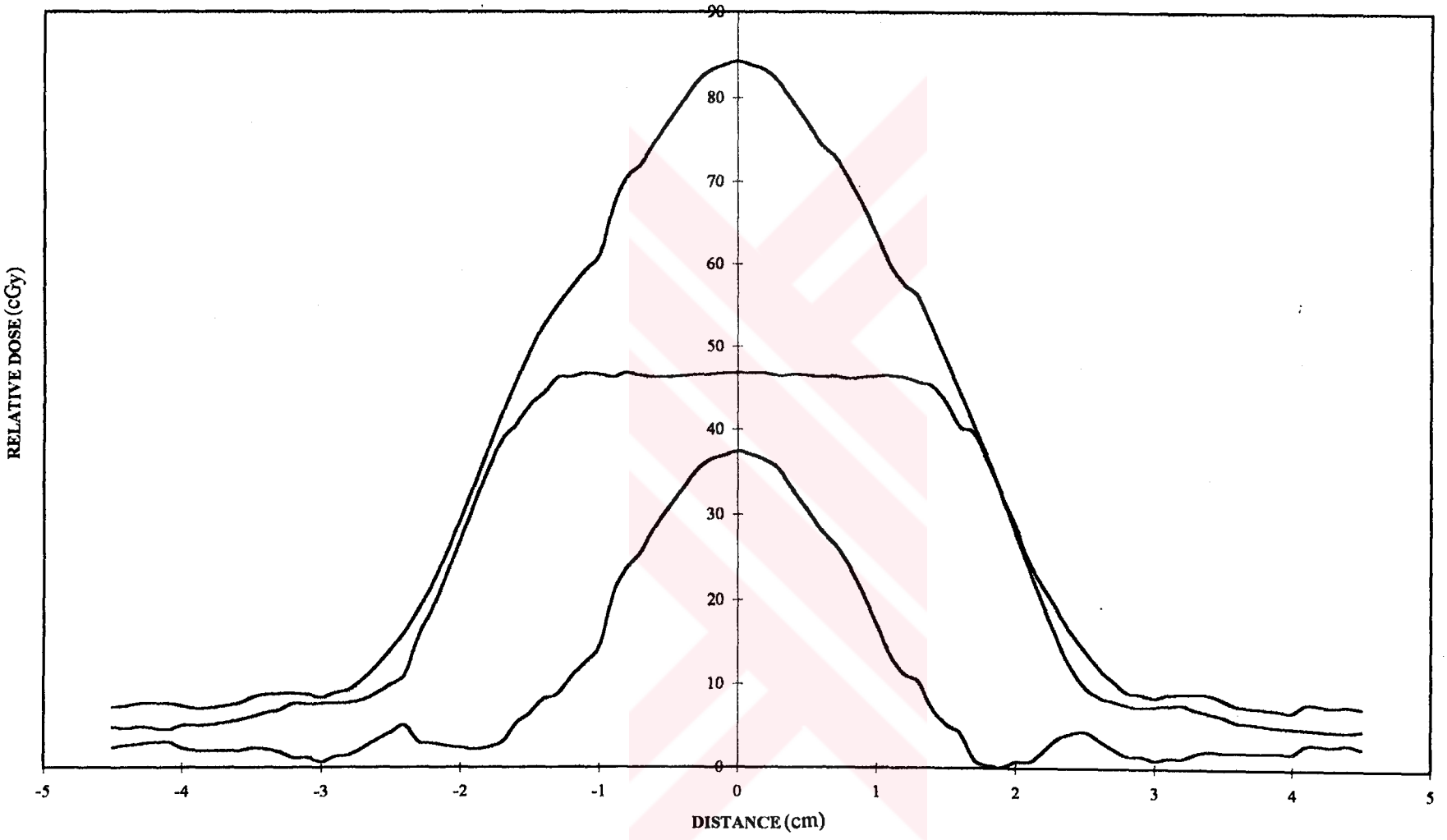

Figure 6.16. Electron Dose Profile for E=16 MeV, x=35+0 cm and lead sheet thickness=4 mm.

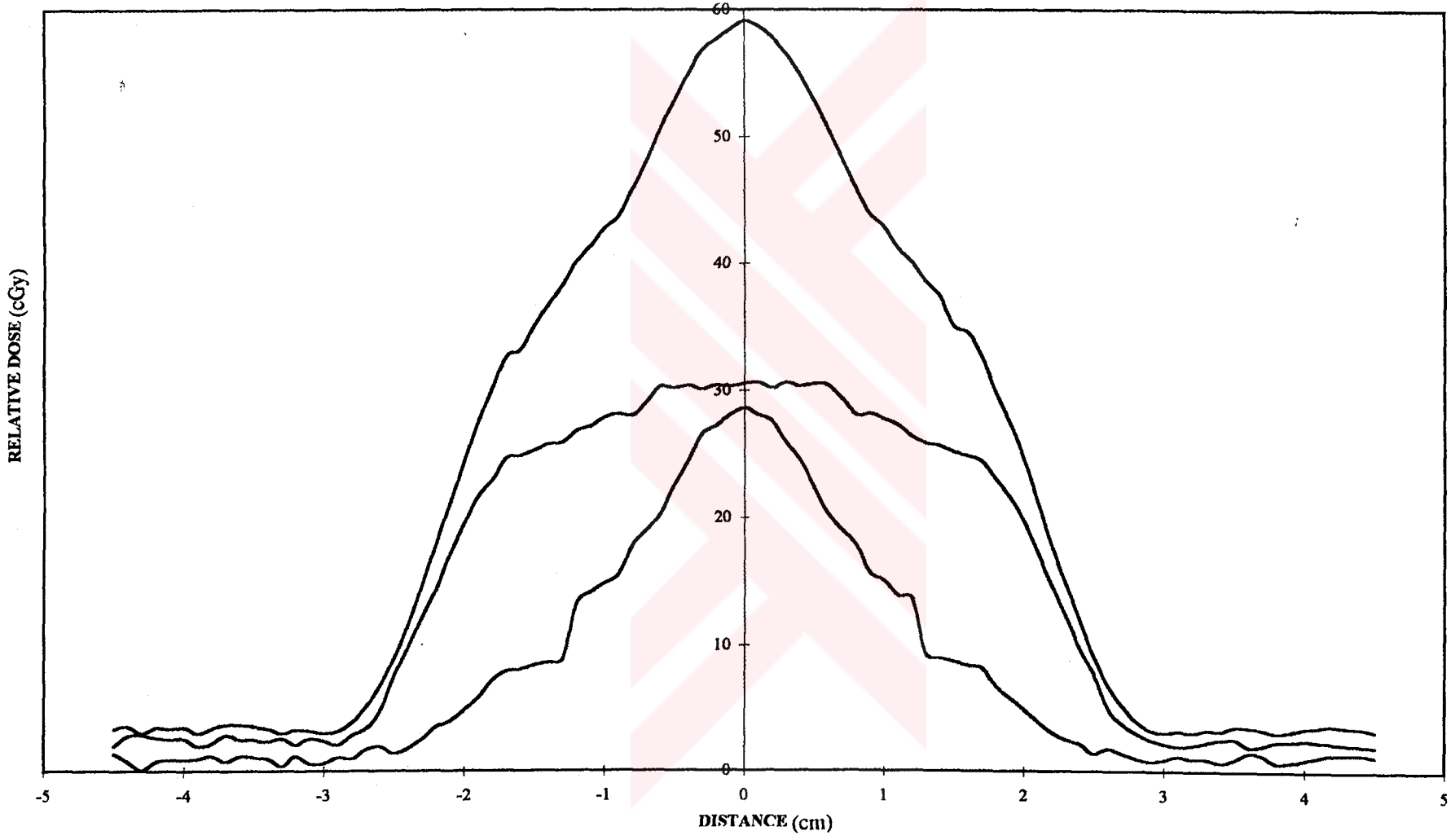

Figure 6.17. Electron Dose Profile for E=16 MeV, x=35+3.2 cm and lead sheet thickness=4 mm.

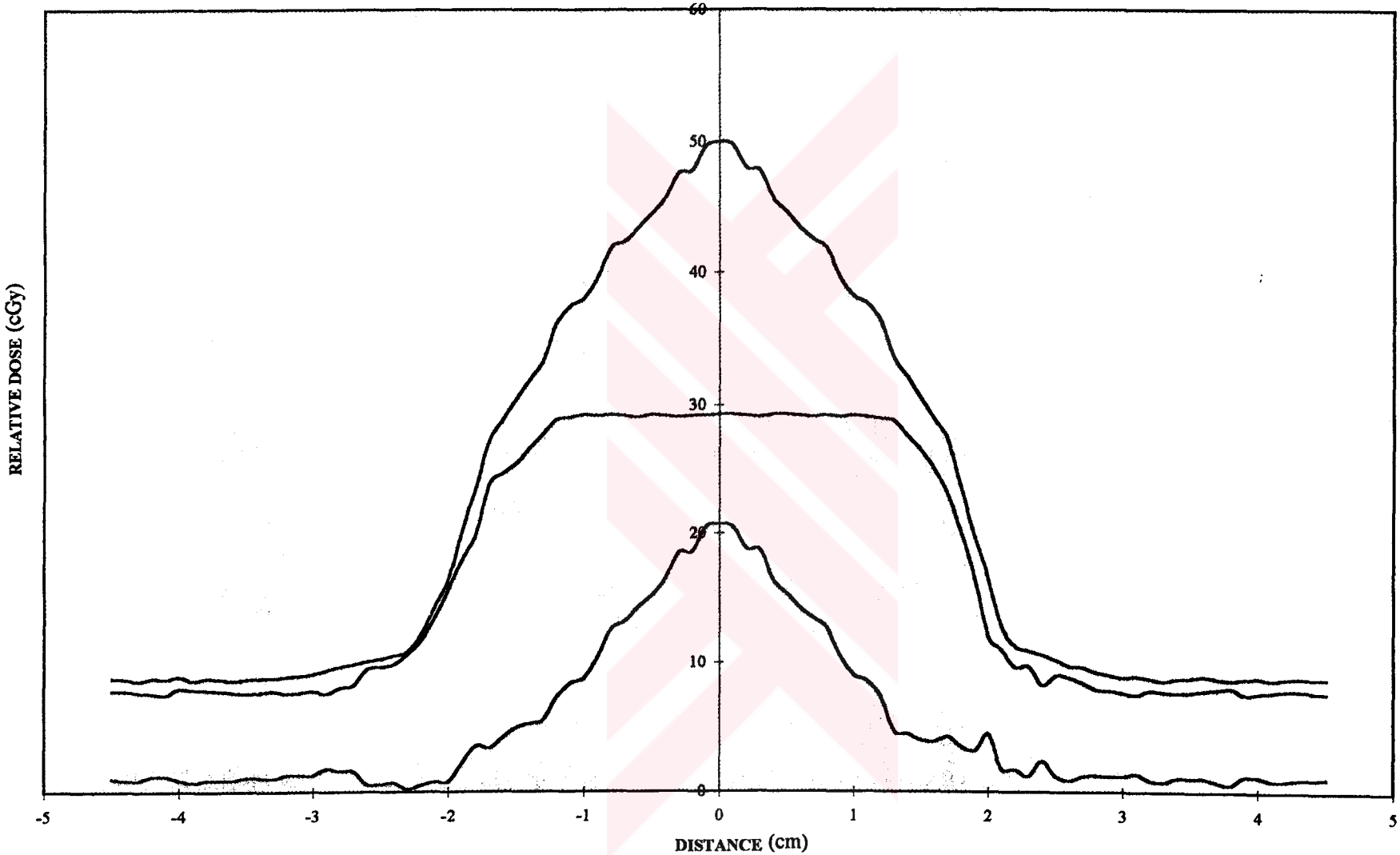

Figure 6.19. Electron Dose Profile for E=16 MeV, x=35+3.2 cm and lead sheet thickness=6 mm.

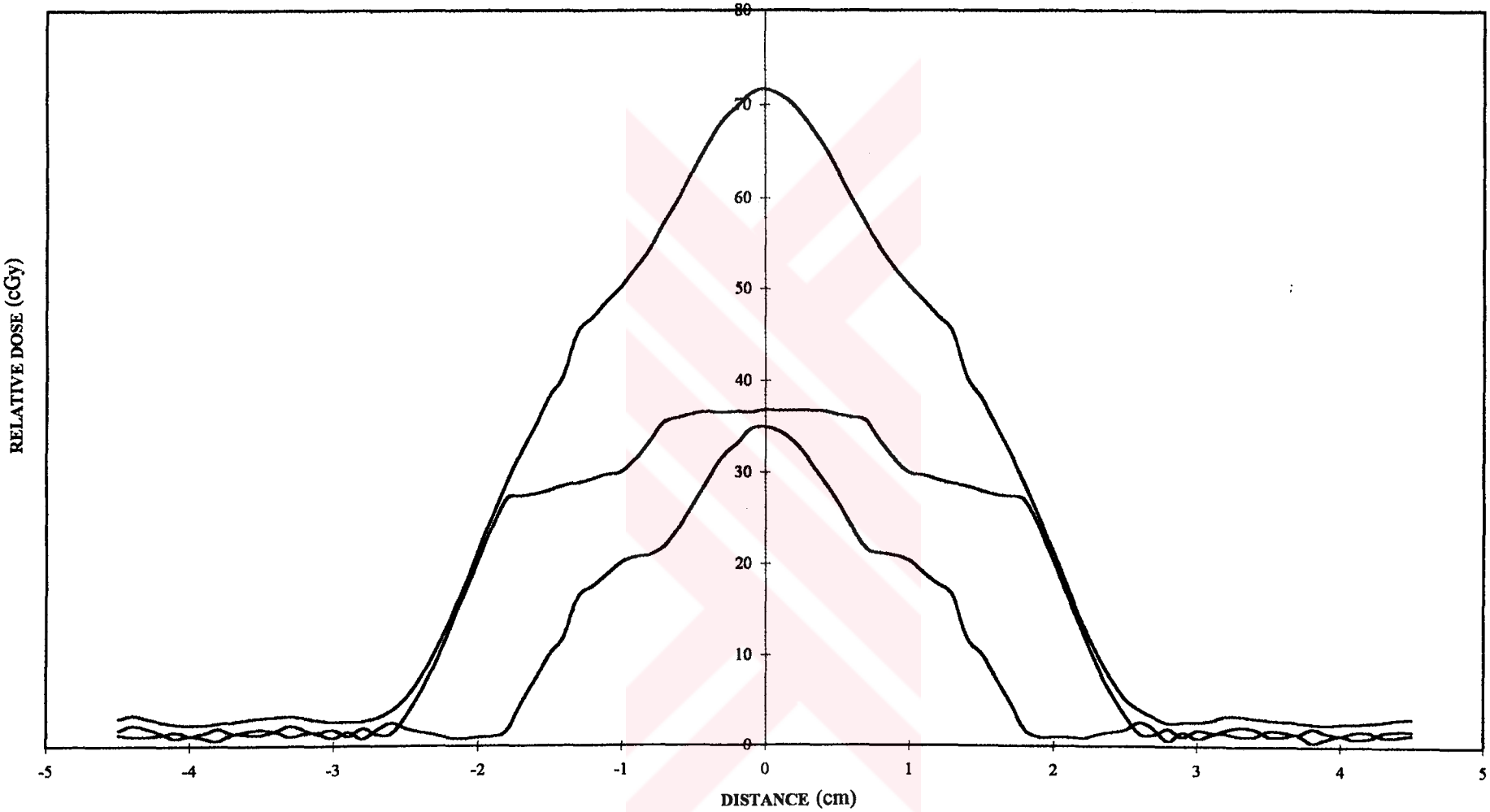

Figure 6.18. Electron Dose Profile for E=16 MeV, x=35+0 cm and lead sheet thickness=6 mm.

VII. CONCLUSION AND DISCUSSION

While high energy electrons pass through a medium, the interactions with nuclei and the orbital electrons cause generally two different phenomena occurring together.The electron loses energy mainly by interacting with the orbital electrons while it changes the direction of motion through the collisions with the nuclei of the atoms in the medium. These two phenomena suggest some methods of measuring the kinetic energy of the electron beams.The range method is based on the practical range of electrons in a medium or the distance where the dose falls to 50% of the maximum dose both of which are due to energy loss. The scattering method related with multiple scattering, is derived from the probabilistic approach of electron interactions and it is shown that the scattering method equations derived analytically, are in a good agreement with the practical results.

In the range method there is reference distances of measurement, field sizes and measurement apparatus; however, in the scattering method, there is no fixed distance for the radiation measuring device or diameter of aperture in the lead sheet for any energy or the thickness of the lead sheet or the field size to be radiated. Because of the lack of such a protocol, it was convenient to perform more measurements to obtain more reliable results by arithmetic means of energies.

The experimental results obtained show that the proposed method can be reliably used in the electron beam energy measurements. Furthermore,this method can also be used as a practical alternative to the range method in clinical setttings by performing a number of enhancements such as designing simple and low cost apparatus for automatic data collection and processing. We think that an important advantage of this method relies in its solid theoretical foundation, making it less prone to variations in different settings.

Further work is needed to optimize the various experimental parameters for a set of standart measurement protocols. Comparison with magnetic spectroscopy can also be useful as a means of validation.The major measurement errors are statistical and

systematic errors, created by mechanical imperfections in the exit hole of electrons and the photon contamination in the background.Compensation techniques should be investigated for minimizing the systematic types of errors. The mass angular scattering power method, which approaches the kinetic energy determination in a probabilistic scattering of electrons in air can be used as an alternative method to the range method.

APPENDIX A

DEPTH DOSE CURVES

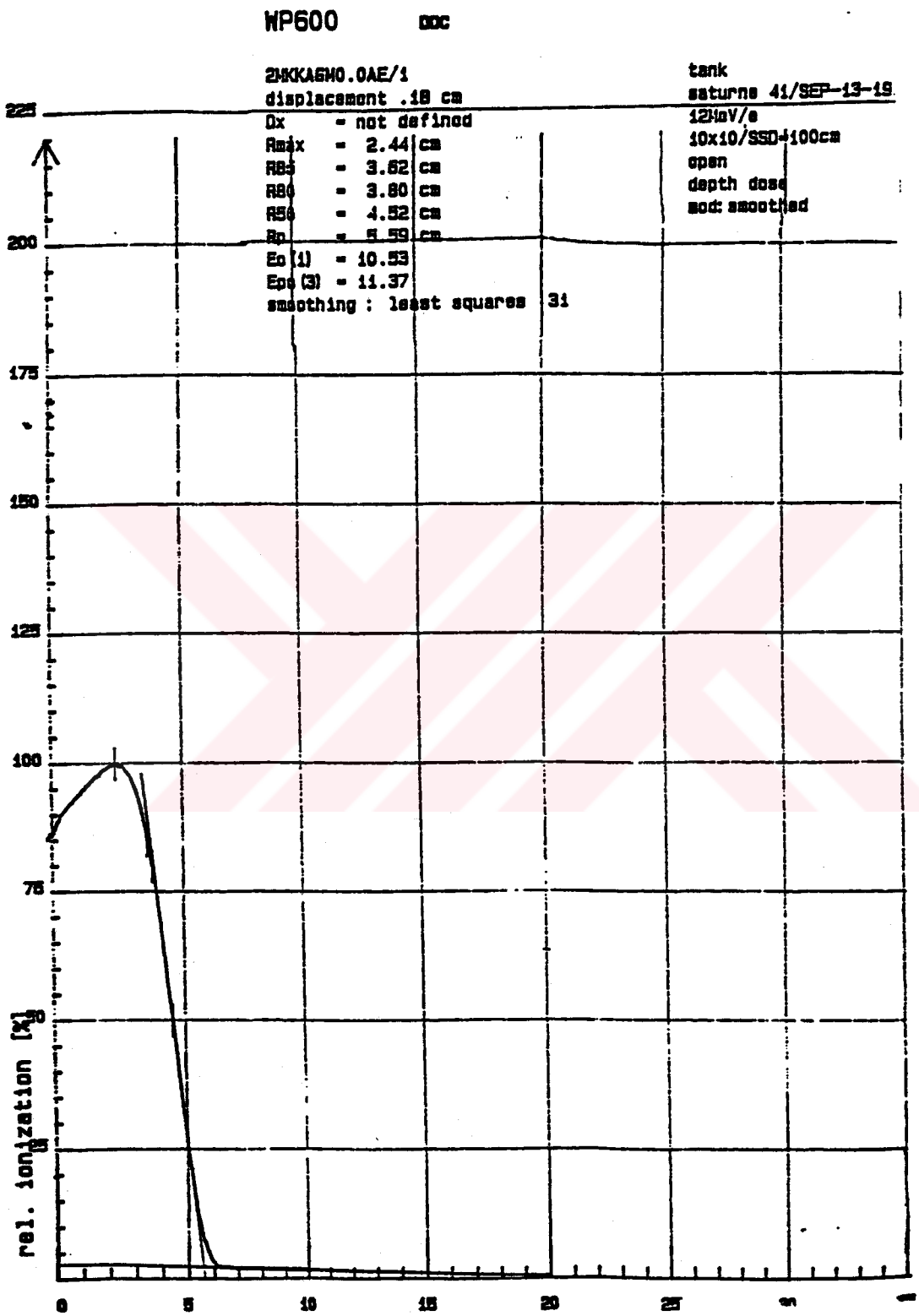
WP600 ooc
2MKKA6M0.0AE/1
displacement .18 cm
Dx = not defined
Rmax = 2.44 cm
R80 = 3.80 cm
R50 = 4.52 cm
Rp = 5.59 cm
Eo (1) = 10.53
Epo (3) = 11.37
smoothing : least squares 31
tank
saturne 41/SEP-13-19
12MeV/e
10x10/SSD=100cm
open
depth dose
mod: smoothed
rel. ionization [%]
225
200
175
150
125
100
75
0
5
10
15
20
25

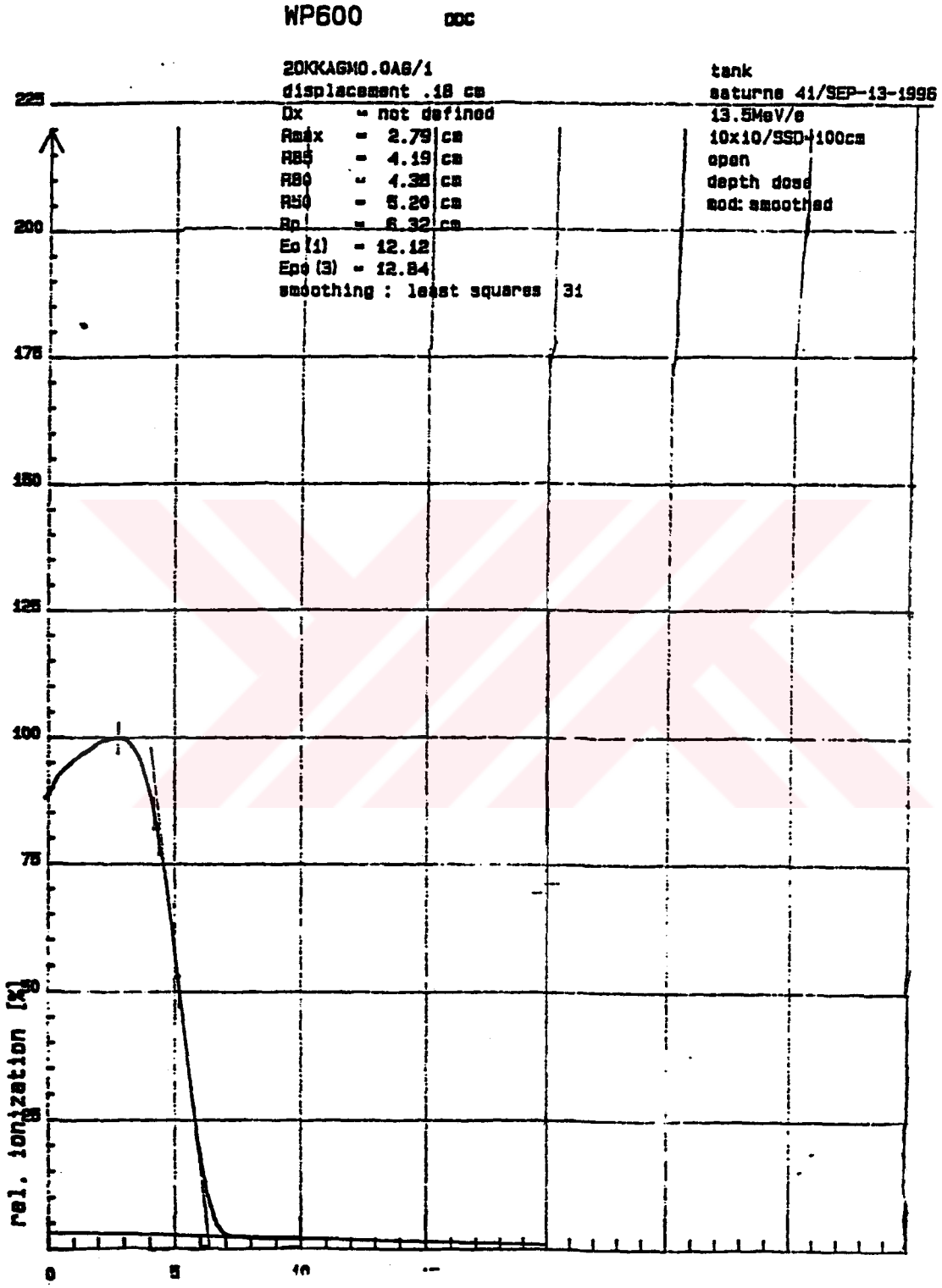
WP600 ooc
20KKAGMO.0A6/1
displacement .18 cm
Dx = not defined
Rmax = 2.79 cm
R80 = 4.19 cm
R80 = 4.38 cm
R50 = 5.20 cm
Rp = 6.32 cm
Eo (1) = 12.12
Epo (3) = 12.84
smoothing : least squares 31
tank
saturne 41/SEP-13-1996
13.5MeV/e
10x10/SSD=100cm
open
depth dose
mod: smoothed
rel. ionization [%]
225
200
175
150
125
100
75
50
25
0
5
10

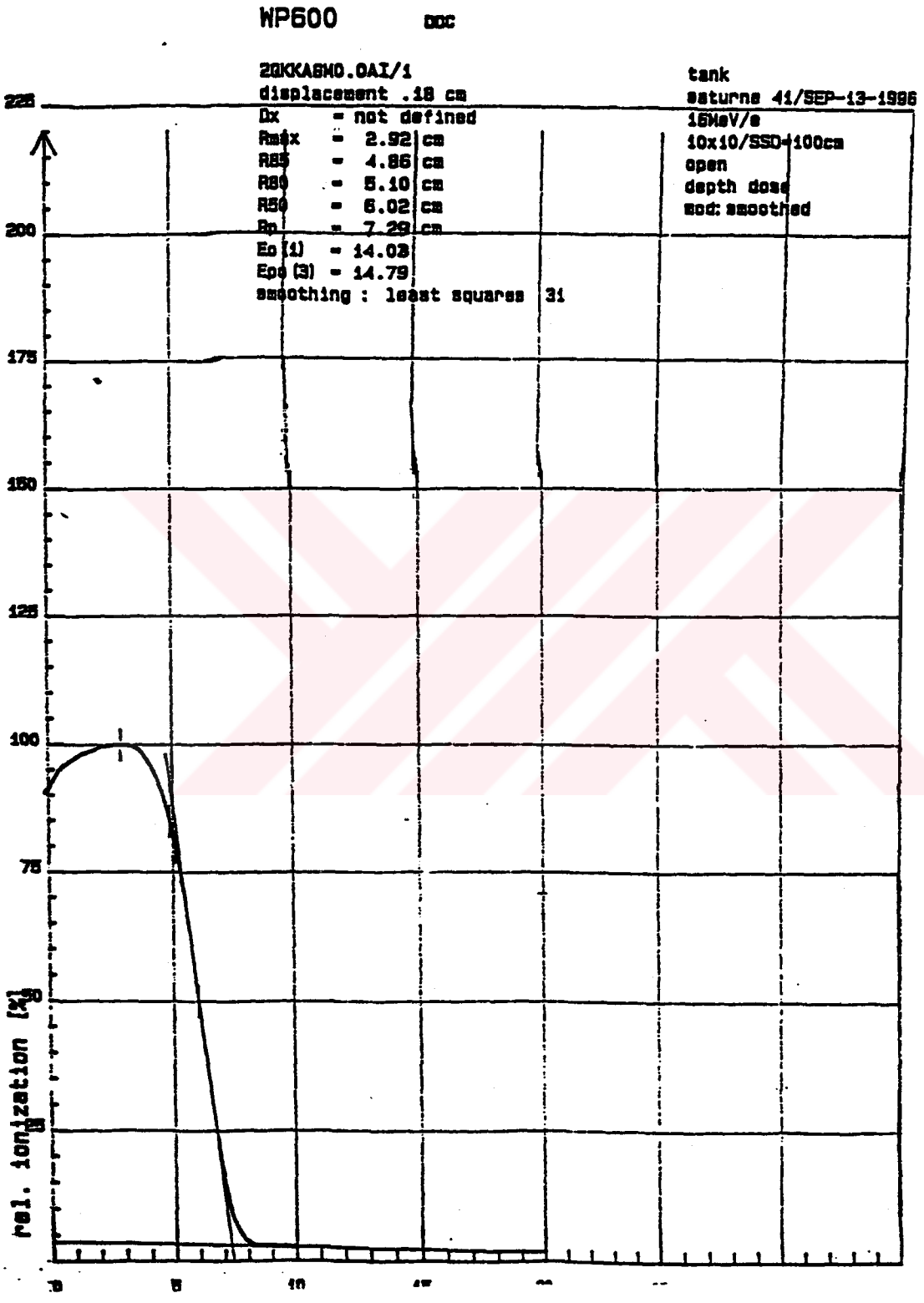
WP600 DOC
20KKA6M0.0AI/1
displacement .18 cm
Dx = not defined
Rmax = 2.92 cm
R85 = 4.86 cm
R80 = 5.10 cm
R50 = 6.02 cm
Rp = 7.29 cm
Eo (1) = 14.03
Epo (3) = 14.79
smoothing : least squares 31
tank
saturne 41/SEP-13-1996
15MeV/e
10x10/SSD=100cm
open
depth dose
mod: smoothed
225
200
175
150
125
100
75
rel. ionization [%]

APPENDIX B

SATURNE 41 PRODUCT DATA

-Europe: Paris, France
Fax: 33 1 40 93 33 33
GE Medical Systems-Americas: Milwaukee, WI, USA
Fax: 1 414 544 3384
GE Medical Systems-Asia: Singapore
Fax: 65 291 7006
YMS: Tokyo, Japan, Fax: 81 425 85 5360

Product Data
93264-E

Saturne 41 F

Linear accelerator (F63321)

Application

The Saturne 41 F is a medical linear accelerator powered by a magnetron operating in the 3000 MHz frequency range. The unit delivers electron radiation beams of six different energies ranging from 4.5 to 15 MeV and photon radiation beams at two energies between 6 and 15 MV.

Configuration

Accelerator

The standing wave accelerator waveguide is mounted on a rotating gantry. The electron gun, the RF window, vacuum pump and bending chamber are all removable for fast, easy system maintenance. The GE-patented magnetic system provides 270° deviation of the electron beam. Energy is defined by the built-in energy selection slit.

Radiation head

The radiation head assembly is mounted on the end of the accelerator waveguide and incorporates all the equipment needed for beam definition and control:
- Double scattering system for electron beam uniformity.
- Optimized photon targets for each energy group.
- Different flattening filters for each photon energy.
- Beam measurements and control by two independent sets of ionization chambers.

Beam limiting system (collimator)

The beam limiting system is mounted beneath the radiation head and may be used in photon mode or with beam applicators in electron mode. The system comprises:
- a pair of independent jaws (X1, X2) enabling symmetrical or asymmetrical movement in relation to the collimator axis,
- a pair of independent jaws (Y1, Y2) enabling symmetrical movement in relation to the collimator axis,
- an automatic wedge filter.

An accessory holder plate is installed at the base of the beam limiting system and is associated with a coding system.

Saturne 41 F linear accelerator

A metallic ring located at the bottom of the collimator stops movements and radiation in the event of accidental collision.

Technical area

The modulator assembly, RF generator, power supply rack and cooling circuit are located at the rear of the gantry behind the wall partition (4.50 m x 2.65 m). Two doors provide access to this area.

Control systems

Accelerator gantry and patient support assembly movements are controlled by a single control box in the treatment room. A control console in the control room is used for:
- system operation and surveillance,
- treatment and safety management.

Operational Features

The Saturne 41 F can operate in electron or photon mode for both stationary or moving-beam (arctherapy) modes.

Electron mode

- Dose rates:

The monitor unit (MU) is defined as being equal to 0.01 Gy ± 2 % for a 10 x 10-cm field and a dose rate of 200 MU/minute. The measurement probe is placed at the isocenter and dose maximum depth. The following dose rates are available for all energies: 200 - 300 - 400 MU / min.

- Field sizes:

Square-cornered fields, as defined by the jaws fitted with their applicators, are visualized by light source projection. Symmetrical fields measured at a distance of 100 cm from the source are continuously variable from 2 cm x 2 cm to 30 cm x 30 cm. In asymmetric mode, the field center may be offset in relation to the collimator axis. The edge of the field defined by each X1 or X2 jaw fitted with its applicator, stops 1 cm from the collimator axis. The maximum offset possible is 7 cm.

87

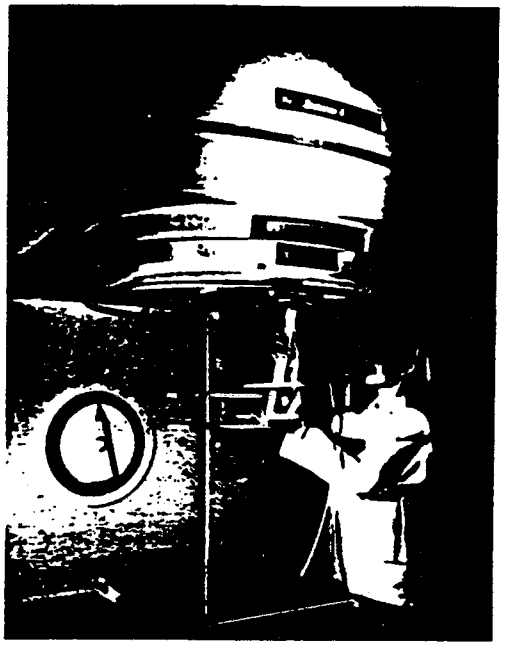

Square-cornered fields, as defined by the jaws fitted with their applicators, are visualized by light source projection.

eld flatness:
l flatness is measured for square
s greater than 10 x 10 cm with the
r-phantom surface in contact with
ipplicators. On either side of the
er along 80 % of the length of the
median lines and along 60 % of
ield diagonals, dose variation
sured at a single point in relation to
rithmetic mean value does not
ed:
6 for E < 6 MeV
6 for E ≥ 6 MeV

eld symmetry
l symmetry is measured at all
gies for a surface defined by 80 %
e length of the median lines and
g 60 % of the field diagonals. The
variation measured at two
netrical points in relation to the
mator axis does not vary from the
metic mean value by more than

: For symmetrical fields, all
surements are made in a water
valent with the gantry at 0°, and in
ne parallel to the surface at a
h of ½Rp (Practical range, IEC
inology). The surface is
endicular to the collimator axis at
tance from the source of:
cm for the flatness and symmetry
surement,
cm for the dose rate
surement.

on mode

rne generates photons by
lerating electrons in a high atomic
ber target.

se rates
monitor unit (MU) is defined as
g equal to 0.01 Gy ± 2 % for a 10 x
n field and a dose rate of 200 MU/
ute. The measurement probe is
ed at the isocenter and dose
mum depth. The following dose
are available:
100 - 200 MU / min at 6 and 8 MV.
100 - 200 - 300 - 400 MU / min at
V and more.

eld sizes
netrical fields with square corners
ontained within a 56 cm diameter
measured at a distance of 100 cm
the target and at dose maximum
h. They are continuously variable
2 cm x 2 cm to 40 cm x 40 cm.
are defined by the contour of the
isodose. The variation measured
ie median lines between the edge
e light field and the 50 % isodose
s than 0.2 cm.
ymmetric mode, the field center can be offset in relation to the collimator axis. Each X1 or X2 jaw stops at the collimator axis. The maximum offset possible is ± 10 cm.

• Field flatness
Field flatness is measured in a plane at a distance of 100 cm from the target and at 10 cm depth in a water-phantom for square fields of 10 x 10 cm to 30 x 30 cm on either side of the center and over 80 % of the length of the median lines and 60 % of the length of the diagonals.
Dose variation does not exceed ± 3 % of the arithmetic mean value. For fields larger than 30 x 30 cm, this limit is ± 5 %.

• Field symmetry
Field symmetry is measured for square fields greater than 10 x 10 cm within an area defined by 80 % of the length of the median lines and 60 % of the diagonals. For all energies, the dose measured at two symmetrical points in relation to the collimator axis, at a 100 cm from the target and at 10 cm depth in a water-phantom, does not vary from the arithmetic mean value by more than 2 %.

• Penumbra
For a square field of 10 x 10 cm at 100 cm from the target and under 10 cm of water, penumbra is defined as being the distance measured on median lines between 80 % and 20 % isodoses.
Penumbra is:
0.6 cm at 10 to 15 MV
0.65 cm at 8 MV
0.7 cm at 6 MV

• Wedge filter
The wedge filter system is installed inside the collimator and covers a maximum field of 20 cm in the X axis and 40 cm in the Y axis centered on the collimator axis. By programming two consecutive irradiation sequences, with and without the filter, the wedge filter makes it possible to obtain a wedge angle of between 0° and about 60° from the X median.

• Radiation leakage rate
Radiation leakage rate is calculated by taking the average of values measured. Leakage through the collimator is less than 0.5 %. This figure is determined by the ratio between the absorbed rate measured in the patient plane at a distance of 100 cm from the target, in a circle of 56 cm diameter centered on the collimator axis. Dose rate is measured for a field of 2 cm x 40 cm. The residual aperture is closed by 10 cm of lead. In the patient plane, radiation leakage rate is:
- less than 0.1 % on average
- less than 0.2 % maximum.
Outside the patient plane: less than 0.1 %. These radiation leakage rates comply with IEC recommendations.

• Moving beam therapy (arctherapy)
Moving beam therapy is possible with Saturne in photon or electron mode (without applicators) over a maximum arc of 360° in both rotation directions. Dose accuracy is better than 3 % or 1 MU.

Dose rate in MU/min.	100	200	400*
Maximum dose per MU degree	2.5	5	10
Minimum dose per MU degree	0.33	0.66	1.33

Rotation of mobile gantry and collimator

Characteristics	Units	Gantry	Collimator
Maximum angle	Degrees	370	370
Mechanical stops	Degrees	185 and	185 and
10° overlap		175	175
Motorized movement	°/min	40 to 300	90 and 360
Positive rotation direction	Clockwise as seen from isocenter		

Mechanical specifications

The isocenter is defined as being the smallest volume described by the rotation axis of the collimator during a complete rotation of the gantry.
- Isocenter volume: r = 0.1 cm max.
- Source to isocenter distance: 100 cm ± 0.2 cm
- Variation for one complete 360° rotation of the gantry 0.2 cm max.
- Isocenter to floor distance 131 cm
- Isocenter to top-cover distance 130 cm
- Isocenter to collimator base distance 50 cm
- Isocenter to base of beam applicators 10 cm
- Collimator axis to gantry mounting wall 240 cm
- Collimator axis to front side of gantry 138 cm ± 1 cm
- Accelerator extremity to gantry mounting wall 330 cm

Control console

The control console comprises:
- A working area with:
an alphanumeric keyboard incorporating a numerical keypad, function keys for each mode, «Beam on» and «Beam off» hard wired pushbuttons and «Irradiation authorization» key, mouse for user interface.
- A shelf for:
a 14-inch (35 cm) color graphics monitor, a printer, a disk drive for patient data (3.5" floppy disk), backlit on/off key, an emergency shut-off control. The shelf is also designed to hold the optional video surveillance monitor(s).
- An electronics cabinet located under the working area with:
two dose backup counters, an operating system floppy disk drive (3.5"), a hard disk, a «physicist» key, maintenance connections and control units, deadman's pedal for arctherapy, RS 232 interface.

Control box

In the treatment room, the control box is used jointly with a control monitor that displays requisite parameters before irradiation can start. The control box has 36 keys grouped as follows: accelerator and patient support assembly parameters, numerical keypad, dedicated function keys, ancillary controls, manual control keys, two deadman's switches on either side of the control box.

The control monitor is wall-mounted on a swivel support. This 19-inch (48 cm) color graphics monitor displays large characters that can be read on screen from a distance of at least four meters (12 feet).

Operation modes

The control console can be used without any previous computer knowledge. The user interface relies on: easy-to-understand screen messages, menu display, dedicated function keys and a mouse, floppy disks.
Two operation modes are available: medical mode and physicist mode. A third mode is reserved for qualified personnel in charge of system monitoring and maintenance.

The start-up procedure (warm-up and self-test), is automatic. The operator simply selects the operation mode desired.

• Medical mode
Medical mode is designed for patient irradiation. It is used to set irradiation conditions, adjust the accelerator and patient support assembly parameters, monitor treatment and generate treatment reports according to the scheduled treatment prescription. The following parameters must be set from the control console before each treatment session:
irradiation mode: stationary or moving-beam therapy (arctherapy: angular positions, and rotation direction),
beam type: type of radiation and energy level, dose rate, total dose,
dose to be administered with wedge filter or filter angle for photon radiation, codes for accessories to be used.
Operator (code), patient and beam identification systems are optionally available.

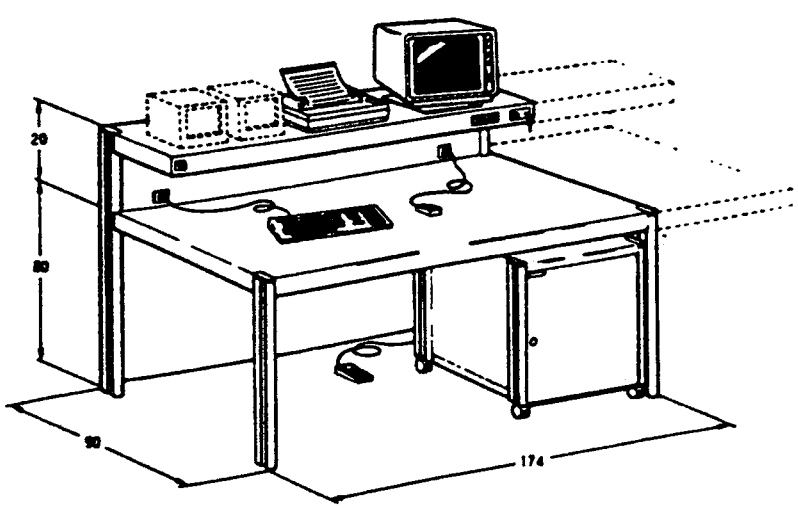

Control console (dimensions in cm).

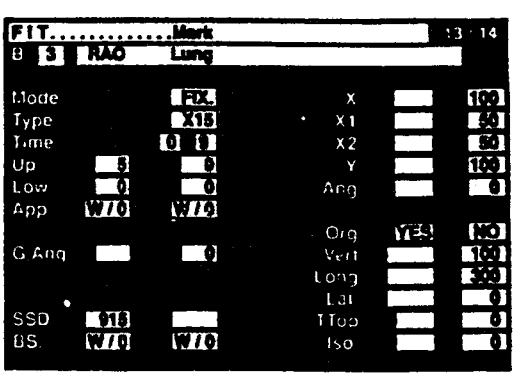

Screen display in medical mode on control monitor in treatment room (actual display in color)

ting up geometric parameters
ing up accelerator and patient
port assembly geometric parameters
ires validation form the operator.
set-up modes are available in the
dard configuration:
ual: after selecting the parameter, operator selects positions with the + keys on the control box. Two ement speeds are available.
t indicators (optical distance cator and cross-hair) and the tions in millimeters or degrees are cated on graduated scales. To make p easier, this information is layed on the control monitor in the tment room.
matic: after selection of the meter, the desired stop position in imeters or degrees is entered on control box. These indications are layed on the control monitor. ement starts when the operator ses the set-up key on the control

at the required position is matic.
rgency shut-off controls are lable on the control box.
m limiting parameters, angular tion of the gantry and patient port assembly parameters may be set n the control console.
ings for automatic positioning may nade from the control box.
meters for the beam limiting ce without applicators and gantry le may be set up globally (with orization) from the control ole. An emergency control for ping movement is available on the trol console.

rify functions
e prescription has been entered on control console before the start of n irradiation session, the system cks that actual parameter settings he accelerator and patient support mbly match the treatment plan. or displays indicate any discrepancy veen prescriptions and actual ngs. During irradiation, the system nitors dose rates and also checks actual current positions of all metric parameters remain equal to e selected at the start of the session. diation is interrupted if repancies are identified.

escription recording
ividual patient prescriptions can be ed on a floppy disk for subsequent tment sessions.
ent prescriptions for daily sessions be generated by GE's Sincer II/MV cription record-and-verify system.

Parameter display in the treatment room

Every movement of the Saturne and patient support assembly has two readouts: mechanical on the graduated scale, digital on the console screen in the treatment room.

	Range	Mechanical	Digital	
		Calibration	Display	Accuracy
Gantry rotation	0° to 359°	degree	degree	±1°
Collimator rotation	0° to 359°	degree	degree	±1°
Photon field size	2 cm to 40 cm	cm	mm	±0.2 cm or ±1 %*
Electron field size	2 cm to 30 cm	cm	mm	±0.2 cm or ±1 %*
Offset field size	0 to 20 cm	0.5 cm	(Jaw position)	±0.2 cm or ±1 %*
PSA	All movements			

* in relation to light field at isocenter

- Ancillary controls
Treatment room lighting and the simulation light can be controlled from the control console or control box. Two keys on the control console are reserved for specific functions such as opening of the treatment room door.

- Irradiation
At the end of the treatment session, a report can be printed automatically or requested by the operator once comments have been entered. This report indicates all parameters, the date and time of the treatment session and the MU calibration factor, if this parameter has been stored in physicist mode. Reports from each irradiation are stored on the patient's floppy disk.

• Physicist mode
Physicist mode comprises three functions: utilities, non-patient irradiation and adjustments.

- Utilities
Utilities are used for the following:
Customization of the system for use in medical mode and with definition of: report headers and indication of the Saturne model used,mandatory and optional items in parameter set-up procedures, permissible beam types (radiation, energy, rate),
preprogrammed angles for the automatic wedge filter,
areas covered by the optional beam stopper,
prescriptions for control irradiation (portfilming option),
definition mode for treatment prescriptions: manual, floppy disks or Sincer II/MV.
Management of patient floppy disks:
Storage of dose Monitor Unit calibration factors.

- Non-patient irradiation
This function is similar to irradiation in medical mode, but is designed to monitor dose rates. It allows:
Irradiation sequencing without re-entering prescriptions.
Set-up of all geometric parameters of the accelerator and patient support assembly from the control console.

- Adjustment
The operator can monitor all system set-up parameters and adjust calibration coefficients of dose Monitor Units.

• Maintenance mode
All geometric and physical parameters are digitally controlled before and during irradiation. Adjustment parameters may be displayed, printed and stored on floppy disk. Saturne operation may be monitored by digital display of all static and dynamic parameters.

Protection

Access to different operation modes is protected as follows:
Passwords.
Operator codes (options). This form of protection uses a list of authorized operators drawn up by the site manager. Irradiation print-out reports include the operator's personal code.
Keys. The first, on the keyboard, allows irradiation; the second is inserted in the electronics cabinet and indicates the system manager's presence.

Patient support assemblies (PSA)

The PSA is not included in the F63321 reference.

760S Isocentric PSA (F64201AA)

The PSA is mounted on a bearing assembly in a 26-cm floor pit. All movements are motorized.
Isocentric rotation: ± 120°
Table top rotation: ± 185°
Vertical movement from floor : ± 74.5 cm to 146 cm
Lateral movement: ± 20 cm
Longitudinal movement: 60 cm
The PSA is delivered with a type B standard tabletop measuring 240 x 53 cm.

Treatment field localization

The light simulation system replaces the source during this procedure. Cross-hairs are placed at the base of the collimator according to the median lines of the fields.
The optical distance indicator projects a light scale calibrated in centimeters from 75 to 140 cm. Distance is read at the intersection of the cross-hairs. Digits are given every 5 cm. Calibration precision: ± 0.2 cm.

RS 232 interface

An RS 232 C serial port allows:
Control console loading with external prescription
Transmission of all geometric and irradiation parameters.
This serial port is used for connection to the Sincer II/MV prescription record-and-verify system.

Options

Additional photon dose rate (F63301DK)

Saturne 41 F is delivered with one photon dose rate as standard. One or maximum two additional photon dose rate can be supplied on option.

Additional electron dose rate (F63301RN)

Saturne 41 F is delivered with one electron dose rate as standard. One or maximum two additional electron dose rate can be supplied on option.

Additional high dose rate (F63301FC)

For any two electron energies chosen from the standard range, Saturne can also supply an additional dose rate of 1000 MU/min.

Preprogrammed portfilming (F63301FA)

Portfilming prescriptions are defined and recorded in physicist mode. They are recalled in medical mode by pressing either the «prescribed field» or «wide field» function keys. The operator may adjust the number of Monitor Units to be administered. The beam limiting device can be set up from the control console. During portfilming irradiation, pressing the «irradiation reset» key regenerates prescriptions defined for the nominal beam.

Additional control monitor in treatment room (F63301FD)

This second 19-inch color monitor is identical to the one supplied in the standard configuration. It displays the same information.

Optical backpointer (F63301FB)

The optical backpointer is installed at the base of the gantry and is used to project a plane of laser light covering the source and gantry rotation axis. The optical backpointer is not compatible with digital portal imaging.

Digital portal imaging (F65101A)

Digital portal imaging allows verification of set-up before or during each treatment, without film and without processing. Treatment quality can be improved without loss of time. Target View provides real-time megavoltage digital imaging for the verification of photon treatment fields.

Accessories

See accessories catalogue.

Interlocks

The Saturne has the following interlocks:
• General interlocks,
- power-on key,
- irradiation authorization key,
- authorization key for physicist mode and resetting of major faults,
- emergency-off switch on control console and emergency-off switches in the treatment room,
- physicist mode password,
- operator codes (protected machine access).
• Movement interlocks
- deadman's switches on the control box,
- control console pedal,
- emergency off switch on the PSA,
- emergency off switch on control console keyboard,
- emergency off switch on the control box,
- anti-collision detection ring around the collimator.
• Heating circuit
- hard-wired interlock system.
• High-voltage circuit
- hard-wired safety circuit authorizing operation of the modulator.
A 15-minute time delay is installed between the heating circuit and the high-voltage circuit.
• Positioning
- safety circuit for positioning of target, scattering and flattening filters, two ionization chambers and wedge filter,
- checking of geometric parameters.
• Before irradiation
- checking of correct operation of the two dose measurement systems,
- integration of treatment door status information (open or closed).
• During irradiation
- Machine on:
- verification of parameters displayed on video screen,
- verification of ionization chamber power voltage,
- verification of pulse levels,
- vacuum monitoring: accelerator waveguide.
- Beam on:
- dose rate per pulse greater than preset threshold,
- dose rate too high or too low,
- dose rate inconsistent with the two dose measurement systems,
- symmetry or uniformity error,
- elapsed time error,
- failure of the first dose measurement system,
- interruption by the second system at prescribed value + 10 %,
- inconsistency between the dose delivered and dose calculated throughout moving-beam therapy,
- angle reached in moving-beam arctherapy.

Saturne complies with recommendations made by the International Electrotechnical Commission (IEC no. 601-2-1 1981, modified in December 1984).

Photon mode

Energies

When purchasing, two energies must be chosen from the following values:
6 - 8 - 10 - 12 - 15 MV

Dose rates

When purchasing, one dose rate must be chosen from the following values:
50 - 100 - 200 MU / min at 6 and 8 MV.
50 - 100 - 200 - 300 - 400 MU / min at 10 MV and more.

Energies

	Units	Values				
Effective energy (*)	MV	6	8	10	12	15
Depth of maximum absorbed dose	cm	1.5	2.0	2.5	2.8	3.0
Surface dose (under 0.05 cm water)	%	29	26	21	20	19
Absorbed dose (under 0.05 cm water)	%	67.7	71	74	75	77
Depth of 50 % dose	cm	15.8	17.3	18.5	19.4	20.0
NACP index (**)		1.67	1.61	1.57	1.55	1.53

(*) British Journal of Radiology, supplement 17. Central Axis Dose Data for Use in Radiotherapy, London 1983.
(**) Nordic Association of Clinical Physicists, Acta Radiologica Oncologica 19-55-79, 1980.

Depth dose curves

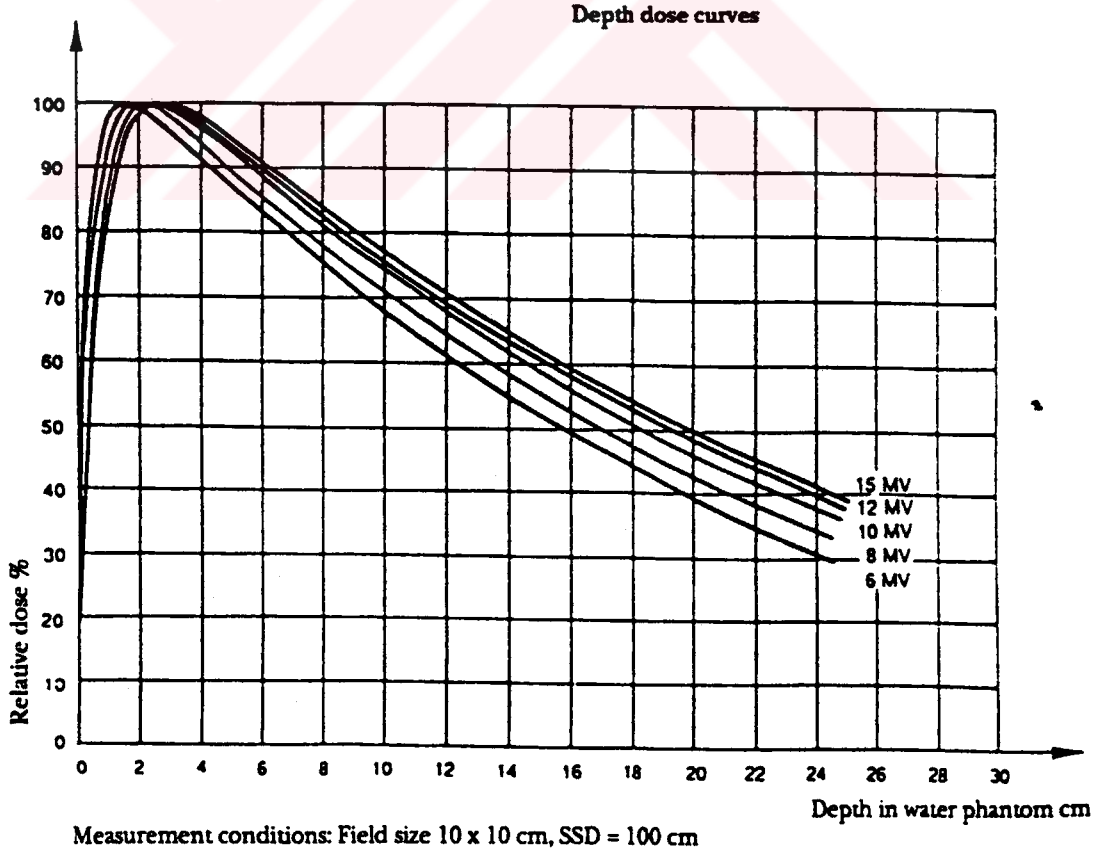

Measurement conditions: Field size 10 x 10 cm, SSD = 100 cm

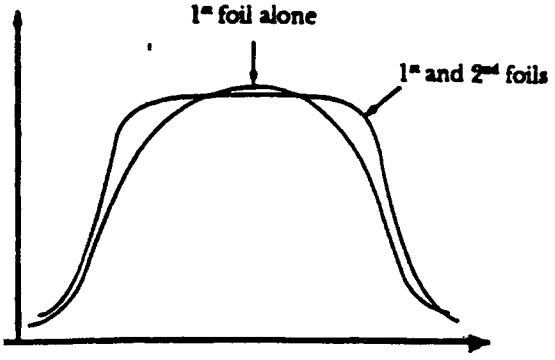

Double scattering

Energies

	Units	Double scattering					
Nominal energy	MeV	4.5	6.0	7.5	9.0	12.0	15.0
Energy in practical range Rp*	MeV	5.1	6.4	7.6	9.0	11.6	14.3
Surface absorbed dose under 0.05 cm water	%	70	72	75	77	81	84
Depth 80 % of dose	cm	1.5	2.0	2.5	3.0	4.0	5.0
Depth 50 %	cm	1.75	2.4	2.9	3.5	4.7	5.9
Depth 20 % of dose	cm	2.1	2.7	3.3	4.0	5.3	6.6
Practical range Rp (*)	cm	2.3	3.0	3.6	4.3	5.7	7.1
Photon contamination less than (**)	%	0.4	0.5	0.6	0.7	1.1	2.0
NACP gradient (***)		2.4	2.5	2.6	2.7	2.8	2.9

Measurement conditions: 10 x 10 cm field, SSD = 100 cm

*) Rp = practical range (IEC definition). Rp precision ± 0.2 cm or ± 3 %, whichever is greater.

**) Measured 10 cm beyond Rp.

***) Nordic Association of Clinical Physicists, Acta Radiologica Oncologia, 19-55-79, 1980.

Depth dose curves

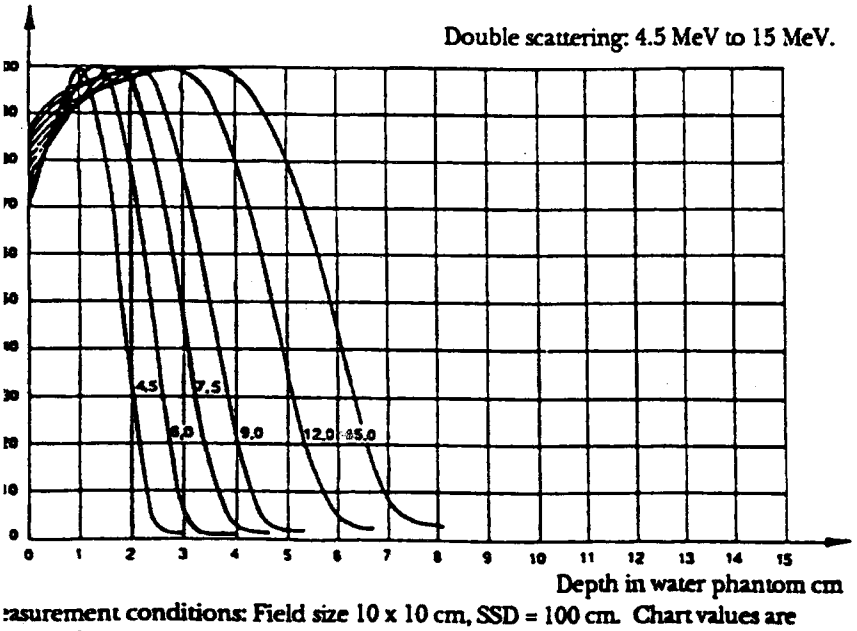

Measurement conditions: Field size 10 x 10 cm, SSD = 100 cm. Chart values are obtained from ionization measurements and corrected according to NACP standards.

Electron mode

The standard configuration of the Saturne 41 F offers 6 electron beam energies. Two scattering foils are used to obtain field flatness. The first foil widens the beam while maintaining maximum dose in the beam axis. The second foil is energy specific, and is used to obtain beam homogeneity over the entire field.
Photon contamination of the electron beam is less than 3 % of the maximum dose.

Dose rates

When purchasing, one dose rate must be chosen from the following values: 200 - 300 - 400 MU / min.

Installation requirements

• Power supply
Voltage: 380 V three-phase ± 7 % + neutral
Frequency: 50 Hz or 60 Hz ± 1 Hz
Ground connection impedance: < 1 Ω
Power (accelerator and control console only): 10 kVA on stand-by, 20 kVA during irradiation
Cos-phi: 0.86 on stand-by, 0.91 during irradiation
Overload: Twice normal current for 20 ms at start of stand-by sequence
PSA 760S: 2kVA
PSA 1100: 2kVA

• Cooling system
Lost water temperature: 6-25° C
Flow rate at 20° C: 5 l/min. to 10 l/min. in stand-by, 10 l/min. to 20 l/min. during irradiation
Filtered water: lime-free, filtered to 100 microns
Dissipated power: 6 kW in stand-by, 12 kW during irradiation
Input pressure: regulated by pressure, (1-5 bar)
Pressure loss during use: 3 bar (max.)

• Air conditioning
The temperature in the different rooms should be between 20° C (min.) and 25° C (max.), relative humidity less than 70 %. Dissipated power levels are:
- control console: 2 kW
- accelerator: 5 kW

• Waveguide pressurization
By gas: hexafluoride gas (SF_6) at 1 bar relative pressure.

Acceptance tests

Acceptance tests for the Saturne 41 F are described in the documents delivered with the equipment.

APPENDIX C

WELLHAUFER DOSIMETER SYSTEM PRODUCT DATA

ASSEMBLY FLOWCHART WATERPHANTOM

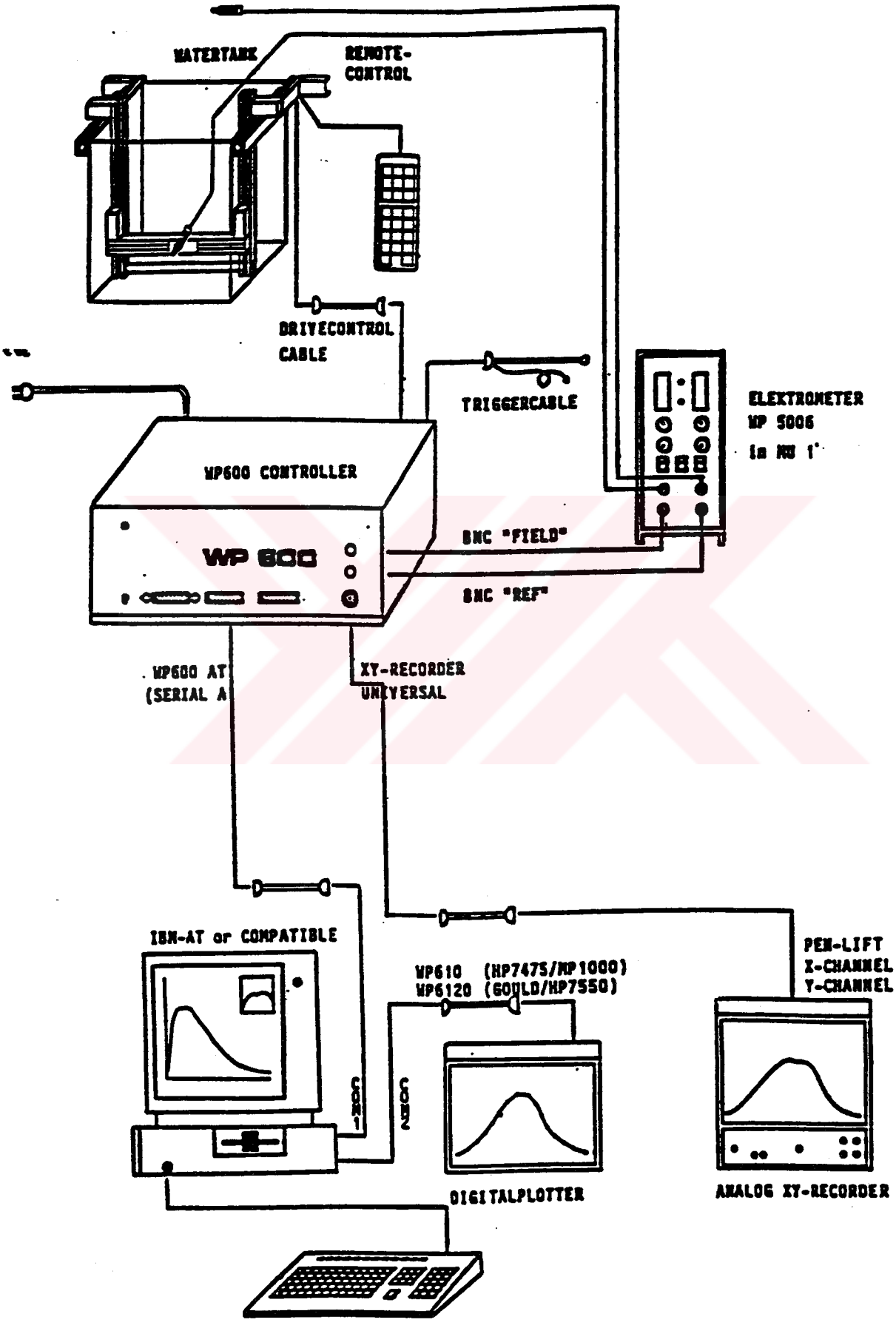

FIGURE 1

WATER TANK DIMENSIONS, COORDINATES AND MECHANICAL LIMITS

(set up example)

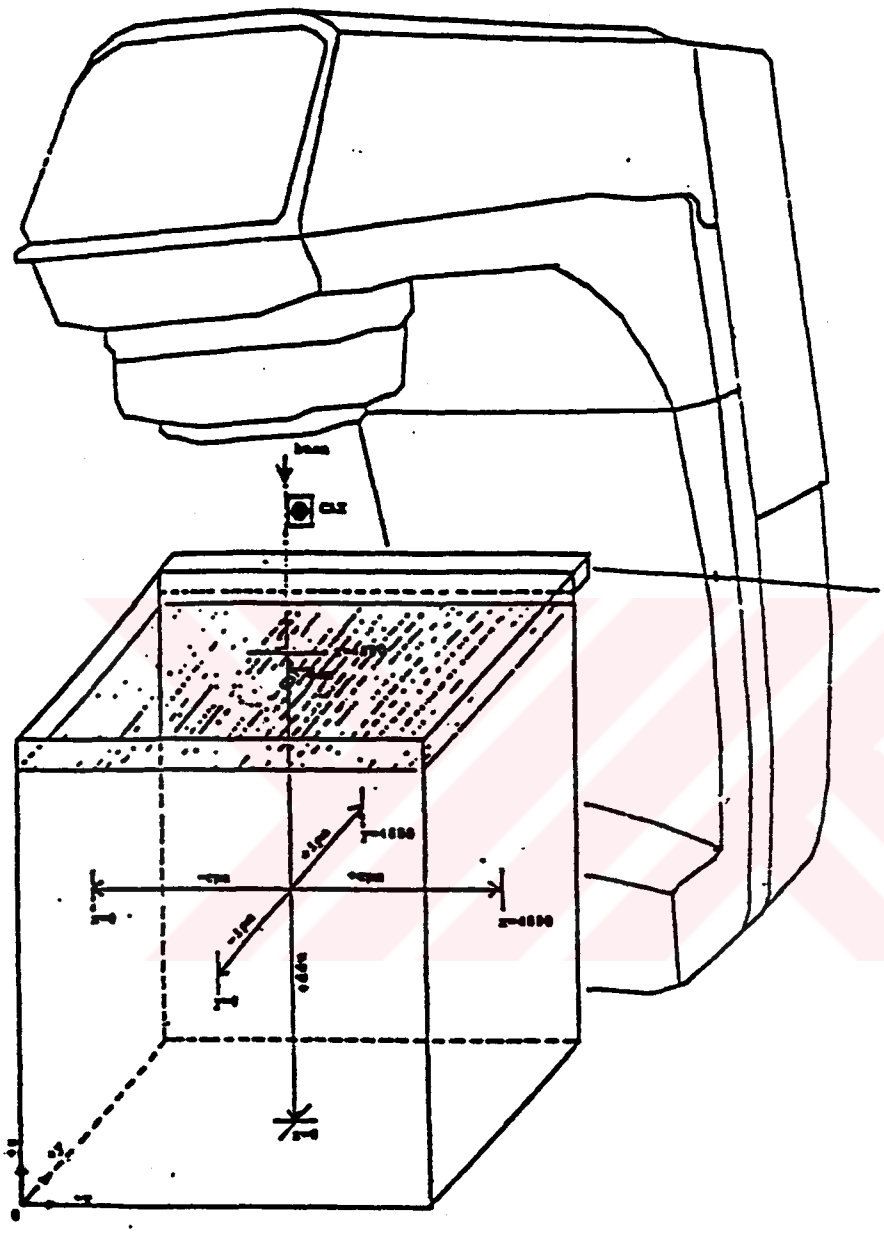

The relative coordinates below are according to the accelerator/phantom set up example shown in this figur For other cases refer to figure 6 and section III - WF software description

x, y, z	: absolute phantom coordinates
ip, cp, dd	: phantom coordinates inplane, crossplane, depth direction relative to isocentre and water surface
y = 0000 / y = 4800	: mechanical limits in y absolute coordinates
-ipm, +ipm	: mechanical limits in relative coordinates inplane
x = 0000 / x = 4800	: mechanical limits in x absolute coordinates
-cpm, +cpm	: mechanical limits relative coordinates crossplane
z = 4800	: mechanical limit in z absolute coordinates above water surface
-ddm	: mechanical limit relative coordinates depth direction water surface
z = 0000	: mechanical limit in z absolute coordinates tank bottom
+ddm	: mechanical limit relative coordinates direction tank bottom
x = 2400 y = 2400 z = 2400	: mechanical centre of phantom in absolute coordinates

FIGURE 5b

Ion Chamber IC 10

Schematics

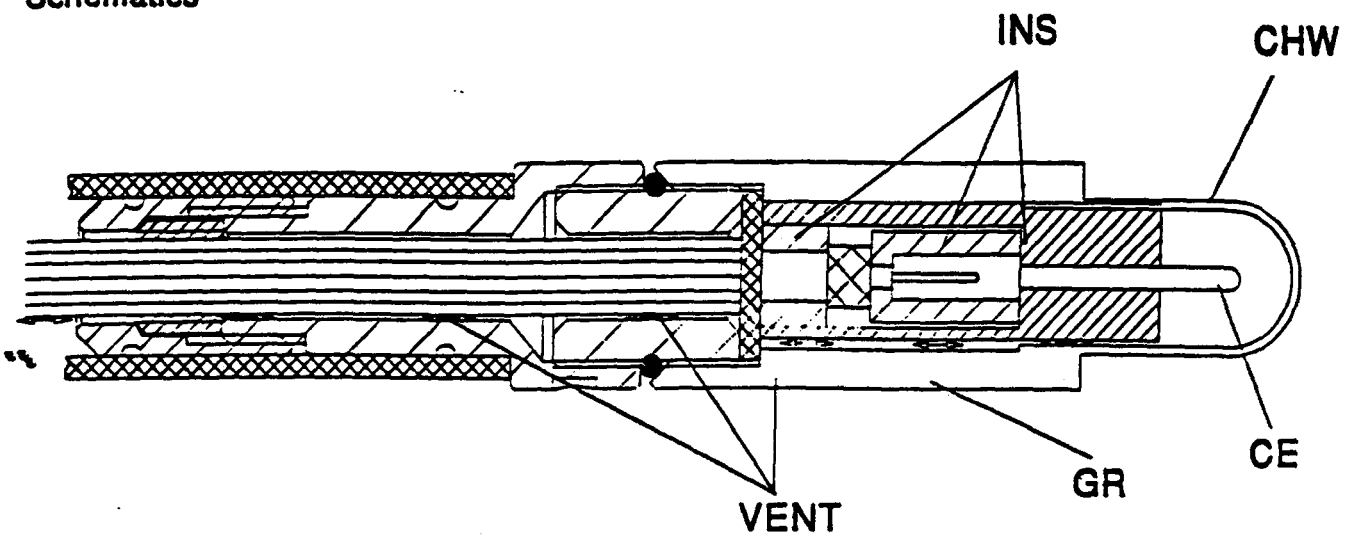

CHW	chamber wall (Shonka C552)
CE	center electrode (Shonka C552)
GR	guard ring (Shonka C552)
VENT	gas ventilation through hose
INS	insulators (Polyphenylenoxid PPO)

effective centre of active volur

waterproof
chamber volume 0.14 ccm
wall thickness 0.4 mm

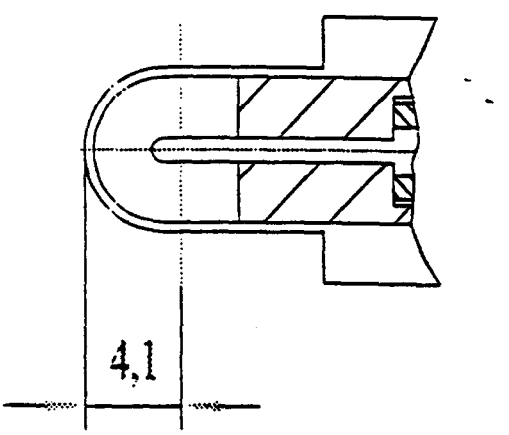

WELLHÖFER DOSIMETRIE

Bahnhofstraße 5
D - 8501 Schwarzenbruck
Tel. 09128-6070
FAX 09128-60710

APPENDIX E

MASS ANGULAR SCATTERING POWER VALUES FROM ICRU 21 AND 35 REPORTS

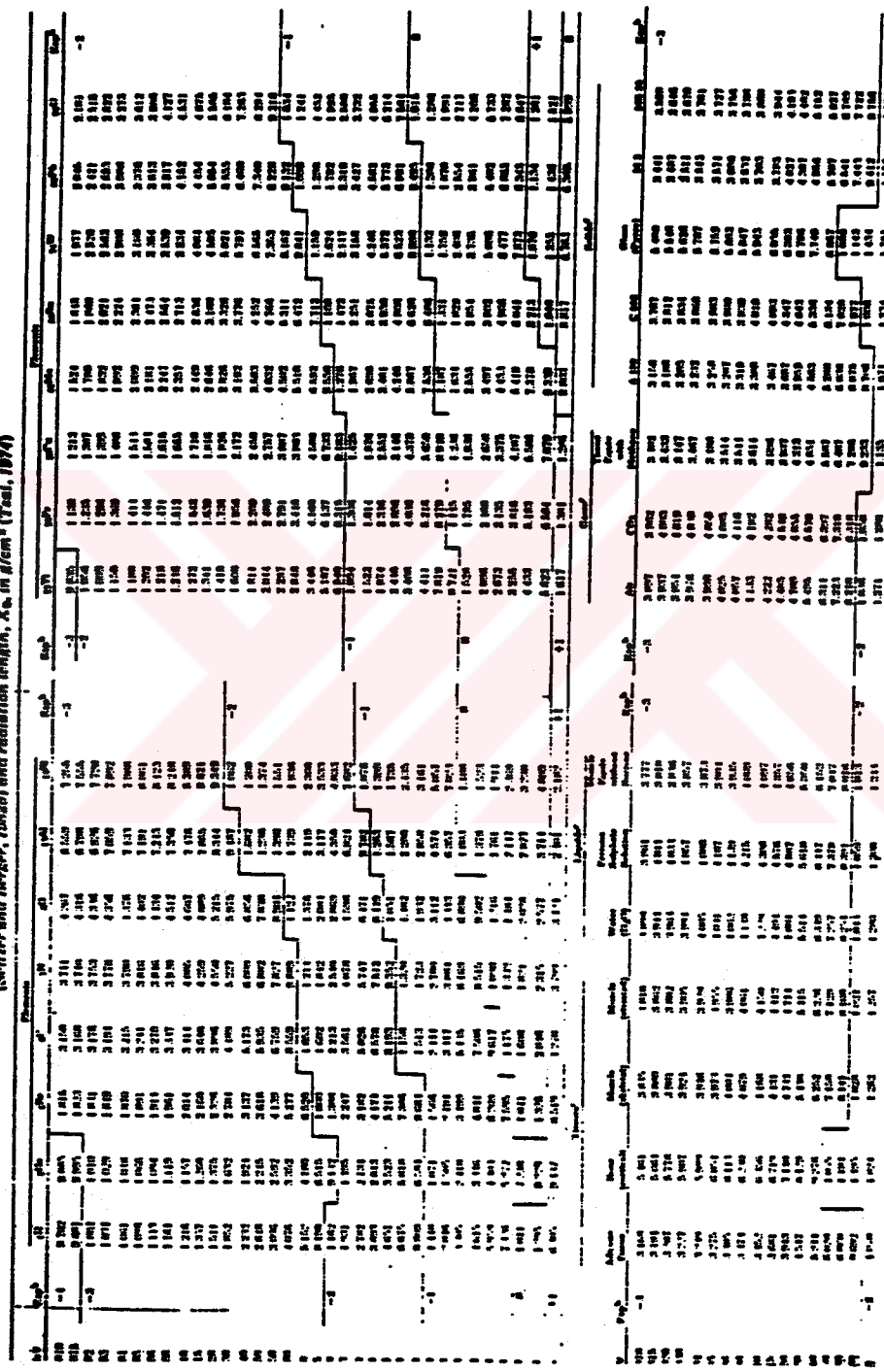

TABLE 2.1—Mass radiative stopping power[a], $(S/\rho)_{rad}$, in MeV cm^2 g^{-1} (Seltzer and Berger, 1982b) and radiation length, X_0, in g/cm^2 (Tsai, 1974)

TABLE 2.3—*Mass angular scattering power,* $\overline{\theta^2}/\rho \cdot l$, *in* $\text{radian}^2 \cdot \text{cm}^2 \cdot \text{g}^{-1}$ *as a function of electron energy (Rossi, 1952)* (*For* 9.08/+2 *read* 9.08×10^2)

E MeV	H (1)	C (6)	N (7)	O (8)	Al (13)	Fe (26)	Cu (29)	Pb	Air[a]	Water	Muscle[a]	Bone[a]	Polymethyl methacrylate	Polyethylene	Polystyrene	Silicon	LiF	Film emulsion[a]
0.010	2.62/+3	6.50/+3	7.43/+3	8.35/+3	1.23/+4	2.15/+4	2.31/+4	1.77/+4	7.75/+3	7.72/+3	7.59/+3	9.33/+3	6.78/+3	5.01/+3	6.20/+3	1.35/+4	7.25/+3	2.01/+4
0.015	1.25/+3	3.14/+3	3.59/+3	4.01/+3	6.00/+3	1.05/+4	1.14/+4	2.58/+4	3.75/+3	3.73/+3	3.67/+3	4.53/+3	3.28/+3	2.87/+3	3.00/+3	6.59/+3	3.51/+3	1.20/+4
0.020	7.39/+2	1.87/+3	2.14/+3	2.41/+3	3.57/+3	6.33/+3	6.84/+3	1.45/+4	2.21/+3	2.23/+3	2.19/+3	2.71/+3	1.95/+3	1.71/+3	1.78/+3	3.95/+3	2.10/+3	7.77/+3
0.030	3.53/+2	9.01/+2	1.01/+3	1.17/+3	1.74/+3	3.10/+3	3.35/+3	7.17/+3	1.08/+3	1.08/+3	1.06/+3	1.32/+3	9.45/+3	8.25/+2	8.61/+2	1.92/+3	1.03/+3	3.82/+2
0.01	2.10/+2	5.41/+2	6.22/+2	7.01/+2	1.04/+3	1.87/+3	2.02/+3	4.30/+3	6.49/+2	6.46/+2	6.35/+2	7.89/+2	5.66/+2	4.91/+2	5.15/+2	1.15/+3	6.06/+3	2.31/+2
0.05	1.41/+2	3.61/+2	4.10/+2	4.72/+2	7.01/+2	1.27/+3	1.37/+3	2.97/+3	4.37/+2	4.36/+2	4.28/+2	5.32/+2	3.84/+2	3.33/+2	3.47/+2	7.79/+2	4.10/+2	1.57/+2
0.08	1.02/+2	2.61/+2	3.01/+2	3.43/+2	5.12/+2	9.21/+2	9.97/+2	2.17/+3	3.17/+2	3.16/+2	3.10/+2	3.87/+2	2.76/+2	2.41/+2	2.52/+2	5.69/+2	2.98/+2	1.14/+2
0.08	6.12/+1	1.60/+2	1.84/+2	2.09/+2	3.11/+2	5.61/+2	6.08/+2	1.33/+3	1.93/+2	1.92/+2	1.88/+2	2.35/+2	1.67/+2	1.46/+2	1.52/+2	3.44/+2	1.80/+2	6.98/+1
0.10	4.15/+1	1.00/+2	1.25/+2	1.42/+2	2.13/+2	3.84/+2	4.16/+2	9.15/+2	1.31/+2	1.31/+2	1.28/+2	1.60/+2	1.11/+2	9.03/+1	1.01/+2	2.35/+2	1.23/+2	4.78/+1
0.15	2.08/+1	5.40/+1	6.33/+1	7.15/+1	1.07/+2	1.95/+2	2.12/+2	4.68/+2	6.61/+1	6.59/+1	6.47/+1	8.09/+1	5.75/+1	5.00/+1	5.23/+1	1.19/+2	6.21/+1	2.44/+2
0.20	1.29/+1	3.42/+1	3.91/+1	4.40/+1	6.70/+1	1.22/+2	1.32/+2	2.95/+2	4.12/+1	4.10/+1	4.03/+1	5.05/+1	3.58/+1	3.11/+1	3.25/+1	7.43/+1	3.87/+1	1.53/+2
0.30	6.08/ 0	1.78/+1	2.00/+1	2.33/+1	3.51/+1	6.42/+1	6.99/+1	1.50/+2	2.15/+1	2.14/+1	2.11/+1	2.61/+1	1.87/+1	1.62/+1	1.70/+1	3.90/+1	2.02/+1	8.04/+1
0.4	4.24/ 0	1.14/+1	1.31/+1	1.49/+1	2.24/+1	4.11/+1	4.46/+1	1.00/+2	1.37/+1	1.37/+1	1.34/+1	1.69/+1	1.19/+1	1.04/+1	1.08/+1	2.49/+1	1.29/+1	5.16/+1
0.5	3.00/ 0	8.07/ 0	9.32/ 0	1.05/+1	1.60/+1	2.93/+1	3.18/+1	7.17/+1	9.71/ 0	9.71/ 0	9.53/ 0	1.20/+1	8.40/ 0	7.35/ 0	7.68/ 0	1.77/+1	9.10/ 0	3.68/+1
0.6	2.26/ 0	6.11/ 0	7.06/ 0	7.99/ 0	1.21/+1	2.23/+1	2.41/+1	5.45/+1	7.38/ 0	7.36/ 0	7.23/ 0	9.09/ 0	6.41/ 0	5.56/ 0	5.82/ 0	1.34/+1	6.91/ 0	2.80/+1
0.8	1.46/ 0	3.95/ 0	4.56/ 0	5.17/ 0	7.83/ 0	1.44/+1	1.57/+1	3.55/+1	4.77/ 0	4.75/ 0	4.67/ 0	5.88/ 0	4.14/ 0	3.59/ 0	3.70/ 0	8.68/ 0	4.49/ 0	1.82/+1
1.0	1.03/ 0	2.81/ 0	3.25/ 0	3.68/ 0	5.58/ 0	1.03/+1	1.12/+1	2.55/+1	3.40/ 0	3.39/ 0	3.32/ 0	4.19/ 0	2.95/ 0	2.56/ 0	2.67/ 0	6.19/ 0	3.20/ 0	1.30/+1
1.5	5.50/−1	1.51/ 0	1.74/ 0	1.97/ 0	3.00/ 0	5.55/ 0	6.03/ 0	1.38/+1	1.82/ 0	1.82/ 0	1.78/ 0	2.25/ 0	1.58/ 0	1.37/ 0	1.43/ 0	3.33/ 0	1.71/ 0	7.01/ 0
2.0	3.49/−1	9.58/−1	1.11/ 0	1.26/ 0	1.91/ 0	3.54/ 0	3.85/ 0	8.83/ 0	1.16/ 0	1.16/ 0	1.13/ 0	1.43/ 0	1.01/ 0	8.71/−1	9.11/−1	2.12/ 0	1.09/ 0	4.48/ 0
3.0	1.80/−1	4.97/−1	5.75/−1	6.53/−1	9.85/−1	1.85/ 0	2.01/ 0	4.63/ 0	6.02/−1	6.00/−1	5.89/−1	7.45/−1	5.23/−1	4.52/−1	4.73/−1	1.10/ 0	5.67/−1	2.34/ 0
4	1.11/−1	3.08/−1	3.57/−1	4.05/−1	6.18/−1	1.15/ 0	1.25/ 0	2.89/ 0	3.74/−1	3.72/−1	3.66/−1	4.62/−1	3.21/−1	2.80/−1	2.93/−1	6.84/−1	3.52/−1	1.46/ 0
5	7.61/−2	2.11/−1	2.45/−1	2.78/−1	4.34/−1	7.89/−1	8.59/−1	1.99/ 0	2.56/−1	2.55/−1	2.50/−1	3.17/−1	2.23/−1	1.93/−1	2.01/−1	4.70/−1	2.41/−1	1.00/ 0
6	5.55/−2	1.54/−1	1.79/−1	2.03/−1	3.19/−1	5.78/−1	6.29/−1	1.46/ 0	1.87/−1	1.87/−1	1.83/−1	2.32/−1	1.62/−1	1.40/−1	1.47/−1	3.44/−1	1.76/−1	7.34/−1
8	3.35/−2	9.34/−2	1.08/−1	1.23/−1	1.88/−1	3.51/−1	3.82/−1	8.87/−1	1.13/−1	1.13/−1	1.11/−1	1.40/−1	9.80/−2	8.48/−2	8.88/−2	2.09/−1	1.07/−1	4.46/−1
9																		
10	2.25/−2	6.20/−2	7.20/−2	8.28/−2	1.27/−1	2.37/−1	2.58/−1	6.00/−1	7.63/−2	7.61/−2	7.47/−2	9.46/−2	6.60/−2	5.71/−2	5.98/−2	1.41/−1	7.10/−2	3.01/−1
15	1.03/−2	3.03/−2	3.52/−2	3.99/−2	5.12/−2	1.15/−1	1.25/−1	2.91/−1	3.69/−2	3.67/−2	3.60/−2	4.57/−2	3.19/−2	2.75/−2	2.88/−2	6.80/−2	3.47/−2	1.46/−1
20	6.38/−3	1.80/−2	2.08/−2	2.37/−2	3.03/−2	6.80/−2	7.41/−2	1.73/−1	2.18/−2	2.17/−2	2.13/−2	2.71/−2	1.89/−2	1.63/−2	1.71/−2	4.03/−2	2.06/−2	8.66/−2
30	3.01/−3	8.51/−3	9.87/−3	1.12/−2	1.72/−2	3.23/−2	3.52/−2	8.00/−2	1.03/−2	1.03/−2	1.01/−2	1.29/−2	8.91/−3	7.73/−3	8.09/−3	1.91/−2	9.75/−3	4.12/−2
40	1.76/−3	4.99/−3	5.79/−3	6.58/−3	1.01/−2	1.88/−2	2.04/−2	4.51/−2	6.00/−3	6.05/−3	5.93/−3	7.54/−3	5.24/−3	4.53/−3	4.74/−3	1.12/−2	5.72/−3	2.38/−2
50	1.16/−3	3.29/−3	3.82/−3	4.34/−3	6.62/−3	1.21/−2	1.31/−2	2.92/−2	1.00/−3	3.99/−3	3.91/−3	4.93/−3	3.46/−3	2.99/−3	3.13/−3	7.35/−3	3.77/−3	1.51/−2
60	8.21/−4	2.31/−3	2.71/−3	3.06/−3	4.62/−3	8.43/−3	9.11/−3	2.03/−2	2.83/−3	2.82/−3	2.76/−3	3.47/−3	2.45/−3	2.12/−3	2.22/−3	5.12/−3	2.65/−3	1.05/−2
80	1.79/−4	1.33/−3	1.53/−3	1.73/−3	2.61/−3	4.76/−3	5.16/−3	1.15/−2	1.60/−3	1.59/−3	1.56/−3	1.96/−3	1.39/−3	1.21/−3	1.26/−3	2.89/−3	1.50/−3	5.95/−3
100	3.14/−4	8.51/−4	9.82/−4	1.11/−3	1.67/−3	3.05/−3	3.31/−3	7.37/−3	1.03/−3	1.03/−3	1.00/−3	1.26/−3	8.91/−4	7.74/−4	8.16/−4	1.86/−3	9.62/−4	3.82/−3

[a] Composition (Fraction by weight)
Air: 0.755 N; 0.232 O; 0.013 A.
Muscle: 0.1020 H; 0.1230 C; 0.0350 N; 0.7200 O; 0.0008 Na; 0.0002 Mg; 0.0020 P; 0.0050 S; 0.0030 K.
Bone: 0.064 H; 0.278 C; 0.027 N; 0.410 O; 0.002 Mg; 0.070 P; 0.002 S; 0.147 Ca.
Film emulsion: 0.0141 H; 0.0723 C; 0.0193 N; 0.0681 O; 0.0019 S; 0.3491 Br; 0.4741 Ag; 0.0031 I.

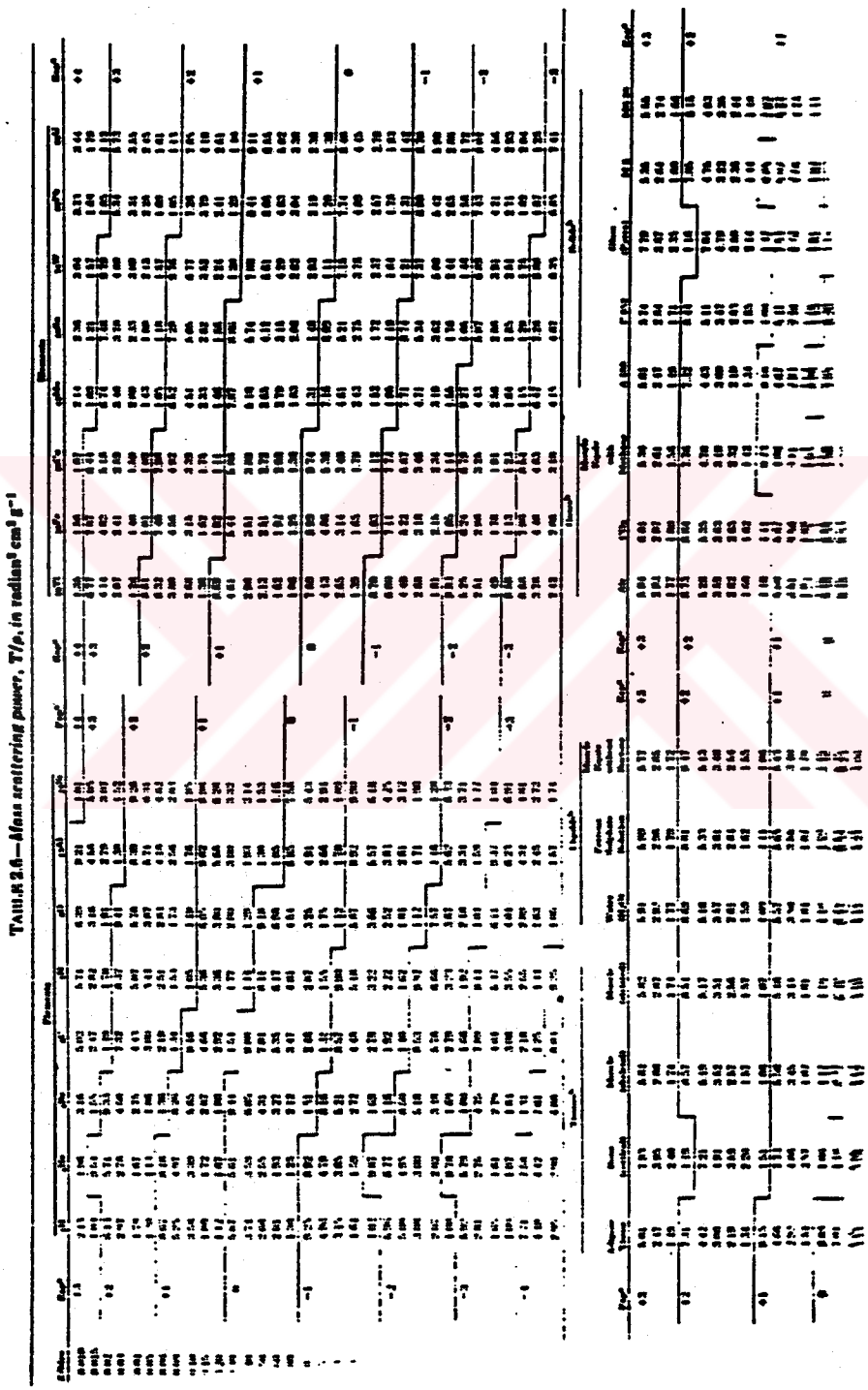

TABLE 2.6—*Mass scattering power, T/ρ, in radian^2 cm^2 g^{-1}*

VIII. REFERENCES

1) Joseph Deasy, Ph. D. Dissertation, *"Electron Energy and Angular Distributions in Radiotheraphy"*, The University of Kentucky, 1992.

2) International Commission On Radiation Units and Measurements Report 35, *"Radiation Dosimetry; Electron Beam with Energies Between 1 and 5 MeV"*, Maryland, U.S.A., 1984.

3) Faiz M. Khan , *"The Physics of Radiation Therapy"*, 2nd Edition, Williams & Williams, Minnesota, U.S.A., 1992.

4) Harold Elford Johns, John Robert Cunningham, *"The Physics of Radiology"*, Fourth Edition, Charles C. Thomas , Illionis, U.S.A., 1993.

5) CGR Handbook, *"Accelerators for Radiotherapy"*, Volume 9, 1985.

6) Robert Stanton, Donna Stinson, *"An Introduction to Radiation Oncology Physics"*, Medical Physics Publishing, Madison, Wisconsin, U.S.A., 1992.

7) S C Klevenhagen, *"Physics of Electron Beam Theraphy"* Adam Hilger Ltd, Bristol and Boston, London, 1995.

8) Peter R. Almond, *"Radiation Physics of Electron Beams"*, Texas, 1985.

9) Jackson J. D. , *"Classical Electrodynamics"*, 2nd Edition, New York, Wiley, New York , U.S.A., 1975.

10) International Atomic Energy Agency, *"Absorbed Dose Determination In Photon and Electron Beams, An International Code of Practice."* Technical Report Series No 277, Vienna, 1987.

11) Bruno Rossi, *"High Energy Particles"*, Printice-Hall, New York, U.S.A. 1952.

12) Noel Blais, Ervin B Padgorsak, *"The Mass Angular Scattering Power Method For Determining The Kinetic Energies of Clinical Electron Beams"*, Phys. Med. Biol., Vol.37, P.1932- 1942, 1992.

13) H.Ogelman, J. R. Wayland, *"Introduction To Experimental Techniques of High-Energy Astrophysics."*, National Aeronautics and Space Administration, Washington D.C. , 1970.

14) Malcolm S. Longair, *"High Energy Astrophysics"*, Volume 1, 2nd Edition, Cambridge University Press, 1992.

15) Brano Rossi, Stanislaw Olbert, *"Introduction to the Physics of Space"*, Mc-Graw-Hill , New York, 1970.

16) W.T.Scott, "The Theory of Small Angle Multiple Scattering of Fast Particles" *Rev. Mod. Phys.* 35, p.231-313, 1963.

17) Brano Rossi, K. Greisen, "Cosmic Ray Theory" *Rev. Mod. Phys.* , Vol.13, P. 240 - 303 , 1941.

18) International Commission On Radiaotion Units and Measurements Report 21, *"Radiation Dosimetry; Electrons with Initial Energies Between 1 and 5 MeV"*, Washington D.C., U.S.A., 1984.

19) David Jette, "Electron Dose Calculation Using Multiple Scattering Theory. A Gaussian Multiple Scattering Theory.", *Med. Phys.*, 15(2), P. 123, 1988.

20) H.L.A. Polman, P.M. Van Der Linden, "Description of the uncollimated electron beam in air by means of a directional pencil beam model", *Phys. Med. Biol.*, 1987, Vol. 32, P.353 - 363, 1987.

21) B.J. Parland, "Using Background Subtraction For Measuring The Dose Distribution Of an Electron Pencil Beam", *Med. Phys.*, 14 (3), P.406-409, 1987.

22) H.L.A. Polman, P.M. Van Der Linden, "Determination of three parameters describing the uncollimated electron beam in air. " *Phys.Med. Biol.*, Vol. 32, P. 345- 353, 1987.

23) *"Saturne 40/41/42/43 800 Series, Advanced Service Manual"*, Technical Publications, GE Medical Systems, 1995.

24) Gavinda Rajan, *"Advanced Medical Radiation Dosimetry"*, Printice-Hall of India, New Delphi, 1992.

25) *"Saturne 40/41/42/43 800 Series,Operator Manual"*, Technical Publications, GE Medical Systems.

26) *"Technical Document for Water Phantom-Systems WP600 and WP700"*, Wellhaufer Dosimetrie, 1996